
Masters Theses

Student Theses and Dissertations

Spring 2012

Laboratory implementations of PMSM drive in hybrid electric vehicles applications

Amir E. Saad

Follow this and additional works at: https://scholarsmine.mst.edu/masters_theses



Part of the [Electrical and Computer Engineering Commons](#)

Department:

Recommended Citation

Saad, Amir E., "Laboratory implementations of PMSM drive in hybrid electric vehicles applications" (2012). *Masters Theses*. 5136.

https://scholarsmine.mst.edu/masters_theses/5136

This thesis is brought to you by Scholars' Mine, a service of the Missouri S&T Library and Learning Resources. This work is protected by U. S. Copyright Law. Unauthorized use including reproduction for redistribution requires the permission of the copyright holder. For more information, please contact scholarsmine@mst.edu.

LABORATORY IMPLEMENTATIONS OF PMSM DRIVE
IN HYBRID ELECTRIC VEHICLES APPLICATIONS

by

AMIR E. SAAD

A THESIS

Presented to the Faculty of the Graduate School of the
MISSOURI UNIVERSITY OF SCIENCE AND TECHNOLOGY

In Partial Fulfillment of the Requirements for the Degree

MASTER OF SCIENCE IN ELECTRICAL ENGINEERING

2012

Approved by

Jonathan W. Kimball, Advisor
Mehdi Ferdowsi
Keith Corzine

© 2012
Amir E. Saad
All Rights Reserved

ABSTRACT

Field Programmable Gate Arrays (FPGAs) are one of the today's most successful technologies for developing systems that require real time operation and providing additional flexibility to the designer. This research is focused on developing a control board for a permanent magnet synchronous machine (PMSM) using an FPGA module. The board is configured for individual use of an FPGA, digital signal processor (DSP) or in combination to control the PMSM by generating the required Pulse Width Modulator (PWM) to the inverter in order to drive and control the speed of the PMSM. Since, the exact rotor position and speed are required to control the motor; a useful method is developed digitally and implemented in the FPGA hardware module. The speed observer (SO), in which the Hall effect signals were used to calculate the speed and the angle of the rotor.

In this thesis, three different techniques of PWM generation were developed and combined with rotor position and speed method. The project is implemented in Altera FPGA using Quartus II software V11.0 with VHDL as the supporting language. The design achieved high performance and accuracy of the detection estimation and control scheme for the Permanent Magnet Synchronous Machine. Error and design analysis has been done also.

ACKNOWLEDGMENTS

I owe my utmost gratitude to my Advisor Dr. Jonathan Kimball, who has the attitude and the substance of a genius: his encouragement, guidance and support from the initial to the final level enabled me to develop and understand the subject, for inspiring and motivating me to overcome all the obstacles in the completion of this work, and for providing the financial support to me and my family through this wonderful period.

I would like to thank my committee members; Dr. Mehdi Ferdowsi and Dr. Keith Corzine, for helping me walk through my academic knowledge and technical participation at the DOE project, providing me the encouragement to achieve the maximum success.

I would like to thank my parents, Elshaikh Saad and Asmaa Saad and my brother Mohamed and also extend my sincere thanks and appreciation to my little family, my dearest wife Hadeel Abdalla and balsam of my life my daughter Leen Saad for their support, patience, and encouragement during these years.

I would like to thank my friends, classmates, the faculty staff, and everyone who helped or encouraged me during my whole life.

Lastly, thank you to the Department of Energy and the Missouri S&T research board for their financial support. This research was sponsored by the Department of Energy under grant DE-EE0002012.

TABLE OF CONTENTS

	Page
ABSTRACT	iii
ACKNOWLEDGMENTS	iv
LIST OF ILLUSTRATIONS	vii
LIST OF TABLES	ix
NOMENCLATURE	x
SECTION	
1. INTRODUCTION	1
1.1. BACKGROUND	1
1.2. PROPOSED APPROACH	1
1.3. LITERATURE REVIEW	4
1.4. THESIS OUTLINE	7
2. SIGNAL PROCESSING AND CONTROL BOARD	8
2.1. INTRODUCTION	8
2.2. SIGNAL CONDITIONING CIRCUIT	8
2.3. FILTER CIRCUIT	10
2.4. LEVEL SHIFTERS	11
2.5. ANALOG TO DIGITAL CONVERTERS	12
2.6. ISOLATOR CIRCUIT	14
2.7. CAN TRANSCEIVER CIRCUIT	14
2.8. DIFFERENTIAL INPUT CIRCUIT	15
2.9. DSP CIRCUIT	16
2.10. FPGA CIRCUIT	17
2.11. POWER SUPPLY BOARD	19
2.12. PULL-UP RESISTOR CIRCUIT	21
2.13. ERRATA	22
3. PULSE WIDTH MODULATOR	23
3.1. INTRODUCTION	23
3.2. DIGITAL PWM GENERATION TYPES	23

3.2.1. Up-Mode Counter.....	24
3.2.2. Down-Mode Counter.....	24
3.2.3. Up-Down Mode Counter.....	25
3.2.4. PWM with Dead-Band.....	26
4. PMSM ROTOR POSITION MEASUREMENT	30
4.1. INTRODUCTION	30
4.1.1. Optical Encoder.....	30
4.1.2. Resolver.....	31
4.1.3. Full Observer.....	31
4.1.4. Hall Effect Sensors.....	32
4.2. HYBRID SPEED OBSERVER.....	33
5. RESULTS AND SYSTEM VALIDATION	43
5.1. MODELSIM RESULTS.....	43
5.2. HARDWARE RESULTS.....	46
6. CONCLUSION AND FUTURE SCOPE.....	51
APPENDICES	
A. PRINTED CIRCUIT BOARDS DESIGN.....	52
B. VHDL CODES OF THE DESIGN.....	71
BIBLIOGRAPHY.....	88
VITA	91

LIST OF ILLUSTRATIONS

	Page
Figure 1.1. PCB0021 Control Board.....	3
Figure 1.2. The Control Board and the Inverter.....	3
Figure 2.1. Gains and Offset Circuit.....	8
Figure 2.2. Generic Sallen Key Filter Topology.....	10
Figure 2.3. CMOS Hex Voltage –Level Shifter.	12
Figure 2.4. AD7276 Block Diagram.....	13
Figure 2.5. AD7329 Block Diagram.....	13
Figure 2.6. ADUM1412 Block Diagram	14
Figure 2.7. 65HVD251Funcional Diagram	15
Figure 2.8. Differential Amplifier Circuit.....	16
Figure 2.9. TMS320F28335.....	17
Figure 2.10. Structure of the FPGA.....	18
Figure 2.11. Altera Design Flow Chart.....	19
Figure 2.12. PES and PET Type Connectors.....	20
Figure 2.13. PCB0025.....	20
Figure 2.14. Pull-up Resistor for Open Collector Configuration.....	21
Figure 3.1. PWM Block Diagram.....	23
Figure 3.2. Up Mode Counter.....	24
Figure 3.3. Down Mode Counter.....	25
Figure 3.4. Up-Down Mode Counter.....	25
Figure 3.5. Signals of Interest.....	26
Figure 3.6. PWM Schematic Diagram.....	28
Figure 4.1. Optical Encoder.....	30
Figure 4.2. Resolver Schematic	31
Figure 4.3. Full Adaptive Observer	32
Figure 4.4. Three Hall Effect Sensors and Their Related Signals	33
Figure 4.5. High-Performance BLDC.....	34
Figure 4.6. Hybrid Observer Bounding Functions.....	36

Figure 4.7. Hybrid Observer Block Diagram [26].....	39
Figure 4.8. Speed Observer Schematic in VHDL.....	40
Figure 4.9. PCB0006 Experiments Board.....	41
Figure 4.10. The Experiment dc Motor.	42
Figure 5.1. The Simulation Results of the Up-Mode Counter.....	43
Figure 5.2. The Simulation Results of the Down-Mode Counter.....	43
Figure 5.3. The Simulation Results of the Up-Down Counter.	44
Figure 5.4. Screen Shot (1) for Parameters Results of the SO.....	44
Figure 5.5. Screen Shot (2) for Parameters Results of the SO.....	45
Figure 5.6. Screen Shot (3) for Parameters Results of the SO.....	45
Figure 5.7. Screen Shot (4) for Parameters Results of the SO.....	46
Figure 5.8. The Rising-Edge Counter Delay.	46
Figure 5.9. The Falling-Edge of the Fed Counter.....	47
Figure 5.10. Hall Effect Signals.....	47
Figure 5.11. The SO Output in 59.86 Hz Hall Effect Signals Input.	48
Figure 5.12. The Absolute Error vs. m Bits.	49
Figure 5.13. The Total Logic Elements vs. m Bits.	49
Figure 5.14. The $\sin(\theta_{rh})$ Output.	50
Figure 5.15. Zoom in Results of $\sin(\theta_{rh})$	50

LIST OF TABLES

	Page
Table 2.1. Maximum and Minimum Voltage Range.	9
Table 2.2. The Resistor Values for Fig. 2.1.	9
Table 2.3. Capacitor and Resistor Values.	11
Table 2.4. Power Modules and Corresponding Voltages.	21
Table 4.1. Bounding Functions vs. Hall States.	35
Table 4.2. State Transition Points.	35
Table 4.3. Initial Conditions.	37
Table 4.4. The Motor Parameters.	42

NOMENCLATURE

Symbol	Description
HEVs	Hybrid Electric Vehicles
EMs	Electric Motors
CAN	Computer Automotive Network
RTDC	Resolver-to-Digital Converter
SO	Speed Observer
PMSM	Permanent Magnet Synchronous Machine
FPGA	Field Programmable Gate Array
Q	Quality factor
f_c	Cutoff frequency
\hat{i}	Observed current
\hat{v}	Observed voltage
h_a, h_b, h_c	Hall effect sensor signals
ω_r	Rotor angular speed
$\hat{\omega}_r$	Rotor estimated speed
θ_r	Rotor electrical position

1. INTRODUCTION

1.1. BACKGROUND

Electric motors (EMs) and generators are the primary workhorses in hybrid-electric vehicles (HEVs). The generators convert mechanical power from the engine electrical power in order to charge the batteries and operate the motors. Then motors produce the required torque to drive the wheels. There are many types of motors and generators used in HEVs: induction, switched reluctance, and permanent magnet. Each type requires the occurrence of a magnetic field. Reluctance and induction motors use an external source to provide the magnetic field, while the permanent magnet motors use permanent magnets for this purpose. The critical factors for these components are power, efficiency, controllability, cost, and durability [1-3].

PMSMs have been generally used in the HEV over the last two decades because of their high efficiency, high-power density and lack of a dc field winding in the rotor; however, they are more expensive than alternatives [2]. It is usually accepted that precise control of a PMSM requires exact rotor position and speed information. The methods to detect the rotor position are basically divided into two categories. One is the rotor position detection by a position sensor mounted on the machine rotor, and the other is a sensor-less method based on indirect rotor position estimation techniques [3].

In this thesis, a control board for a PMSM is constructed with advanced electronic techniques in order to offer the best type of control for a PMSM in a HEV application. The board contains many different signal processing circuits in addition to the flexibility of using microcontroller or FPGA module to apply different control applications. Rotor speed and position scheme is implemented in the FPGA using VHDL language. The method used is the Hall effect sensors to estimate the rotor speed and position [4].

1.2. PROPOSED APPROACH

In order to estimate the rotor position and control the PMSM, a signal processing control board is necessary to study, investigate and apply many different control techniques. The circuits in the board have been simulated using MATLAB SIMULINK and SPICE for the sake of accuracy and stability of the system. Then CADSOFT EAGLE

PCB design software was used to layout the board. The board uses two different technologies to control the motor: a digital signal processor (DSP) and a FPGA. The Altera Cyclone II FPGA module delivers high performance and low power consumption at a cost that rivals that of ASICs. Altera's modules are supported by the easy-to-use and Quartus II licensed or free Edition design software.

The control board has the capability of working in three modes, the DSP only, the FPGA only, or the DSP-FPGA share mode. In the DSP mode only, all the signals are forwarded towards the DSP for either generating a special signal such as PWM or reading an external signal such as dc bus voltage, current sensors, or Hall effect signals to make other control decisions. The FPGA is being developed to have the same functionality as the DSP. Furthermore, these two devices can share all the control operation if needed, due to the high performance of the FPGA which runs at 24 MHz in this particular module or even up to 400 MHz in some other families.

Signal conditioning circuits are added to the board in order to offer the compatibility for the DSP to read external signals from the inverter (Semikron Box), current sensors or the dc bus. Another differential input circuit has been implemented in case applications require different ground reference. Also, level shifter circuits from +3V to +15V and +15V to +3V are needed to condition the PWM signals to be compatible with the Inverter gates threshold or receive fault signals respectively.

Sallen-Key Filters were added to the board for converting signals from digital to analog for monitoring some interesting parameters. Communication is very important in this type of applications, thus, Computer Automotive Network (CAN) transceivers were added to the board. For extra design flexibility, digital Input/Outputs and relay contractors were added to the board for future uses. External Analog to Digital Converters (ADCs) were added in case of the DSP ADCs failure and to speed up the DSP's processing by passing them through the FPGA. Another 16 channel serial ADC was added to offer digital signal to the FPGA.

Figures 1.1 and 1.2 illustrate the control board block diagram and the real board attached to the inverter screen shot.

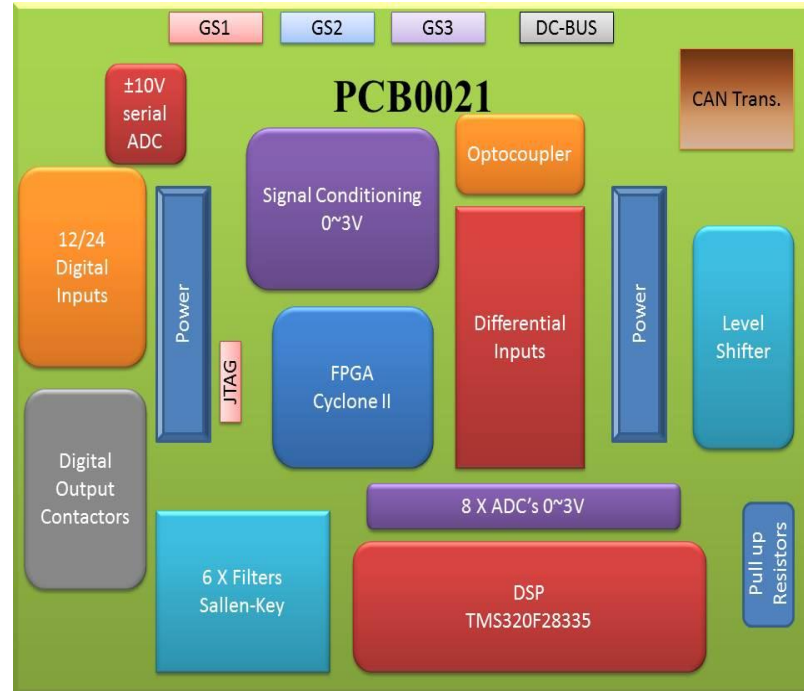


Figure 1.1. PCB0021 Control Board.

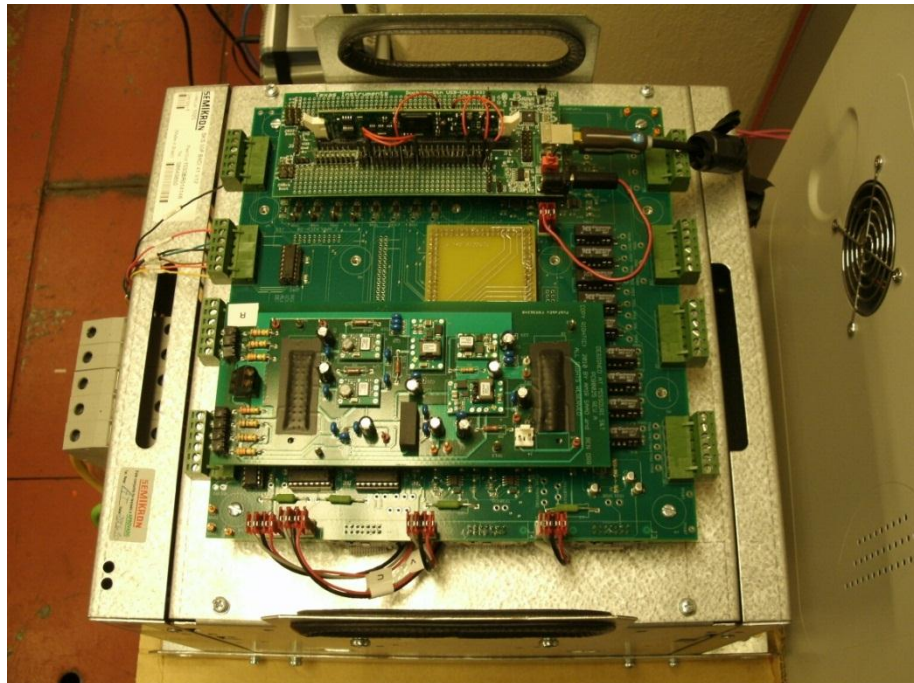


Figure 1.2. The Control Board and the Inverter.

1.3. LITERATURE REVIEW

The existing literatures on the rotor speed and position estimation are studied in this section along with literature that focuses in type of observing methods to estimate these characteristics. A common type of motor that has been used in HEVs is the PMSM [2]. Therefore, this literature will be around this type of a motor.

A proposal of self-sensing technique is proposed in [4]. The technique functions in a manner similar to a resolver and resolver-to-digital converter (RTDC) sensing system, in this technique the motor acts as the electromagnetic resolver and the power converter applies carrier-frequency voltages to the stator which produce high-frequency currents that proportional with position. The sensed currents are processed with a heterodyning technique that provides a signal that is nearly proportional to the difference between the actual rotor position and an estimated rotor position.

Another proposal of a self-sensing technique and high-frequency injection in [5] is based on tracking observer to correct the limitation in [4]. This method uses a rotating vector, a carrier signal, and a tracking observer. In this method, high-frequency injection makes low and zero speed detection possible.

The authors in [6] proposed a FPGA based scheme in which the rotor position can be estimated by using three symmetrical locked Hall effect position sensors. This scheme is implemented using the Altera FPGA, by assuming the time interval between adjacent changes Hall effect sensor signal is Δt and calculating the average electric angular velocity ω_r is,

$$\omega_r = \pi / (3\Delta t) \quad (1)$$

The estimated dynamic error is

$$\delta\theta_{Dmax} = \frac{\pi}{2} - \frac{p}{2a} \left(\omega_2 + \sqrt{\omega_2^2 - \frac{a\pi}{p}} \right) \left(-\omega_2 + \sqrt{\omega_2^2 + \frac{a\pi}{p}} \right) \quad (2)$$

Where a is the motor's acceleration, p is the number of pole pair, and ω_2 is the angular velocity that corresponds to the switching point of the Hall interval.

A scheme of modeling and cosimulation of the PMSM control system using an FPGA is proposed in [7], This method uses the Space Vector Pulse Width Modulator (SVPWM), D - Q transformation and PI controller as a control scheme. During the design, the cosimulation between the function model and the VHDL model has been implemented. The cosimulation between the function model and VHDL model realizes the timing and control simulation by using Link-for Modelsim[®] in MATLAB.

The high frequency signal injection method proposed in [8] to improve the detection accuracy. A DSP (TMS320F2812) is used to implement this method and 4-pole PMSM is selected as experiment subject. The position detection scheme shows high accuracy and reduces the error.

Mathematical modeling of a PMSM and the flux-linkage observer is proposed in [9]. The mathematical model is used to approximate the nonlinear system of PMSM. Due to the present modification scheme with error-correction, the rotor position and machine speed can be estimated; even in the transient state the system has the capability of the smooth starting and reversing. In addition, the system with the flux-linkage is very robust and can tolerate variations in PMSM parameters.

The Hall effect method proposed in [10]; uses a simple algorithm that combines the measurements of a Hall effect sensor with a “sensorless” method. In this method, the Hall effect position sensor is used instead of a resolver as the mechanical sensor, to allow vector control of a PMSM with a sinusoidal back-EMF. As a Hall effect sensor provides only six measurements per electrical turn, the position error between the actual rotor position and the measured position can potentially reach 30° electrically. This error affects the control performances and causes significant torque oscillations and over currents, which are not suitable in transportation systems applications. This method is easy to implement, but it can not offer continuous precise information of the rotor position.

A Flux linkage method is proposed in [11] and uses the flux linkage signals to calculate the rotor position based on trigonometric approximations. The flux linkage signals can be measured by accessing the neutral point of the PMSM. Regarding the

software implementation, the PMSM is modeled in Maxwell, where the nonlinear magnetic flux density B and the magnetic flux intensity curves are also considered.

Multiple geometric and saturation induced saliencies based on a stator-oriented magnetic circuit approach is introduced in [12], it introduces a new modeling approach of a nonlinear machine model. The advantage of this method is that all kinds of saliencies that occur in the electrical machine can be considered simultaneously. Moreover, modeling in the stator coordinates leads to a physically motivated explanation when the cross saturation effect can occur in a PMSM.

The vector-tracking position observer is proposed [13], it is an improved approach for estimating the rotor positions in PMSM drives with low-resolution Hall effect sensors. A vector-tracking position observer in conjunction with a discrete Hall effect sensor's output signal has been proposed, which is similar to a phase-locked loop structure. It consists of a position error detector, based on the vector cross product of the unit back-electromotive-force vectors obtained from a stator electrical model, and a proportional–integral type controller, to make the position error rapidly converge to zero. This structure does not only compensate the misalignment effect of the Hall effect sensors, but also enhance their transient operating capability. This structure allows the proposed approach to provide useful position information even at and around zero speeds where the vector-tracking correction loop cannot correctly operate. Above zero speeds, the proposed approach provides the high-resolution position information, where the position estimation error rapidly converges to zero regardless of the misalignment of Hall's sensors and the excessive average-speed error, particularly speed transient operation. Through the experiments during the steady-state, start-up, speed transient, and load transient operations, the effectiveness and the dynamic performance of the proposed approach have been evaluated and verified.

Most of the literature focuses on how to implement different techniques using mathematical modeling through MATLAB SIMULINK and implement it into a microcontroller. However, a few authors had tried to implement the algorithms in an FPGA. Moreover, all the previous studies did not discuss the error analysis of the hybrid speed observer in which the rotor speed and positions can be determine from the Hall effect sensors' signals.

1.4. THESIS OUTLINE

This section deals with general introduction for the HEV and the importance of the PMSM in the implementation also brief detail of the existing observation and estimation of the rotor speed and angle and how these techniques can help on the control of the motor.

Section 2 describes the control board implementation and the electronic related circuits design configurations and calculations.

Section 3 provides an introduction to the Pulse Width Modulator and different approaches of PWM signal generation by using the FPGA or Microcontroller.

Section 4 describes the Hybrid Speed Observer technique for detecting the rotor speed and position using the Hall effect signals and the physical implementation in the FPGA using the Quartus II software and the error analysis.

Section 5 presents the system validations after the implementation in the FPGA and connecting the board to the PMSM. The results are presented in this section to show the possibility of substituting the Microcontroller with an FPGA or sharing the operations.

Section 6 presents the conclusions. Design problems and recommendations for future research are also discussed in this chapter.

2. SIGNAL PROCESSING AND CONTROL BOARD

2.1. INTRODUCTION

The control board consists of 15 different circuit blocks. Each block has been developed and simulated using SIMULINK or PLECS before the physical implementation to ensure desired results. Numerical calculations were used to determine the right values for the components. All components were chosen based on cost, efficiency, and minimum losses. This section of the thesis will explain the purpose of each circuit associated with a step by step design calculation and circuit configuration.

2.2. SIGNAL CONDITIONING CIRCUIT

Most of the digital devices are compatible with an interface of 0-3V as standard I/O. Both the DSP and the FPGA in this design are compatible with 0V as the OFF state and +3.3V as the ON state. On the other hand, analog signals that need to be processed can be at any range. In this specific design, the analog signal from current sensors (LA 100-p) is $\pm 10V$. An operational amplifier (Op-Amp) TLE-2082 from Texas Instruments (TI) will be used to offer the desired gain and offset. The signals are scaled from $\pm 10V$ to 0-3V in order to be compatible with DSP and The FPGA. Figure 2.1 illustrates the circuit diagram of non-inverting gain offset amplifier. The value of the resistors R_1 , R_2 , and R_3 can be determined by the following equations [14], and Table 2.1 illustrates the amplifier desired parameter to achieve the targeted voltage scale while Table 2.2 showing the selected value of these resistors.

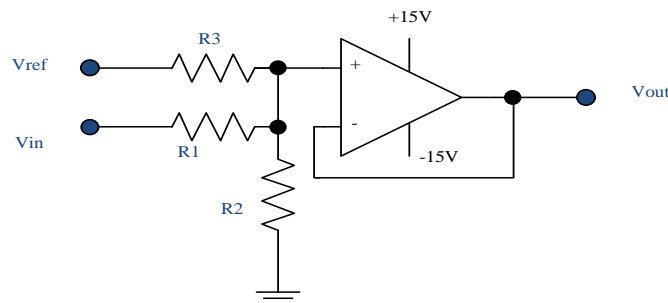


Figure 2.1. Gains and Offset Circuit.

Table 2.1. Maximum and Minimum Voltage Range.

V _{out,min}	0V
V _{out,max}	3V
V _{in,min}	-10V
V _{in,max}	+10V
V _{ref}	+10V
m	0.15
b	1.5

$$V_{out} = m \times V_{in} + b \quad (3)$$

$$m = \frac{\frac{1}{R_1}}{\frac{1}{R_1} + \frac{1}{R_2} + \frac{1}{R_3}} \quad (4)$$

$$b = V_{ref} \times \frac{\frac{1}{R_3}}{\frac{1}{R_1} + \frac{1}{R_2} + \frac{1}{R_3}} \quad (5)$$

Table 2.2. The Resistor Values for Fig. 2.1.

R ₁	49.9 kΩ
R ₂	10.7 kΩ
R ₃	49.9 kΩ

2.3. FILTER CIRCUIT

Filter circuits usually are crucial and require precision. The Sallen Key filter is very popular active filter topology. It is used to implement second order filters or higher with different gain factor, high-quality factor, and simple configuration for the second-order type and can be constructed with following equations from [15, 16]. Figure 2.2 [16] illustrates the generic Sallen Key filter configuration.

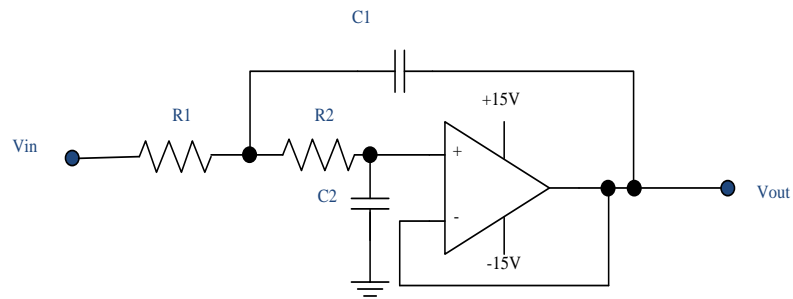


Figure 2.2. Generic Sallen Key Filter Topology.

The cutoff frequency f_c and the quality factor Q are

$$f_c = \frac{1}{2\pi\sqrt{R_1 C_1 R_2 C_2}} \quad (6)$$

$$Q = \frac{\sqrt{R_1 R_2 C_1 C_2}}{C_2 (R_1 + R_2)} \quad (7)$$

For simplicity of the design, a good assumption is to equalize all the resistors.

$$R_1 = R_2 = R \quad (8)$$

This assumption simplifies the equations of the quality factor and the cutoff frequency as follows.

$$Q = \frac{\sqrt{C_1 C_2}}{2C_2} = \frac{1}{2} \sqrt{\frac{C_1}{C_2}} \quad (9)$$

$$f_c = \frac{1}{2\pi R \sqrt{C_1 C_2}} \quad (10)$$

$$C_1 = \frac{2Q}{R\omega_0} \quad (11)$$

$$C_2 = \frac{1}{2RQ\omega_0} \quad (12)$$

In this design, the desired cutoff frequency is $f_c = 3$ KHz and quality factor is $Q = 0.6$ for a better response. After using equations (9), (10), (11), and (12) the values of the design are shown in Table 2.3.

Table 2.3. Capacitor and Resistor Values.

C_1	142pF
C_2	100pF
R	2.2k Ω

2.4. LEVEL SHIFTERS

The microcontroller and FPGA outputs are limited to +3.3V logic signal while the inverter module needs about +15V to turn the gate of the insulated gate bipolar transistors

(IGBTs) on and also the fault signals that need to be interfaced to the DSP or FPGA are +15V. A logic level shifting circuit is needed therefore; the CD4504B voltage level-shifter from Texas Instruments consists of six circuits, which shift the input signals from the V_{CC} logic level to the V_{DD} logic level. For example, to shift from TTL logic signals to CMOS logic scale, the SELECT pin-13 input is at the V_{CC} high logic state. And when the SELECT pin is at low logic state “GND”, each circuit translates the signals from one CMOS to another [17]. Figure 2.3 [17] illustrates the internal block diagram and the pin out for CD4504B.

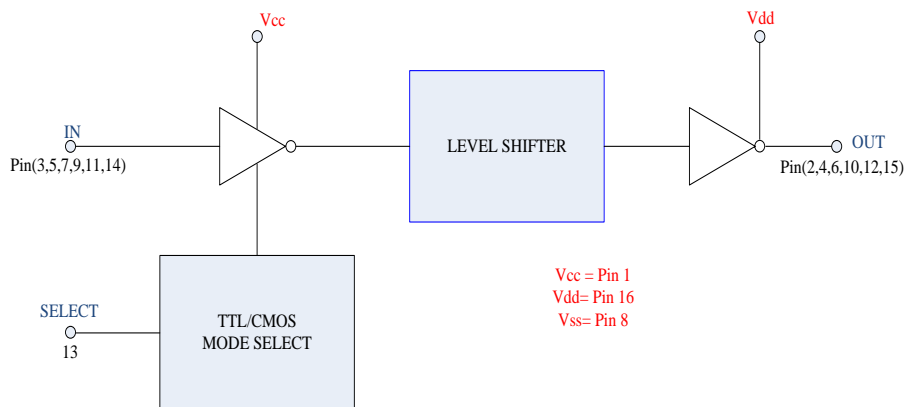


Figure 2.3. CMOS Hex Voltage –Level Shifter.

2.5. ANALOG TO DIGITAL CONVERTERS

The outputs of the current, voltage, and temperature sensors are analog. In order to process these signals by using DSP, analog to digital converters are needed. Eight AD7276 12-bit, high speed, and low power ADCs from Analog Devices are used to convert the sensors' analog signals to digital signals in order to interface it to the DSP or the FPGA [19]. Figure 2.4 [18] shows the block diagram of AD7276. Another serial analog to digital converter AD7329 has been added to the design because of extra

flexibility to process $\pm 10V$ analog signals without any signal conditioning. Figure 2.5 [19] shows the block diagram of the 8-channel AD7329 serial ADC.

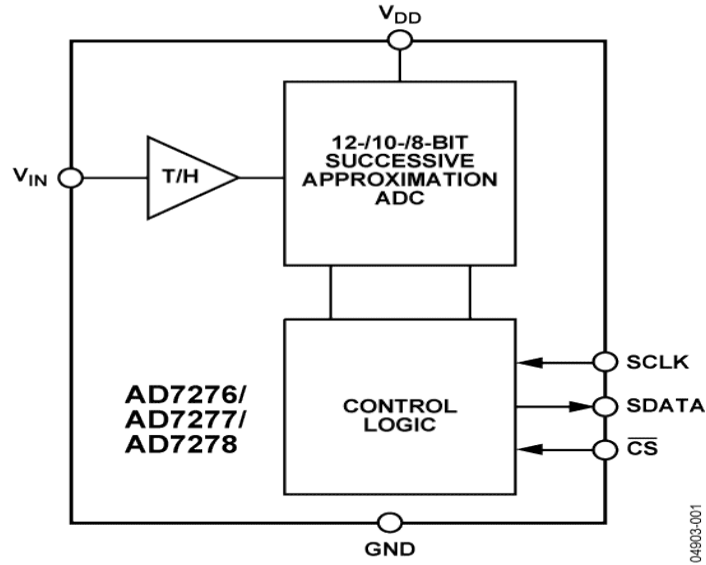


Figure 2.4. AD7276 Block Diagram [18].

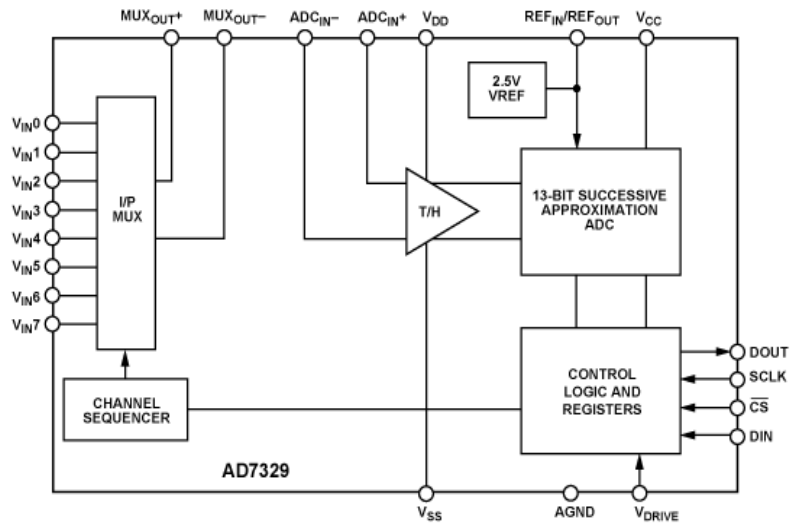


Figure 2.5. AD7329 Block Diagram [19].

2.6. ISOLATOR CIRCUIT

Isolator circuits are usually used when a certain signal needs to be transferred from one circuit to another without any direct coupling, because these circuits may operate at different voltage levels. This technique is used to decouple the board and the Computer Automotive Network (CAN) a bus signal, ADUM1412 quad-channel digital isolator from Analog Devices is used for this purpose. Figure 2.6 displays the block diagram and the pin out of the ADUM1412.

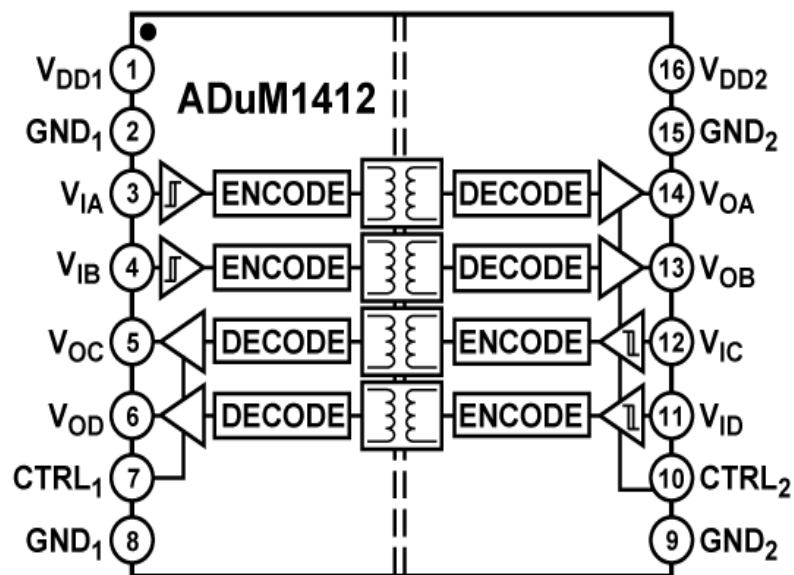


Figure 2.6. ADUM1412 Block Diagram [20].

2.7. CAN TRANSCEIVER CIRCUIT

A controller area network (CAN) transceiver circuit is used to communicate between the board and the CAN controller through a CAN bus. It is useful to send or receive CAN messages to the control board such as the dc bus voltage, the current at any phase, or any other signal condition. Figure 2.7 [21] illustrates the pin out and the functional diagram of 65HVD251 CAN transceiver from TI.

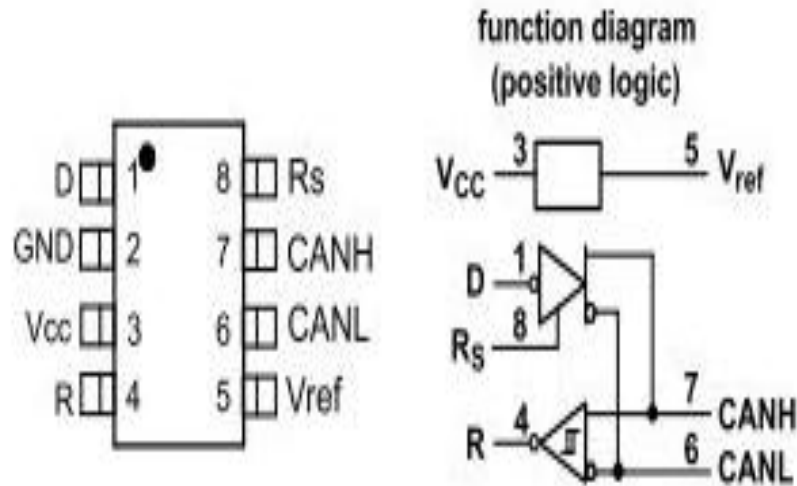


Figure 2.7. 65HVD251Funcional Diagram [21].

2.8. DIFFERENTIAL INPUT CIRCUIT

A differential amplifier amplifies the difference between two voltages and rejects the average or common mode value of these voltages. Figure 2.8 shows the differential amplifier configuration. The equation for this type of amplifier is presented in [22].

$$V_{\text{out}} = V_2 \left(\frac{(R_3 + R_1)R_4}{(R_4 + R_2)R_1} \right) - V_1 \left(\frac{R_3}{R_1} \right) \quad (13)$$

If $R_1=R_2$ and $R_3=R_4$ then

$$V_{\text{out}} = \left(\frac{R_3}{R_1} \right) (V_2 - V_1) \quad (14)$$

The simple case is used to obtain a unity gain, when

$$R_1 = R_2 = R_3 = R_4 = 10K\Omega \quad (15)$$

Then,

$$V_{\text{out}} = (V_2 - V_1) \quad (16)$$

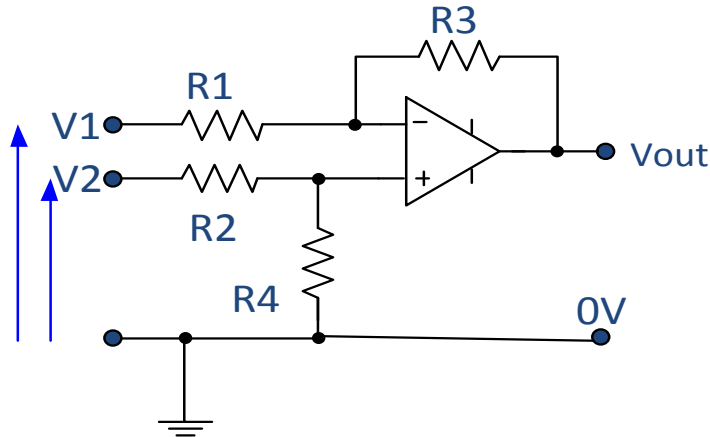


Figure 2.8. Differential Amplifier Circuit.

2.9. DSP CIRCUIT

The Digital Signal Processor is chosen to be TI (TMS320F28335) [23], recommended by TI for motor control applications. The computing unit of this DSP consists of a 32-bit CPU and a single precision 32-bit floating-point unit (FPU), which enables the floating-point operations to be accomplished in hardware. The CPU has 8-channels, which allows the CPU to execute 8 different instructions simultaneously in one clock cycle. The DSP has a system clock of 150MHz generated by an on-chip oscillator and Phase Locked Loop (PLL). The oscillator generates only 50MHz clock that is tripled by the PLL to achieve 150MHz. The DSP also has a physical memory of 34K x 16 single-access random-access memory (SARAM), 8K x 16 read-only memory (ROM), a 1K x 16 one-time programmable memory (OTP) and registers. The DSP has a capability of five types of an interface: serial communication interface (SCI), controller area

network (CAN), inter-integrated circuit (I2C), serial peripheral interface (SPI), and multichannel buffered serial port (McBSP). This allows flexibility in the interfacing between the DSP to any other devices such as motors or communication peripherals. The DSP board also allows for JTAG interface to program the DSP chip.

Figure 2.9 shows, the TMS320F28335 DSP and its control dock. TI offers a friendly user interface Code Composer V4.0 (CCV4.0) to program this type of the microcontroller.

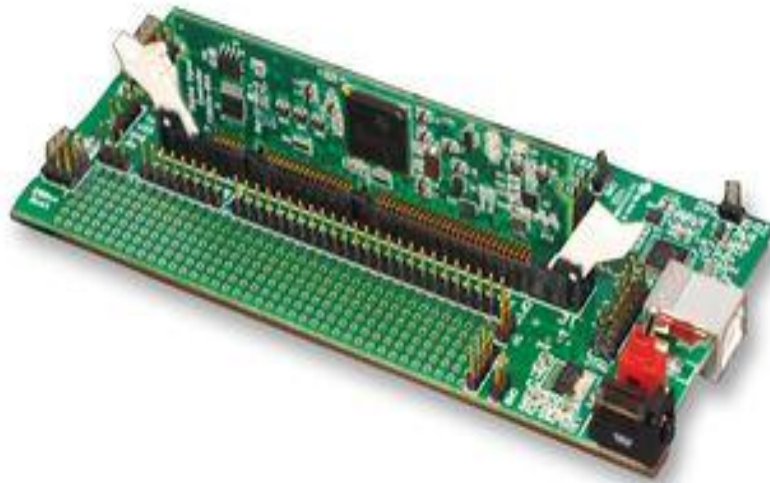


Figure 2.9. TMS320F28335.

2.10. FPGA CIRCUIT

The FPGA is an integrated circuit that contains many duplicate logic cells that can be seen as standard components. Each logic cell can individually take on any one of a limited set of personalities. The individual cells are interrelated by a matrix of wires and programmable switches as it shown in Figure 2.10.

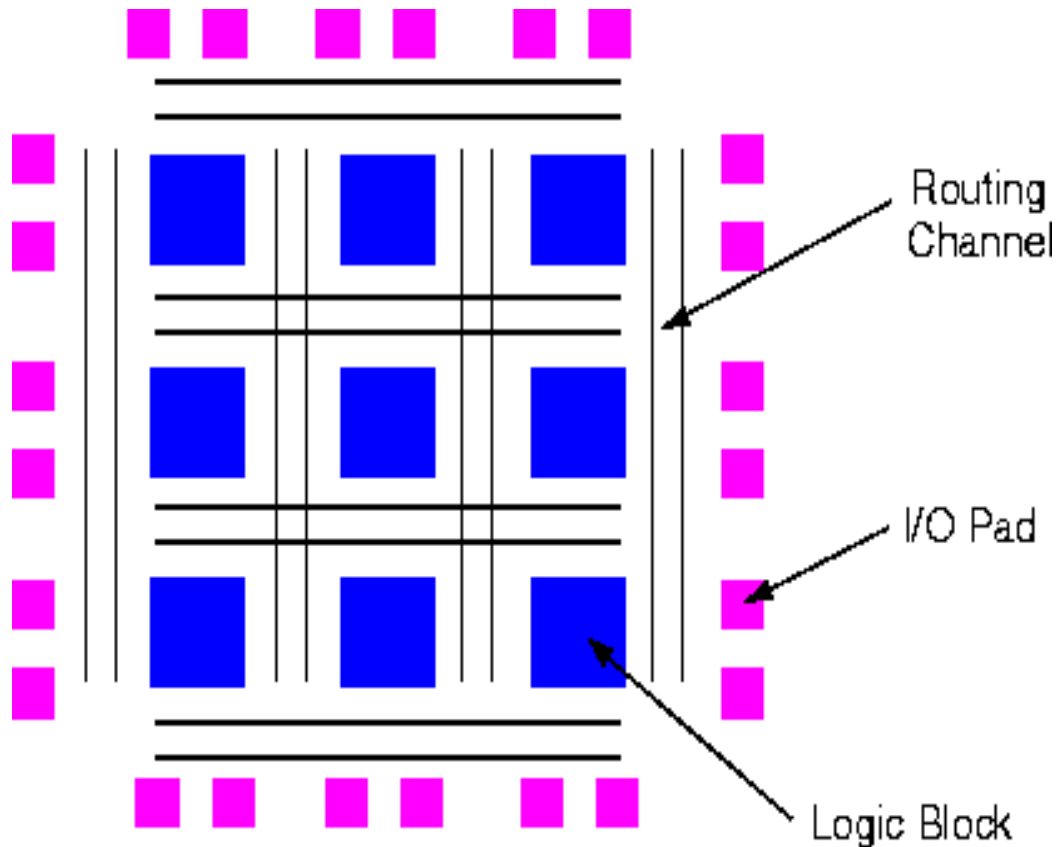


Figure 2.10. Structure of the FPGA.

A user's design can be implemented by specifying the simple logic function for each cell and selectively closing the switches in the interconnection matrix. The array of logic cells and interconnects form a fabric of basic building blocks for logic circuits. Complex designs are created by combining these basic. The FPGA's functions are defined by a user's program rather than by the manufacturer of the device.

A typical integrated circuit performs a particular function defined at the time of manufacture. In contrast, the FPGA's function is defined by a program written by someone other than the device manufacturer. Depending on the particular device, the program is either burned in permanently or semi-permanently as part of a board assembly process, or is loaded from an external memory each time the device is powered up.

Figure 2.11 illustrates a typical flow chart for Altera's FPGA design process, which has been used in this design.

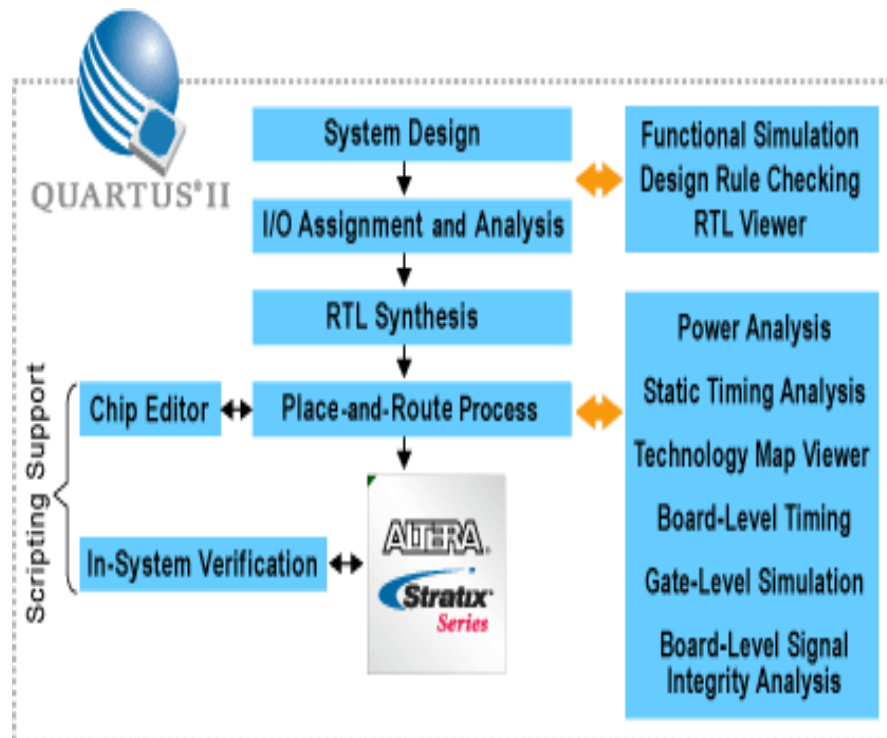


Figure 2.11. Altera Design Flow Chart [24].

This programmability gives the user access to complex integrated designs without the high engineering costs associated with application specific integrated circuits.

2.11. POWER SUPPLY BOARD

The power supply is designed in a different printed board (PCB0025) and attached to the main board through male and female six position power terminals (PES type and PET type) from SAMTEC Inc. as shown in Figure 2.12 [25], respectively.

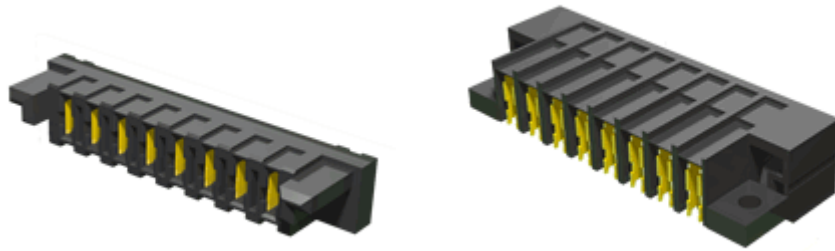


Figure 2.12. PES and PET Type Connectors [25].

Power modules are used in order to generate seven different voltages as in Table 2.4. Figure 2.13 shows PCB0025 and the next table shows the voltages and the corresponding parts. The board layout and schematic are attached in appendix A.



Figure 2.13. PCB0025.

Table 2.4. Power Modules and Corresponding Voltages.

Voltage	Power Module
+1.2V	PTH04000W
+3.3V	PTH04000W
+3.3V ANA	TPS79333DBV
+5.0V	PTN78060W
+5.0V ISO.	TMH2405S
+15.0V	PTN78060H
-15.0V	PTN78000A

2.12. PULL-UP RESISTOR CIRCUIT

Pull-up resistors are used for the open collector encoder in order to read the Hall effect signals. The configuration of this circuit is shown in Figure 2.14.

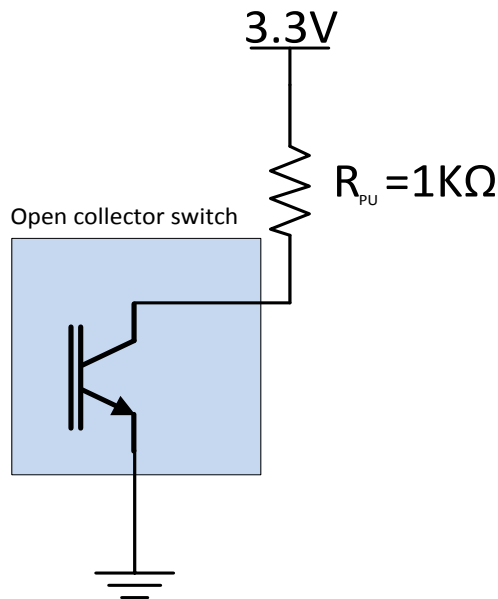


Figure 2.14. Pull-up Resistor for Open Collector Configuration.

2.13. ERRATA

After testing the board, there were some errors, defects, and considerations for new version of the board.

- The gate signal socket package was inverted in eagle. It has been corrected in the Lib_DOE_transportation_electrification.lbr in the server.
- The DSP package needs to be implemented in the Board as one unit to minimize the electromagnetic interference (EMI).
- R₂₅ has been changed to 2.2k Ω .
- R₆₅ and R₆₆ values need to be swapped.
- U₃₆ pin 2 and 3 need to be swapped.
- U₄₁ pin 1 should be connected to +5V (board defect). Pull-up resistors of 1k Ω need to be added to the Hall effect signals input terminal J₂₁.
- Ground terminal needs to be added to J₂₁.
- GPIO34 and GPIO 28 need to be swapped.
- In PCB0025, pin 1 at U₁ and U₄ needs to be connected to the ground.

3. PULSE WIDTH MODULATOR

3.1. INTRODUCTION

Pulse Width Modulation (PWM) is a technique for controlling analog devices with digital signal format. This signal can be generated using a simple analog circuit or a Microcontroller Unit (MCU). This technique is widely used in communication and power electronics circuits for control purposes such as controlling the motor speed, by increasing or decreasing the duty cycle of this digital signal. The traditional way to generate a PWM signal is to compare an analog or dc signal as reference to a carrier signal. Usually, the carrier signal is a triangular or a sawtooth signal. Figure 3.1 illustrates the PWM block diagram.

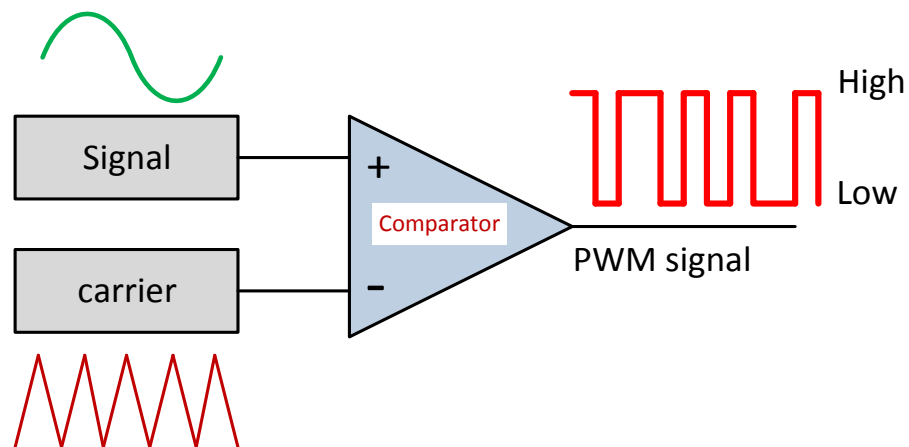


Figure 3.1. PWM Block Diagram.

3.2. DIGITAL PWM GENERATION TYPES

The PWM signals can be generated digitally inside the MCU or FPGA by substituting the carrier signal with a counter. The counter determines when to turn the

PWM signal ON or OFF based on a certain value or reference signal. The counter can be used at any of the following modes:

- Up Mode Counter.
- Down Mode Counter.
- Up/Down Mode Counter. This results in center-aligned PWM.

3.2.1. Up-Mode Counter. In this mode, the counter starts from zero and increments until it reach the desired final value. When the counts reach the maximum, the program will reset the counter to zero and repeat the same procedure again. Figure 3.2 illustrates the up mode counter.

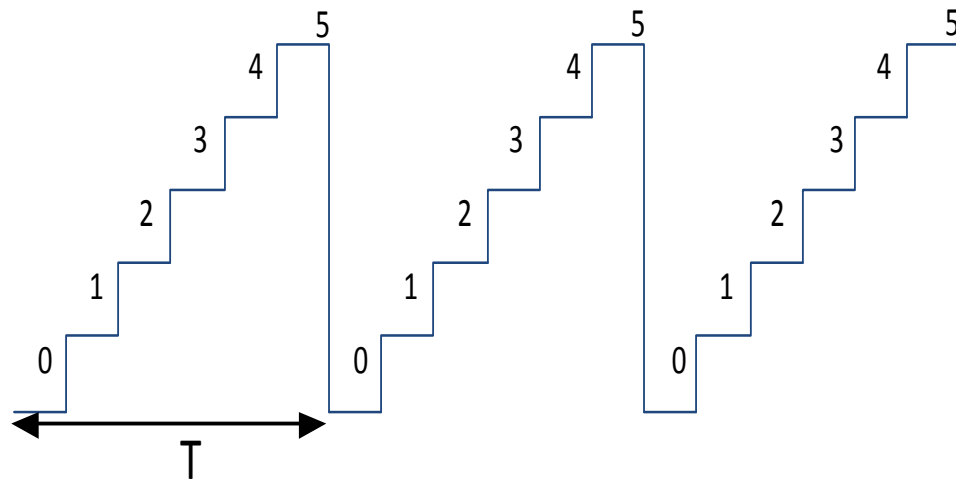


Figure 3.2. Up Mode Counter.

3.2.2. Down-Mode Counter. In this mode, the counter will start to count from the maximum value and decrements until it reaches zero. When it reaches the zero, the counter will be reset to the maximum value and repeats the pattern. Figure 3.3 illustrates the down mode counter.

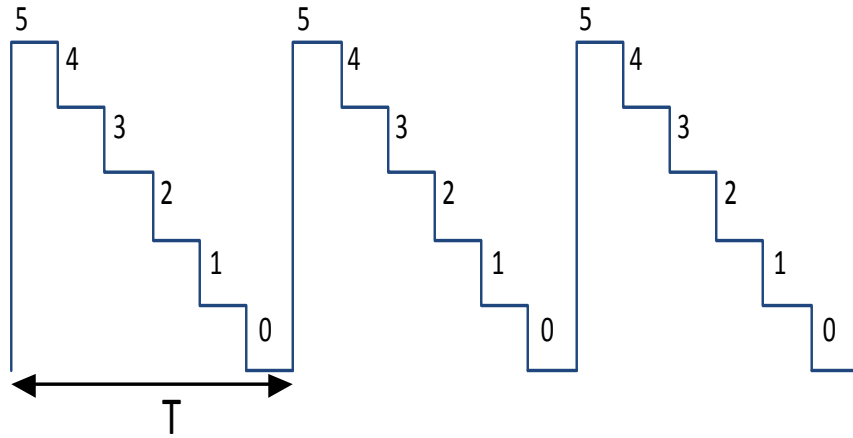


Figure 3.3. Down Mode Counter.

3.2.3. Up-Down Mode Counter. In this mode, the counter will start counting from zero and increments until it reaches the maximum value, then it will start to decrements until it reaches the zero value and keeps repeating the pattern. Figure 3.4 illustrate the Up-Down counter.

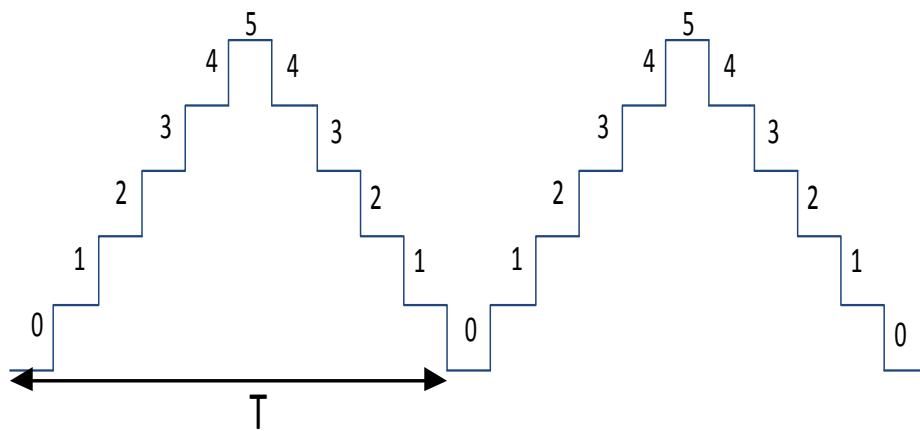


Figure 3.4. Up-Down Mode Counter.

3.2.4. PWM with Dead-Band. In power control applications, it is necessary to have complementary PWM signals with a dead time between them in order to control individual power switches such as MOSFETs or IGBTs or modules like Inverters. Two extra counters are used to create the dead-band. The first counter is the Rising Edge counter (Red_Count), and the second counter is the Falling Edge counter (Fed_Count). These counters create the signal delay in both edges of the PWM signal. Figure 3.5 shows the main Up/Down mode counter and other two up counters representing the Rising and the Falling edges counters. RED and FED are the reference values for rising edge counter and falling edge counter respectively, and they determine the time delays in both edges. The desired duty ratio (D) is used to set and reset the Up-Down mode counter and produce the ON time of the PWM signal.

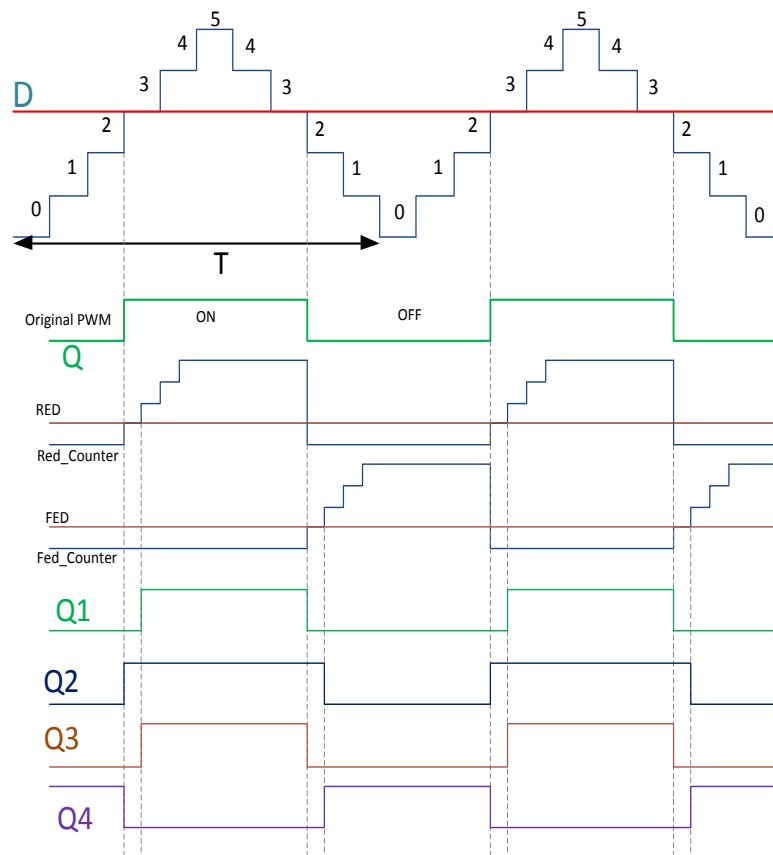


Figure 3.5. Signals of Interest.

Figure 3.6 illustrates the schematic diagram of the up-down counter PWM that has been implemented using Altera's Quartus II software. The block diagram composed of five main blocks and an OR gate.

The first block is the phase locked loop (PLL). The PLL has one input pin (CLKIN) and two output pins: clock out and LOCKED, a flag indicating that the PLL has locked to the input. The clock pin is used as clock reference to all blocks while the locked pin is used to synchronize all blocks in the design. This block is triggered by an external crystal oscillator (24 MHz) on the module and connected to PLL through pin A12. This PLL can either increase the frequency in this module up to 48 MHz or decrease it down to 2.4 MHz in this particular module, in this experiment the clock is chosen to be 24 MHz.

The second block is the PWM constants. This block has no inputs and provides five constants with different word lengths. The constants are iRed (3 bits), iFed, iPulseWidth (3 bits), iD (12 bits), and iClkdiv (3 bits). The iRed and iFed is used to configure the delay in the rising edge and the falling edge respectively. The iPulseWidth is used to configure the start pulse width in the next block. The iD can be connected to the PWM block as known data for testing purposes while iClkdiv is connected to ADC block as clock divider signal in order to slow down the clock inside the block.

The third block generates a start pulse. This block has three inputs and only one output. The inputs are the clock and locked signals from PLL in block one and the iPulseWidth signal from the second block. The output is a single pulse used to trigger the ADC block for the first time through an OR gate. The iPulseWidth signal determines the length of the start pulse.

The fourth block is the ADC block. This block has five inputs and four outputs. The inputs are iClk, iStart, iClkdiv, iReset, and iSDO (12 bits). The block starts running as soon as it receives the iStart pulse from the previous block. This block is a software written in VHDL for AD7276 [18] to read the serial digital data output through the iSDO input from the external chip and process it and generate the four output signals which are the output value (oValOut, 12 bits), serial clock (oSCK), chip select (oLD), and the done pulse (oDone).

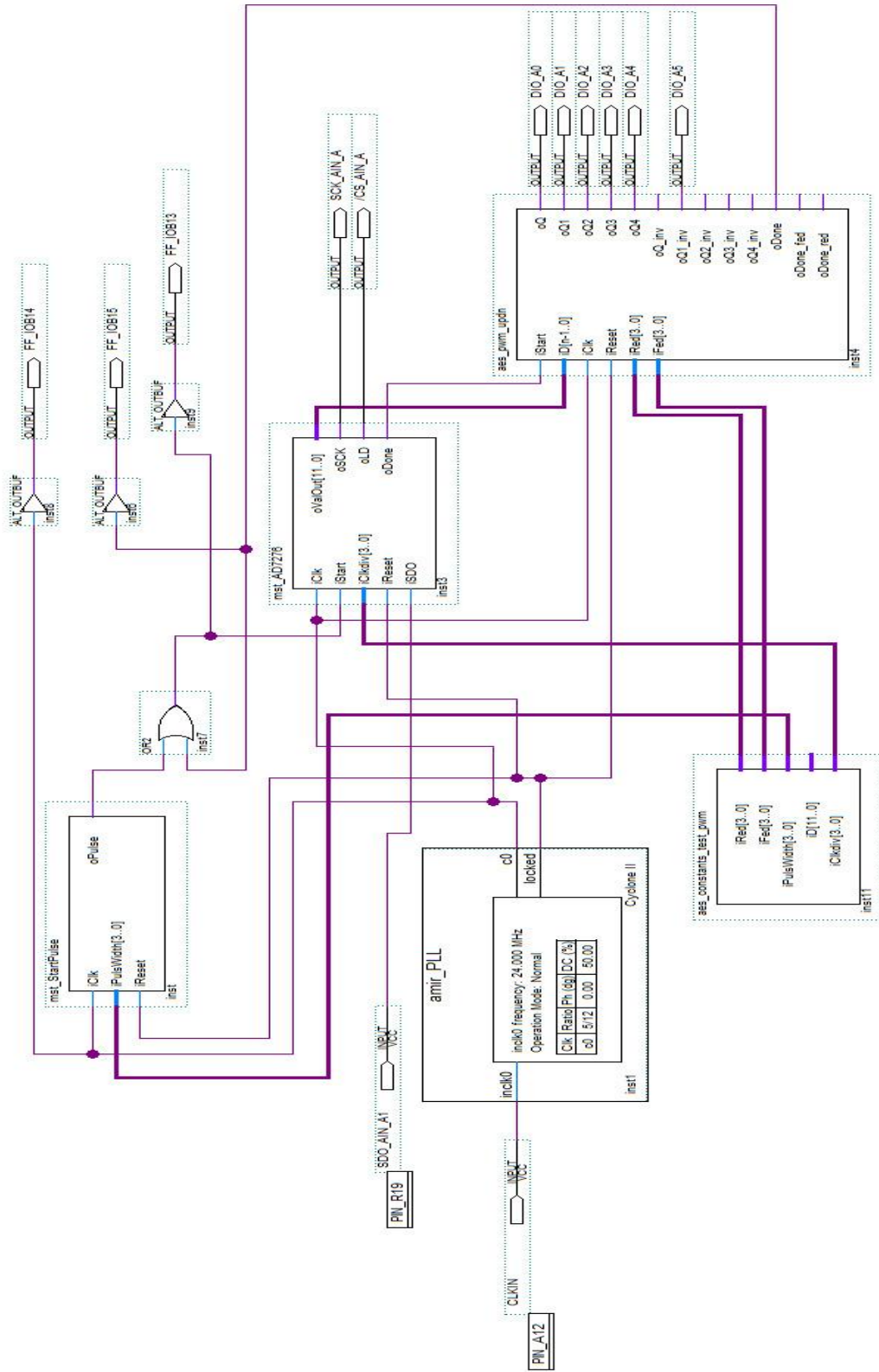


Figure 3.6. PWM Schematic Diagram.

The last one is the main block which the PWM block. This block has six inputs which are iStart, iD, iReset, iRed, and iFed. Also, it has thirteen outputs: oQ through oQ4, oQ_inv through oQ4_inv, oDone, oDone_red, and oDone_fed. The oQx signals are as shown in Figure 3.5 (with or without inversion). The oDone signals indicate that the cycle is complete and the next cycle can begin.

The signal flow through these blocks starts with the clock generated from the PLL to start pulse. The start pulse block generate a single pulse to trigger the ADC block at (iStart) input to start read the input digital signal oSDO from the real chip. When this block finishes its process, it generates the serial clock (oSCK), chip select (oLD), output value (oValOut), and (oDone) which is used to trigger the next block (PWM) at the (iStart) input to receive the (oValOut) from the ADC through (iD) serial input data terminal. The PWM block process that data and generate the desired duty ratio. Also, it uses the constants (iRed) and (iFed) to determine the delay in the rising and falling edges. After the block finishes the process the generated done pulse is rerouted to the OR gate so that the process runs continuously.

4. PMSM ROTOR POSITION MEASUREMENT

4.1. INTRODUCTION

PMSM control requires the continuous sensing of the rotor position and speed in order to apply the control algorithms. There are four common methods for measuring the PMSM rotor position [26].

4.1.1. Optical Encoder. It is the most popular type, which consists of a rotating disk, a light source, and a photo detector. The disk, which mounted on the drive shaft of the motor, has coded patterns of opaque and transparent sectors. When the shaft is rotated, eventually it will rotate the disk and these patterns will interrupt the light emitted onto the photo-detector and generating a pulse signal output that can determine the rotor position and the speed. Figure 4.1 [20] displays the optical encoder.

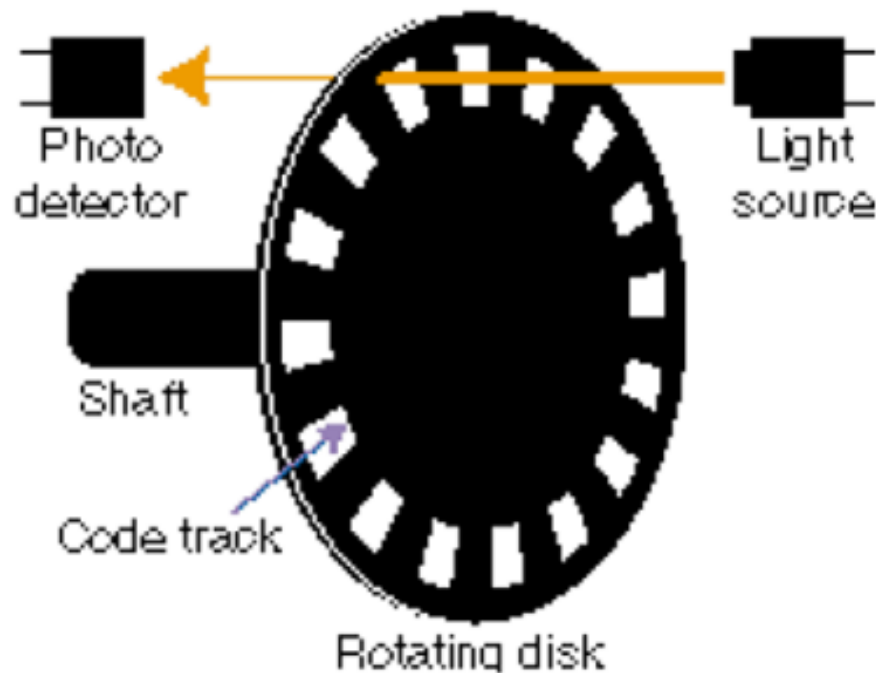


Figure 4.1. Optical Encoder [20].

4.1.2. Resolver. The common type is the Transmitter Resolver; it looks like a small electric motor with a stator and a rotor. The stator consists of three winding configurations: an exciter and a two two-phase winding (X and Y), in which there is 90° phase shift. The output of the Resolver is sine and cosine of an angle θ that corresponds to the shaft position and direction [27]. Figure 4.2 [28] shows the resolver schematic.

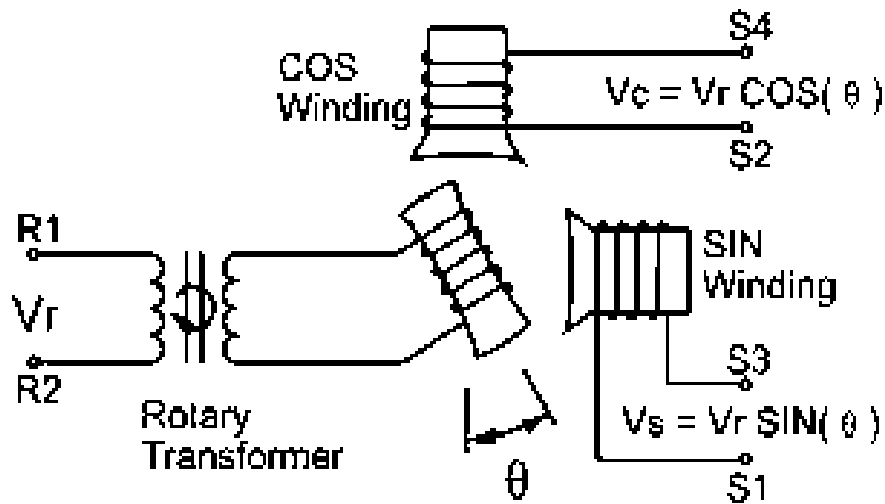


Figure 4.2. Resolver Schematic [28].

4.1.3. Full Observer. The Full Observer uses the characteristics of the Back Electromotive Force and the voltage generated on the windings due to the BEMF. The polarity of the current induced in the winding due to the BEMF is determined by the motor rotating direction. The amplitude of the induced current is proportional to the speed of the rotors. Many manufacturers have implemented this type of observer into electronic chips.

Figure 4.3 illustrates a diagram of a commonly used Full Observer that uses the current i , and voltage v , as references through a Proportional Integral (PI) controller

associated with State Space Matrix analysis in order produce an observed current \hat{i} and voltage \hat{v} to detect the error [29, 30].

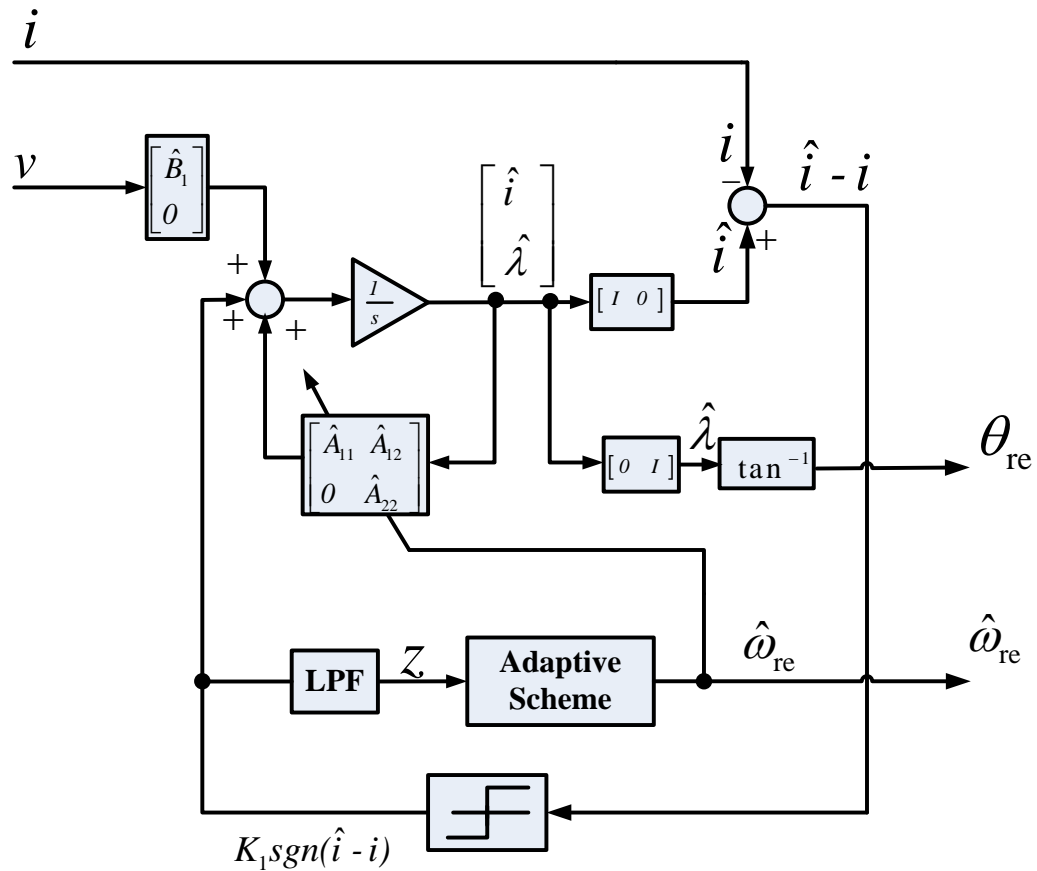


Figure 4.3. Full Adaptive Observer [29].

4.1.4. Hall Effect Sensors. The theory behind this type of sensors is that when a conductor that carrying current is placed into a magnetic field, a voltage will be generated due to the effect of the magnetic field and the direction of that voltage is perpendicular to the current [31]. These sensors are inexpensive, small, and have low resolution. Figure

4.4 shows 2-pole 3-phase PMSM and three Hall effect sensors accompanied by their 120° shifted signals.

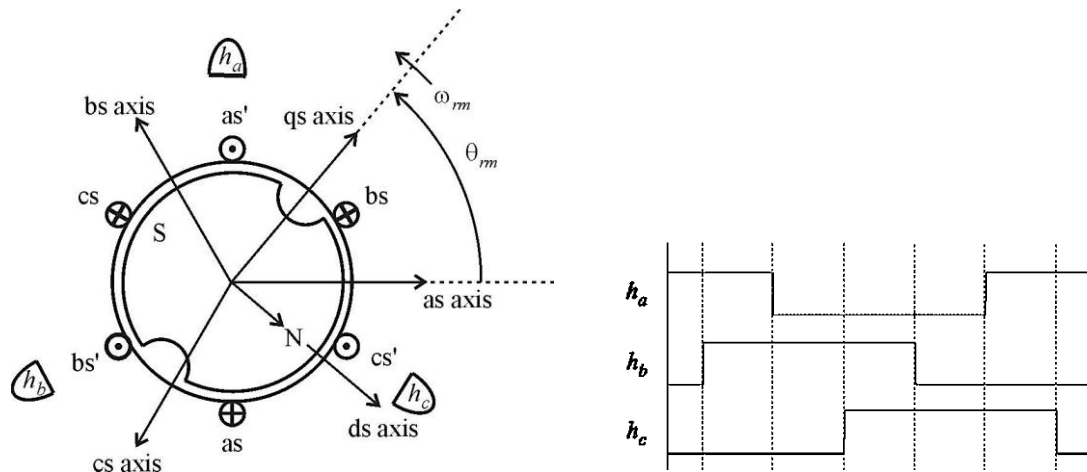


Figure 4.4. Three Hall Effect Sensors and Their Related Signals [26].

4.2. HYBRID SPEED OBSERVER

It is very common in the Brushless dc motor (BLDC) does not have a resolver or optical encoder for couple reasons. One reason is to minimize the motor price and size. Another reason is to offer the flexibility of coupling. The PMSM has different parameters and characteristics and to control two motors will require some sort of harmony. Thus, it will be easier to eliminate the mechanical detection parts.

The Hall effect sensors discussed in section 4.1.4 are a successful solution for sensorless problem due to their low-cost and light weight. Hybrid Observer [32], uses the Hall effect sensors to estimate the rotor position and speed, with accuracy and low cost. The setup in Figure 4.5 illustrates an example of a high-performance BLDC. The system also includes the inverter, observer, speed control and delta-modulated current control [32].

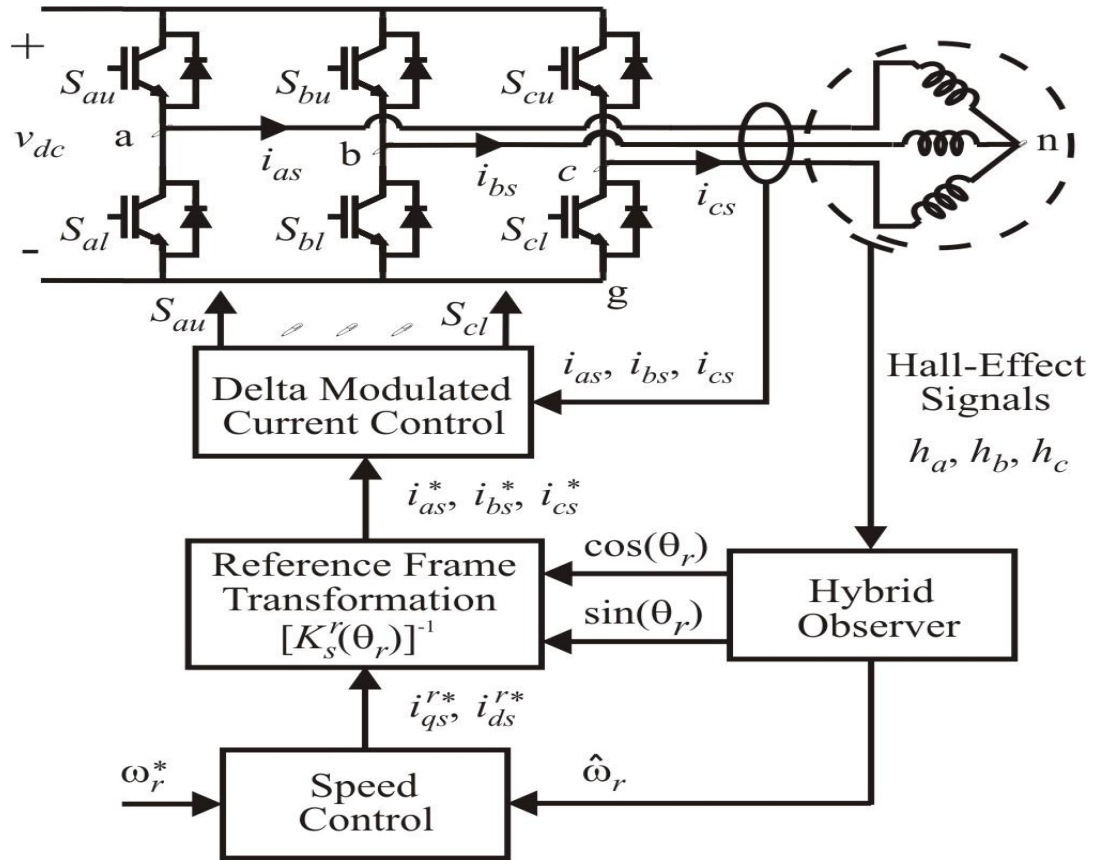


Figure 4.5. High-Performance BLDC [32].

The hybrid observer can be represented by the following differential equation.

$$\frac{d}{dt} \begin{bmatrix} \cos(\theta_{th}) \\ \sin(\theta_{th}) \end{bmatrix} = \begin{bmatrix} 0 & -\omega_r \\ \omega_r & 0 \end{bmatrix} \begin{bmatrix} \cos(\theta_{th}) \\ \sin(\theta_{th}) \end{bmatrix} \quad (17)$$

If the initial position and the electrical speed are known and equation (17) has a solution with no error, the sine and cosine of the rotor relevant to the Hall effect sensors, then $\sin(\theta_{th})$ and $\cos(\theta_{th})$ could be determined using trigonometric identities. Table 4.1 and Figure 5.2 shows the bounding which are maximum and minimum values of $\sin(\theta_{th})$ and $\cos(\theta_{th})$ for the current Hall effect sensor states (h_a, h_b, h_c).

Table 4.1. Bounding Functions vs. Hall States [32].

Hall State			Bounding Functions			
h_a	h_b	h_c	$\max\sin(\theta_h)$	$\min\sin(\theta_h)$	$\max\cos(\theta_h)$	$\min\cos(\theta_h)$
0	0	1	-1/2	-1	0	$-\sqrt{3}/2$
0	1	0	1	1/2	0	$-\sqrt{3}/2$
0	1	1	1/2	-1/2	$-\sqrt{3}/2$	-1
1	0	0	1/2	-1/2	1	$\sqrt{3}/2$
1	0	1	-1/2	-1	$\sqrt{3}/2$	0
1	1	0	1	1/2	$\sqrt{3}/2$	0

The values $\sin(\theta_m)$ and $\cos(\theta_m)$ can be found based on the state transition points.

Table 4.2 shows these values based on the signal states.

Table 4.2. State Transition Points [32].

Sensor Transition	h_a	h_b	h_c	$\sin(\theta_m)$	$\cos(\theta_m)$
h_a	x	0	1	-1	0
h_a	x	1	0	1	0
h_b	0	x	1	-1/2	$-\sqrt{3}/2$
h_b	1	x	0	1/2	$\sqrt{3}/2$
h_c	0	1	x	1/2	$-\sqrt{3}/2$
h_c	1	0	x	-1/2	
x= don't care					

Figure 4.6 illustrates how the sine and cosine the angle could be estimated based on known initial conditions and the bounding conditions of that angle. It also shows the three different three Hall effect signals are shifted by 120°. At any transition point, the rotor speed can be estimated based on the time between the transition occurrences,

$$\hat{\omega}_r = \frac{\Delta\theta_{rh}}{\Delta t} \quad (18)$$

The final calculations to implement the hybrid observer to determine the sine and cosine of the electrical rotor position are

$$\theta_r = \theta_{rh} + \phi_h \quad (19)$$

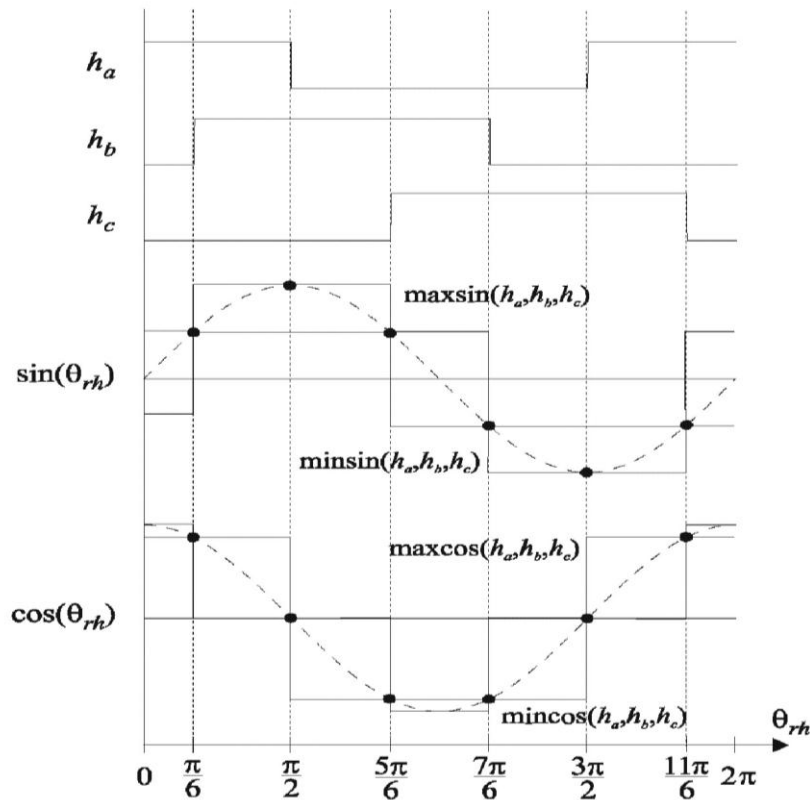


Figure 4.6. Hybrid Observer Bounding Functions [26].

$$\sin(\theta_r) = \sin(\theta_{rh}) \cos(\phi_h) + \cos(\theta_{rh}) \sin(\phi_h) \quad (20)$$

$$\cos(\theta_r) = \cos(\theta_{rh}) \cos(\phi_h) - \sin(\theta_{rh}) \sin(\phi_h) \quad (21)$$

The estimated values of $\sin(\theta_{rh})$ and $\cos(\theta_{rh})$ are

$$\sin(\theta_r) = s_{\theta h} \cos(\phi_h) + c_{\theta h} \sin(\phi_h) \quad (22)$$

$$\cos(\theta_r) = c_{\theta h} \cos(\phi_h) - s_{\theta h} \sin(\phi_h) \quad (23)$$

To determine the initial condition for the rotor, the speed is assumed to be zero. Then $s_{\theta h}$ and $c_{\theta h}$ can be determined from the initial readings of the Hall effect sensor. Table 4.3 gives these initial conditions. Figure 4.7 illustrates the block diagram of the hybrid observer.

Table 4.3. Initial Conditions [32].

Initial Hall State			Initial Conditions		
h_a	h_c	h_c	θ_h	$s_{\theta h}$	$c_{\theta h}$
0	0	1	$4\pi/3$	$-\sqrt{3}/2$	-1/2
0	1	0	$2\pi/3$	$\sqrt{3}/2$	-1/2
0	1	1	π	0	-1
1	0	0	0	0	1
1	0	1	$5\pi/3$	$-\sqrt{3}/2$	1/2
1	1	0	$\pi/3$	$\sqrt{3}/2$	1/2

All the above equations, initial conditions table, and the transitional table have been converted into VHDL language in appendix B to estimate the rotor speed and position. Some of these parameters are treated as signals type while the other signals treated as variables. A fixed point package [33] is used to add more precision to the inputs and the estimated outputs. The integration operations are replaced by accumulated addition operations to estimate the sine and cosine of the electrical angle. The Hall effect signals have six possible transitions per period. Each transition is used to trigger a counter to start counting at each transition state and reset itself at the next transition state. The local estimated rotor speed (IWr) is equal to the length of the period ($2\pi/6$) divided by the time between any two (T_1, T_2, T_3) transitions which is equal to the counter value ($ICount$) multiplied by the sampling frequency (T_s) in 34 bits precision. The final value of the rotor speed has only 12 bit precision due to the lack of precision on the digital to analog converter (DAC). The error that occurs due to the change of the precision on the fraction part of the (IWr) is reported and analyzed in chapter five.

Also, the program can estimate the rotor position at any time based on the initial and the bounding conditions that has been translated into VHDL statements. When the program starts it looks at initial conditions first and estimates the sine and cosine of θ_r and store those values. The sine and cosine θ_r can be calculated from equations (20) and (21) respectively.

The new sine and cosine values can be estimated by integrating the equations. This integration can be replaced by accumulated addition operation as follows,

$$\text{Sin}(\theta_{r,\text{new}}) = \text{Cos}(\theta_{r,\text{int}}) - \omega_r \times \text{Sin}(\theta_{r,\text{int}}) \times T_s \quad (24)$$

$$\text{Cos}(\theta_{r,\text{new}}) = \text{Sin}(\theta_{r,\text{int}}) + \omega_r \times \text{Cos}(\theta_{r,\text{int}}) \times T_s \quad (25)$$

On the next clock cycle the program will load the new Hall effect states and the new values of sine and cosine θ_r will become initial values for the next clock cycle. The

program will also check the bounding conditions in Table 4.1 in order not to exceed the maximum or goes below the maximum and minimum bounding conditions.

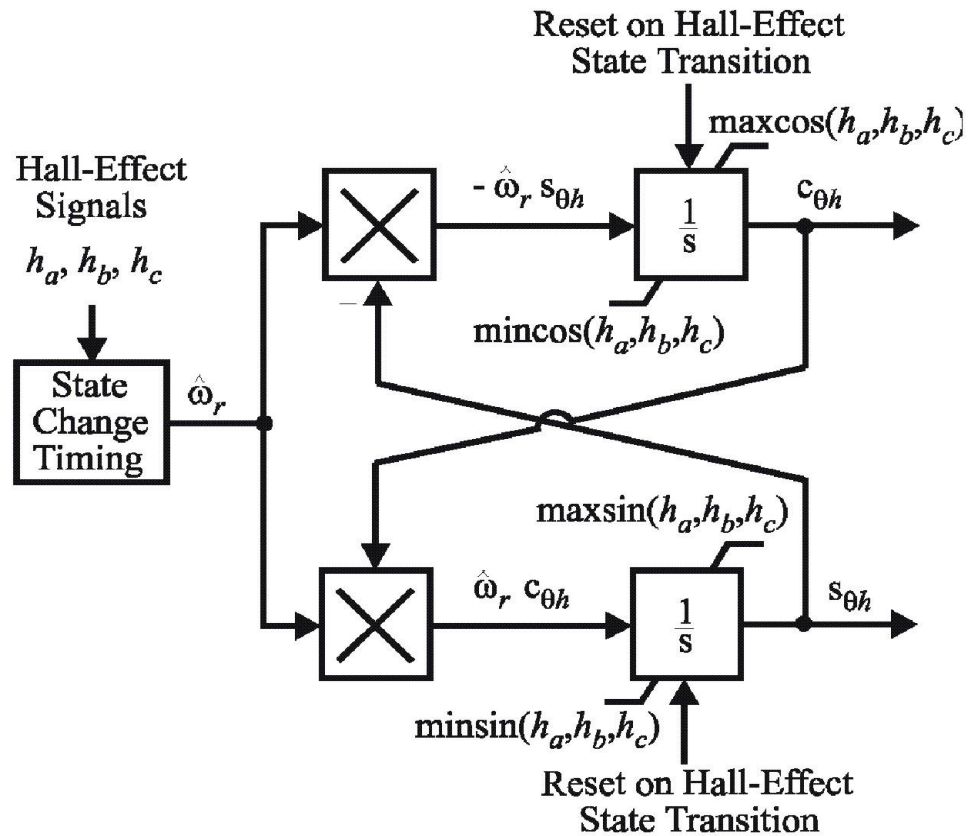


Figure 4.7. Hybrid Observer Block Diagram [26].

This speed observer is built in Quartus II software and VHDL language then simulated at ModelSim, and also implemented and tested in Altera FPGA cyclone II; appendix B shows the program structure. Figure 4.8 shows the schematic view of the hybrid speed observer. Figure 4.9 displays the FPGA experiments board PCB0006 that has been used for the implementation of the hybrid speed observer for testing purposes.

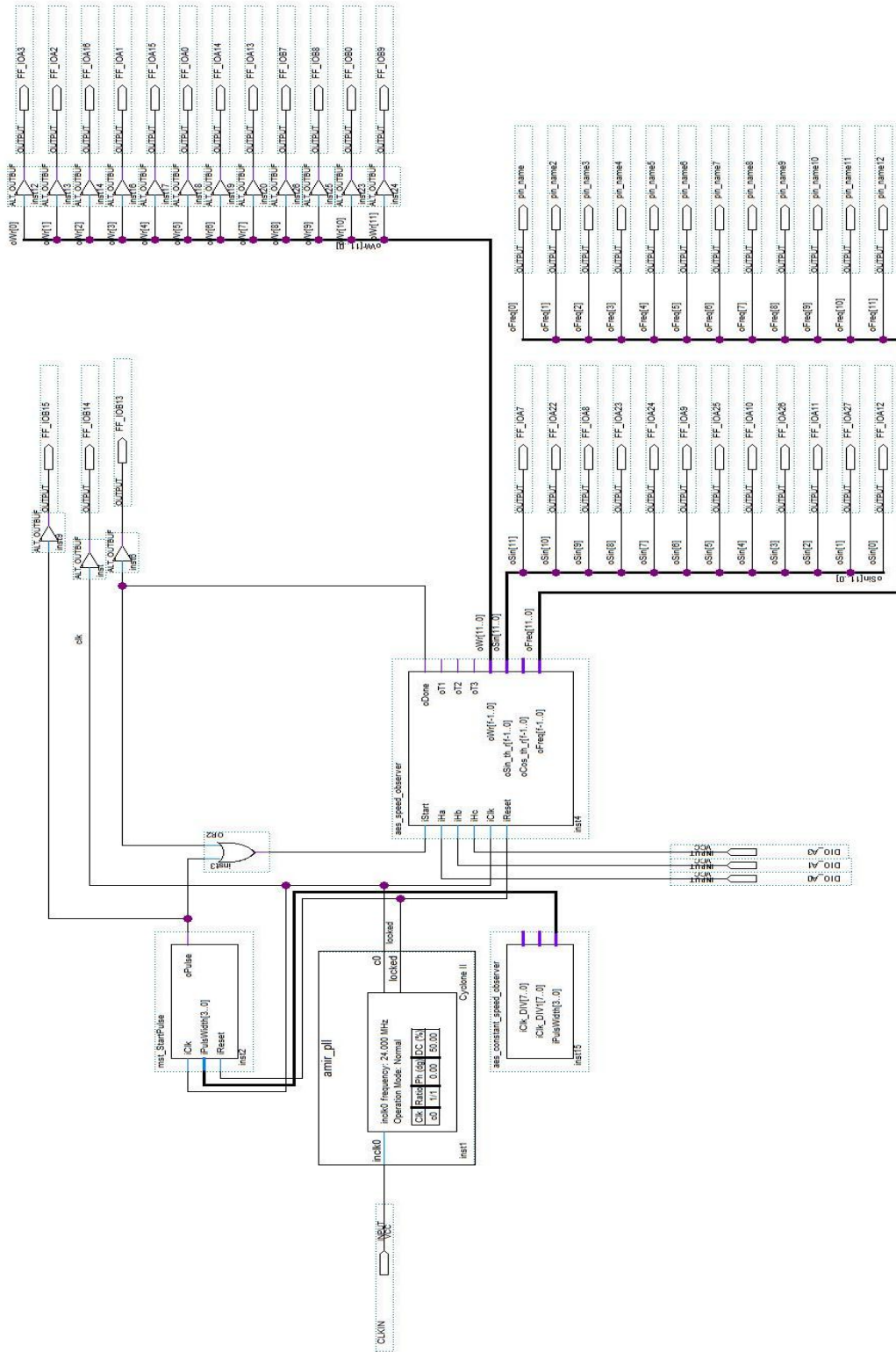


Figure 4.8. Speed Observer Schematic in VHDL.

The signal flow in 4.8 uses the same start procedure in the PWM program in section 3.2.4. Then a single start pulse is used to trigger the speed observer VHDL program in appendix B. The program will start to execute as soon as it receives the start pulse and will provide the results. After the program is finished, it will generate a done pulse that is connected to an OR gate with the start pulse to keep the program continuously working. The Hall effect signals are connected to pins Y22, Y21, and V22. A 24 MHz clock is used to run this experiment.

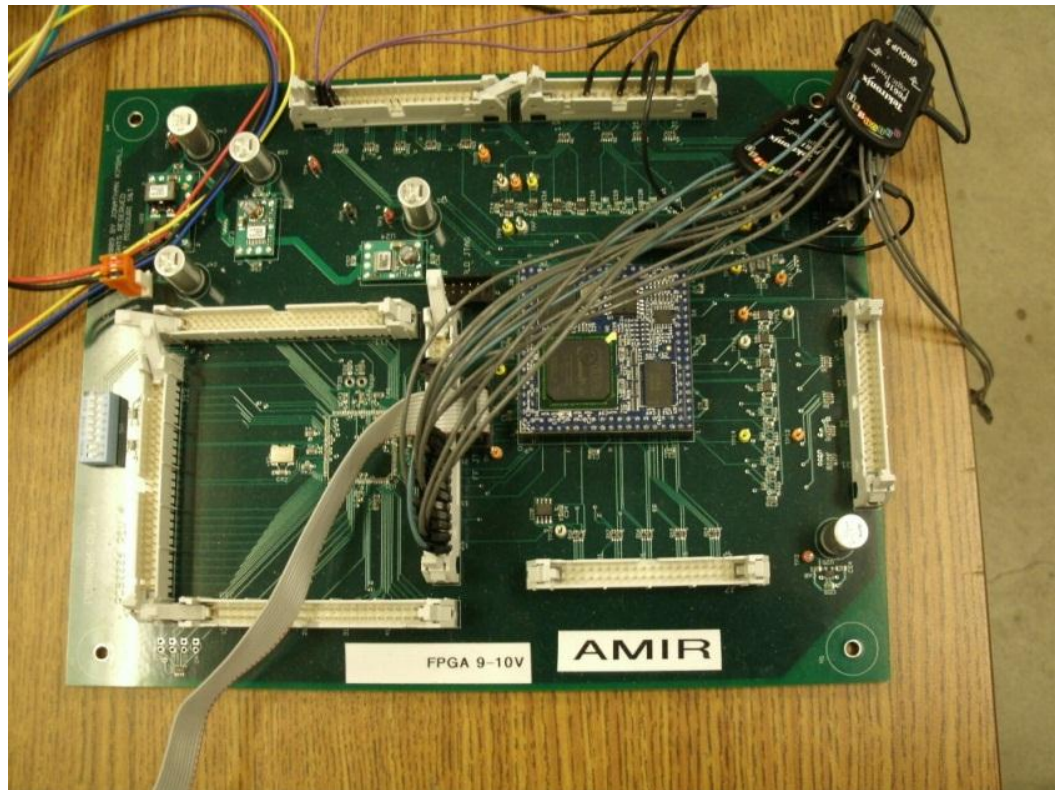


Figure 4.9. PCB0006 Experiments Board.

Figure 4.10 shows the dc motor and the Hall effect sensors encoder type 24A0FEPM from Bodine electric motors that have been involved in this experiment.



Figure 4.10. The Experiment dc Motor.

Table 4.4 illustrates the dc motor parameters and characteristics.

Table 4.4. The Motor Parameters.

Serial number	4440MYEAZ0001
Type	24A0FEPM
Volts	24VDC
F.F	1.0
Amperes	1.2
HP	1/50
INS	B8
RPM	2500

5. RESULTS AND SYSTEM VALIDATION

5.1. MODELSIM RESULTS

The model of the PWM generator has been tested and developed in ModelSim. The next figures show the simulation results for three different techniques. Figure 5.1 illustrates the simulation results of up-mode counter.

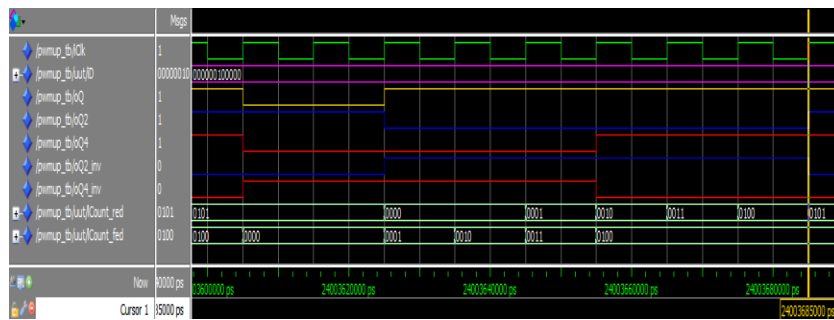


Figure 5.1. The Simulation Results of the Up-Mode Counter.

Figure 5.2 illustrates the ModelSim simulation results of down-mode counter.

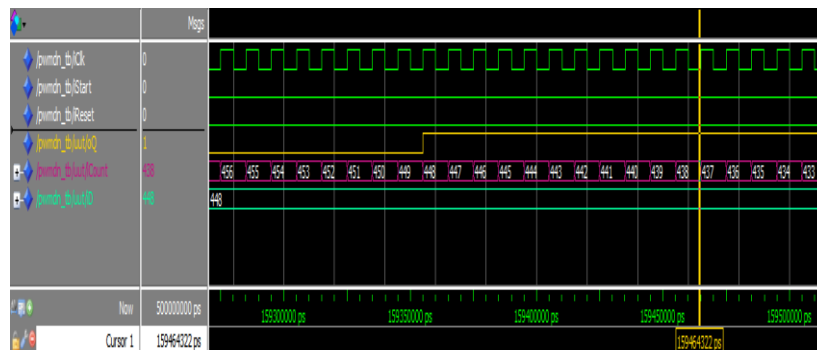


Figure 5.2. The Simulation Results of the Down-Mode Counter.

The simulation test is also applied to the Up-Down mode counter and Figure 5.3 displays the simulation results of this type of counter.

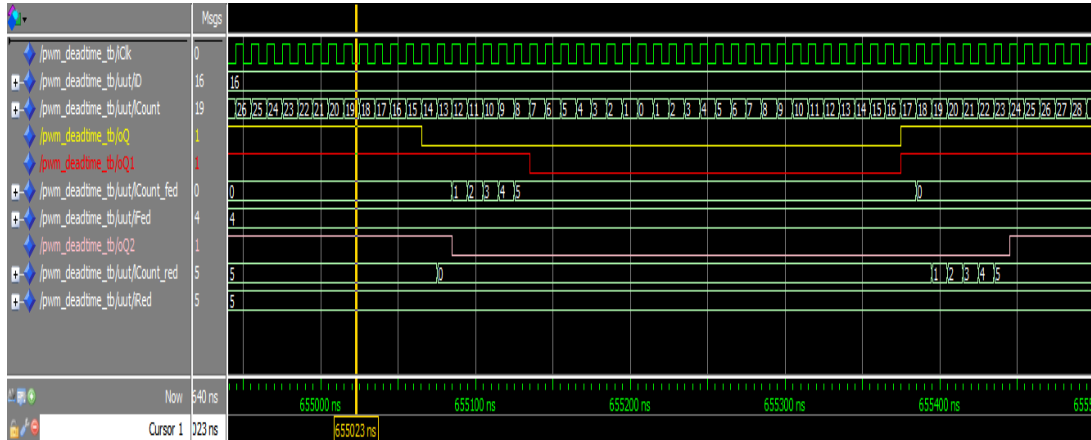


Figure 5.3. The Simulation Results of the Up-Down Counter.

Figures 5.4, 5.5, 5.6, 5.7 illustrate the simulation results of the hybrid speed observer in ModelSim and its related parameters.

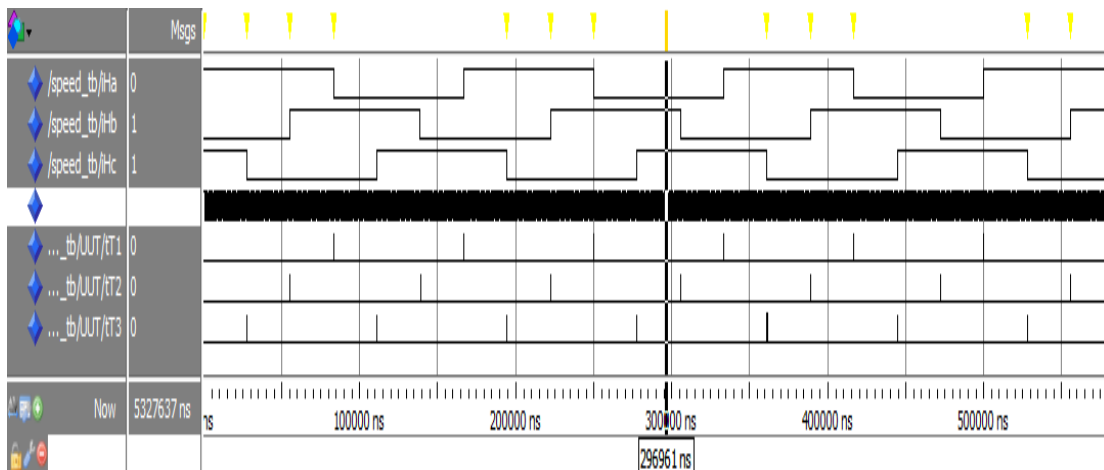


Figure 5.4. Screen Shot (1) for Parameters Results of the SO.

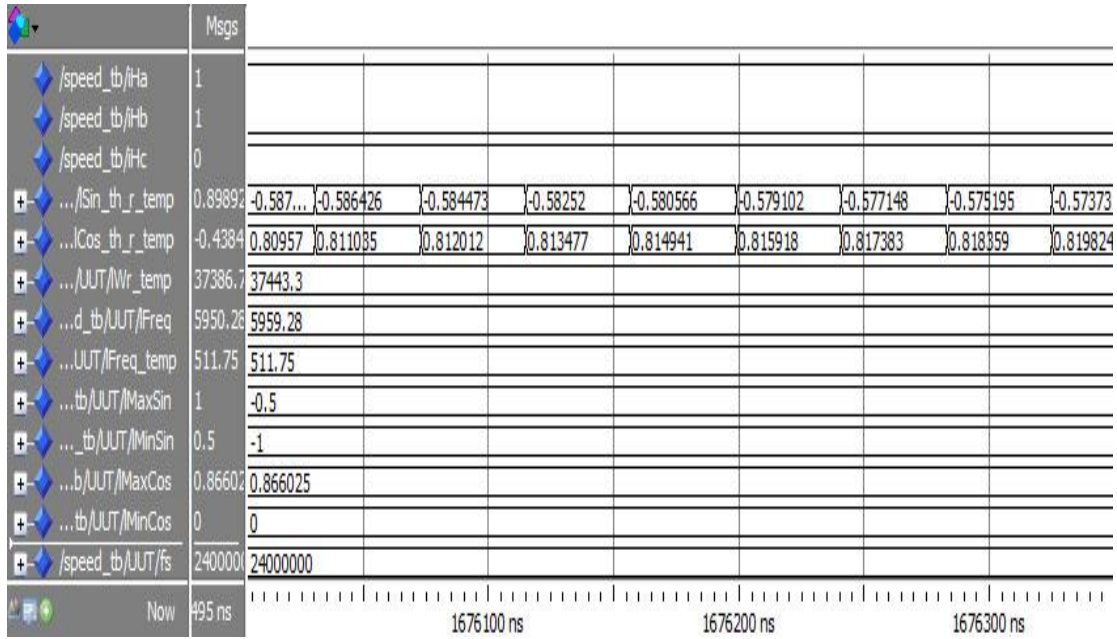


Figure 5.5. Screen Shot (2) for Parameters Results of the SO.

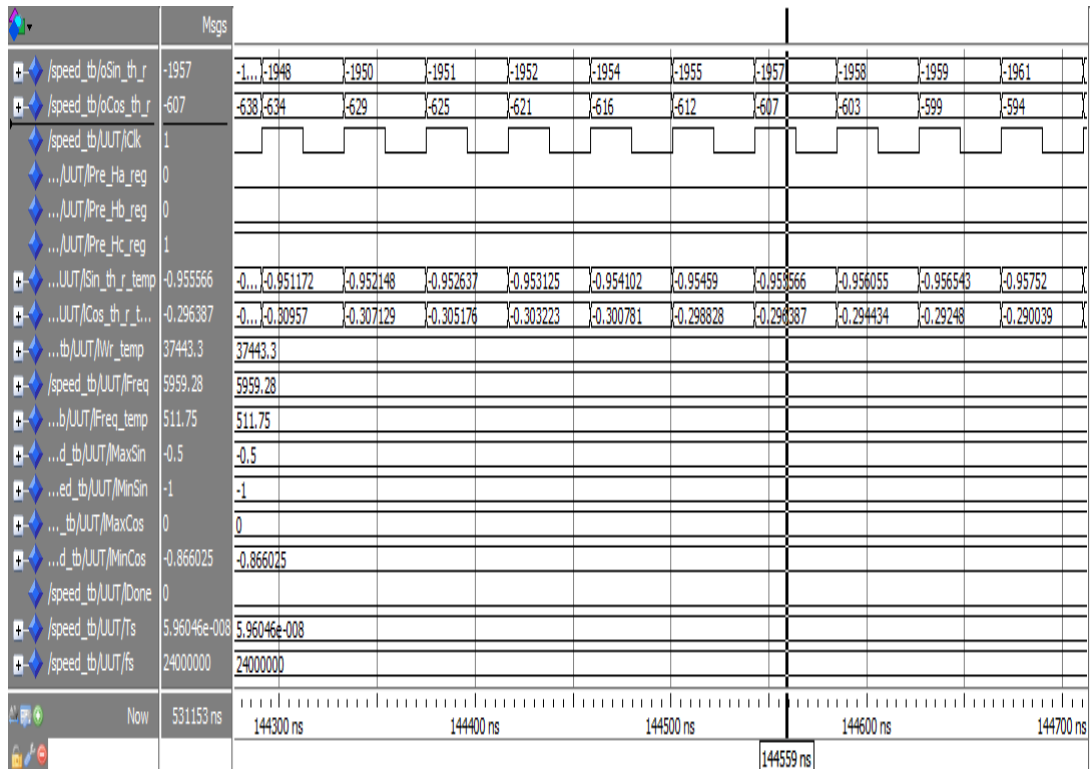


Figure 5.6. Screen Shot (3) for Parameters Results of the SO.



Figure 5.7. Screen Shot (4) for Parameters Results of the SO.

5.2. HARDWARE RESULTS

The PWMs programs are implemented in the FPGA and have been tested to drive synchronous buck converter. The required dead time is about 180 nanosecond which is about 4 clock cycles delay. Figures 5.8 and 5.9 display screen shots for the rising and falling edge of the up-down counter PWM.

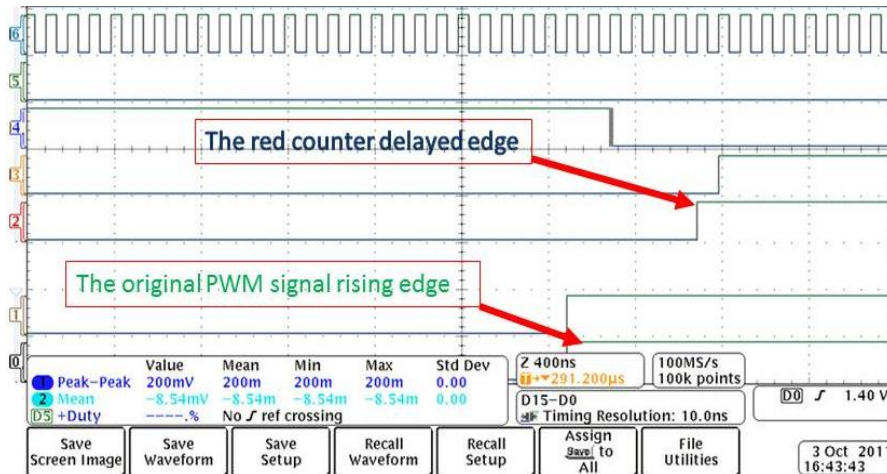


Figure 5.8. The Rising-Edge Counter Delay.

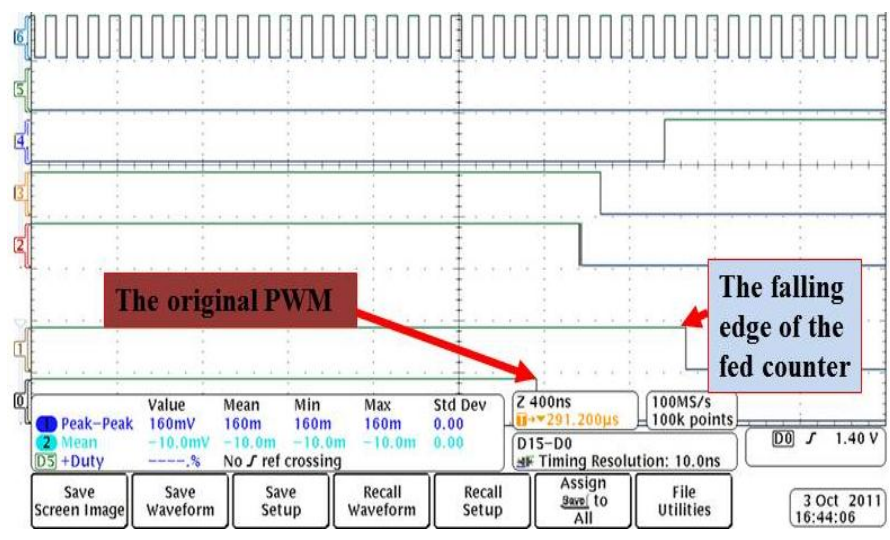


Figure 5.9. The Falling-Edge of the Fed Counter.

Figure 5.10 shows the Hall effect signals from the dc motor in section 5.2.

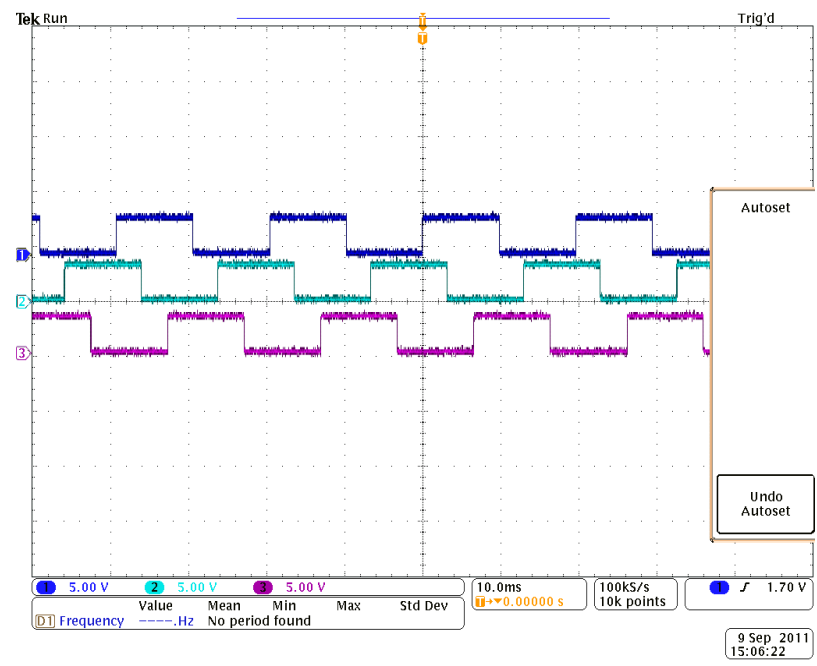


Figure 5.10. Hall Effect Signals.

Figure 5.11 illustrates the output of an experiment that has been prepared for Hall effect signals of 59.86 Hz. The result of ω_r , shown in 12 bit binary bus which included 2 bit of fraction that makes it equivalent to 376 in decimals which is.

$$f = \frac{\omega_r}{2\pi} = \frac{376}{2\pi} = 59.84 \text{ Hz} \quad (26)$$

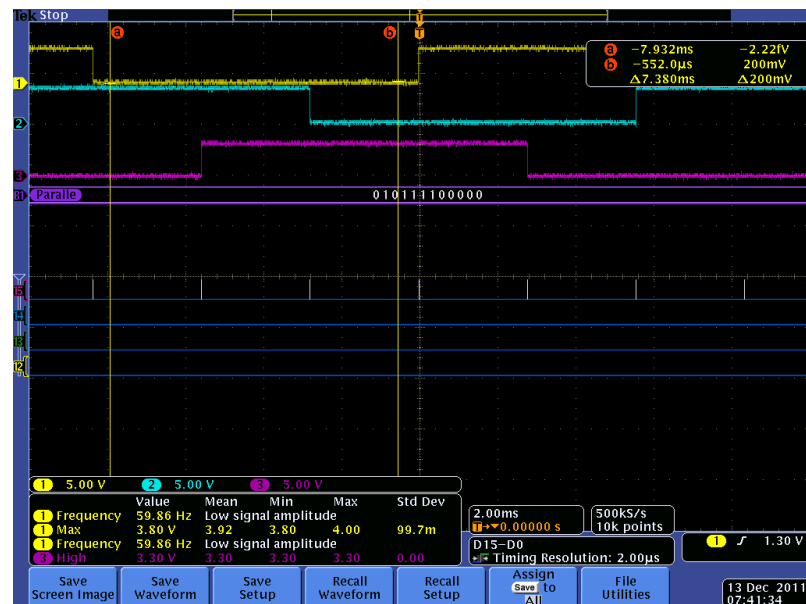


Figure 5.11. The SO Output in 59.86 Hz Hall Effect Signals Input.

The setup has been tested under many different rotating speeds and it always gives excellent results with negligible error due to the approximation of the program and the number of bits m that has been used to calculate ω_r . This error has been detected and analyzed in average form due to the unstable Hall effect signal from the dc motor in addition to the inaccuracy of the scope. The next chart in Figure 5.12 illustrates the absolute average error versus the m bits. Figure 5.13 also illustrates the number of the total logic elements used versus m .

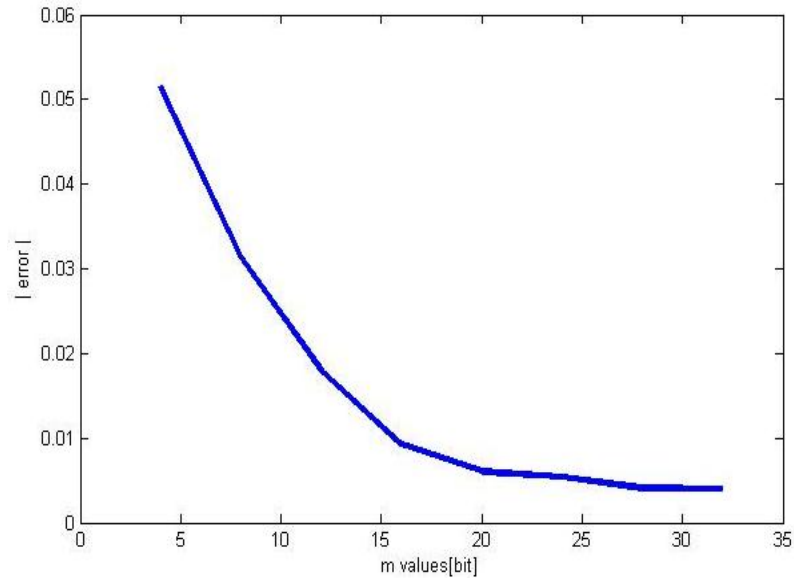


Figure 5.12. The Absolute Error vs. m Bits.

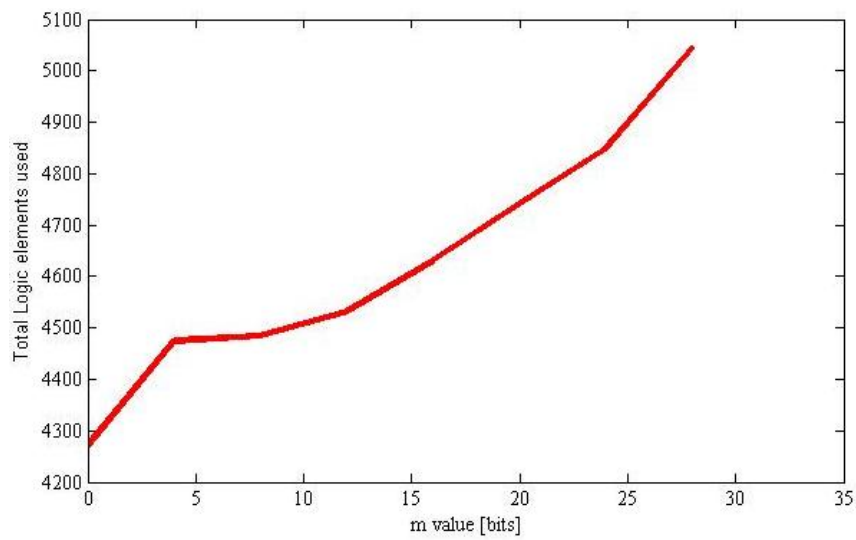


Figure 5.13. The Total Logic Elements vs. m Bits.

Figures 5.14 and 5.15 illustrate the $\sin(\theta_{th})$ output signal from the SO program.

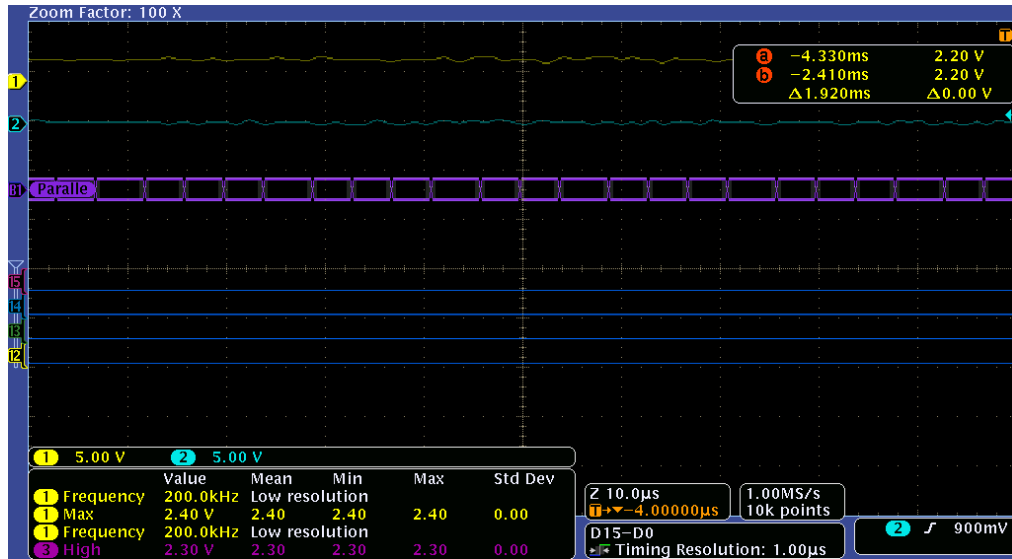


Figure 5.14. The $\sin(\theta_{rh})$ Output.

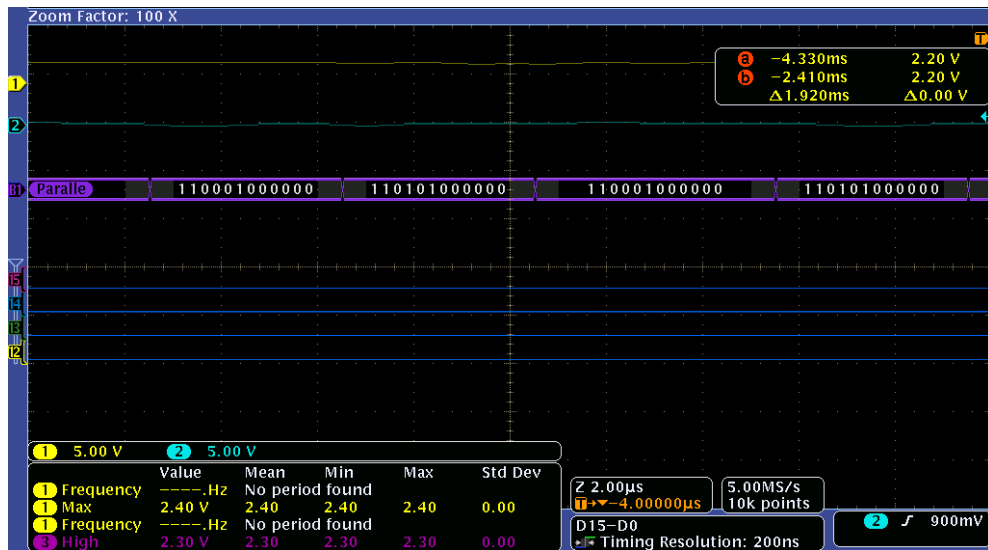


Figure 5.15. Zoom in Results of $\sin(\theta_{rh})$.

6. CONCLUSION AND FUTURE SCOPE

A signal processing board has been designed to control the PMSM and monitor the external parameters. This thesis developed the FPGA to generate special signals and techniques the same as the TI320F28335 does. The PWM signals were tested under different topologies and conditions. These signals include the dead time capability in order to be used in synchronous switching devices that require delay time between the rising and falling edges such as synchronous buck, boost, or buck-boost converters or the modules like a three phase inverters. The hybrid speed observer method is chosen as the rotor position and speed detection technique to control the PMSM. This program has been successfully developed and implemented inside the FPGA and all results are documented and compared to the microcontroller results. The FPGA implementation gives high accuracy and better flexibility in the mathematical operations. Also the resulting error has been analyzed. The system is scalable, so it can control more than one motor due to the better flexibility of FPGA implementation. The future work would be applying some other control methods such as all digital phase lock loop (ADPLL), which is composed of phase and frequency detector, low pass filter (LPF), digital controlled oscillator (DCO), and a divider. Then a useful comparison can be done to illustrate the pros and cons of each method.

APPENDIX A.
PRINTED CIRCUIT BOARDS DESIGN

This appendix includes the signal processing and power supply boards schematics and layouts of the printed circuit boards discussed in Section 2.1 and 2.11 respectively. The board schematic layout for the signal processing is shown in Figure A.1 through A.15 and the schematic and layout of the power supply board is shown in Figure A.16 through A.17.

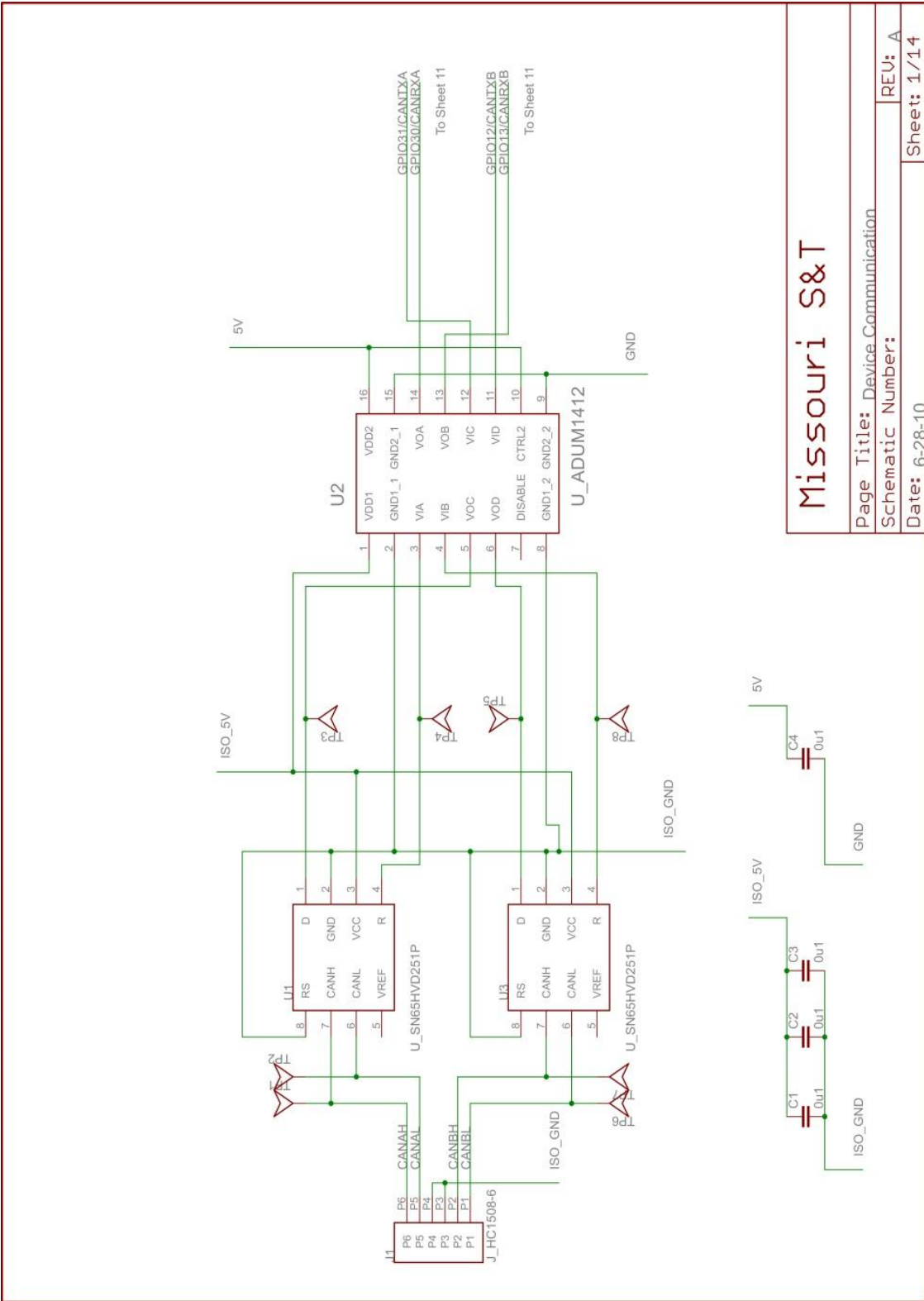
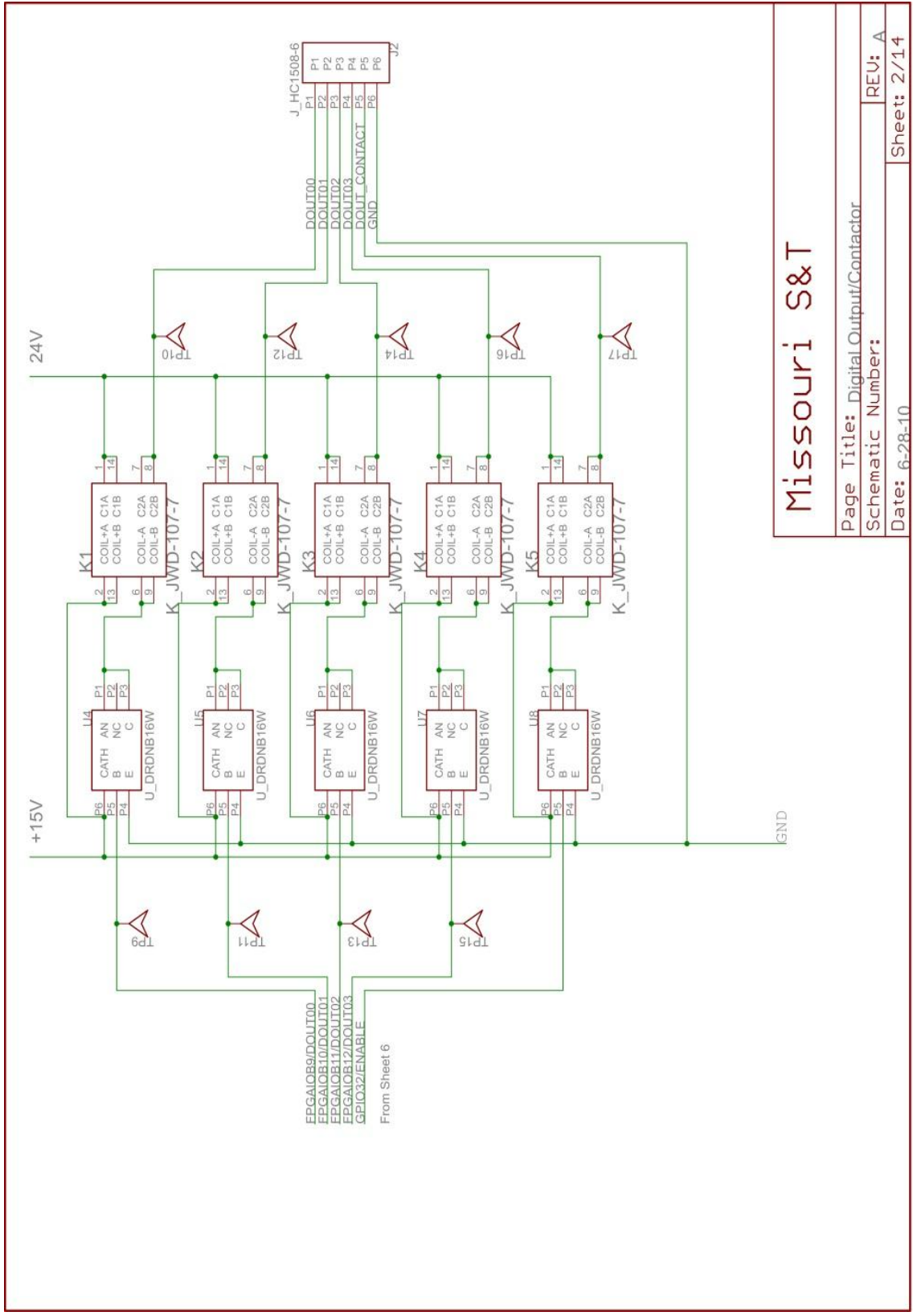


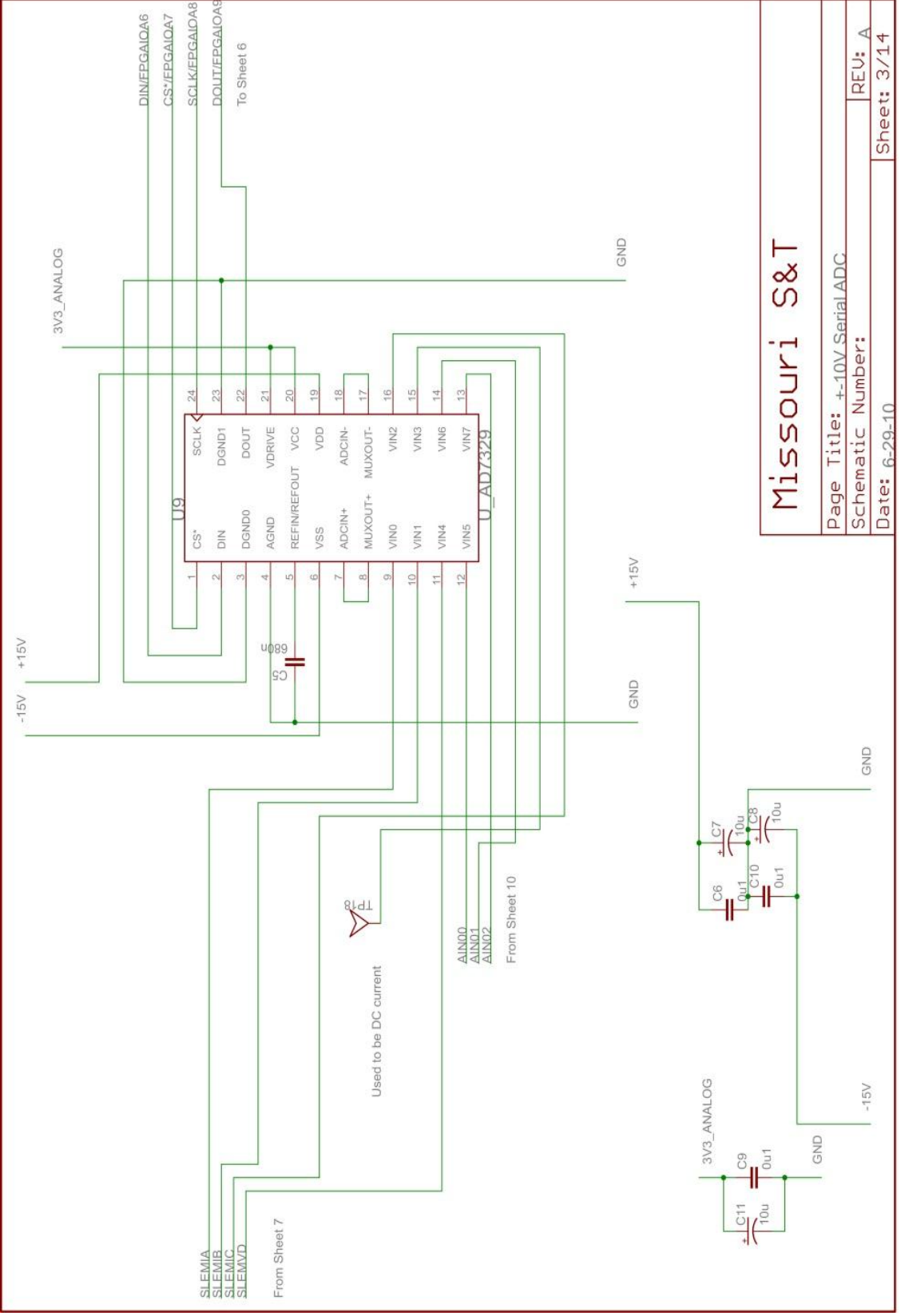
Figure A.1. The CAN Transceiver Circuit.

Missouri S&T	
Page Title: Device Communication	REV: A
Schematic Number:	Sheet: 1/14
Date: 6-28-10	



Missouri S&T	
Page Title: Digital Output/Contactor	REV: A
Schematic Number:	
Date: 6-28-10	Sheet: 2/14

Figure A.2. Digital Output Contactors.



Missouri S&T	
Page Title: +-10V SerialADC.	REV: A
Schematic Number:	Sheet: 3/14
Date: 6-29-10	

Figure A.3. The 8-channel AD7329 Serial ADC Circuit.

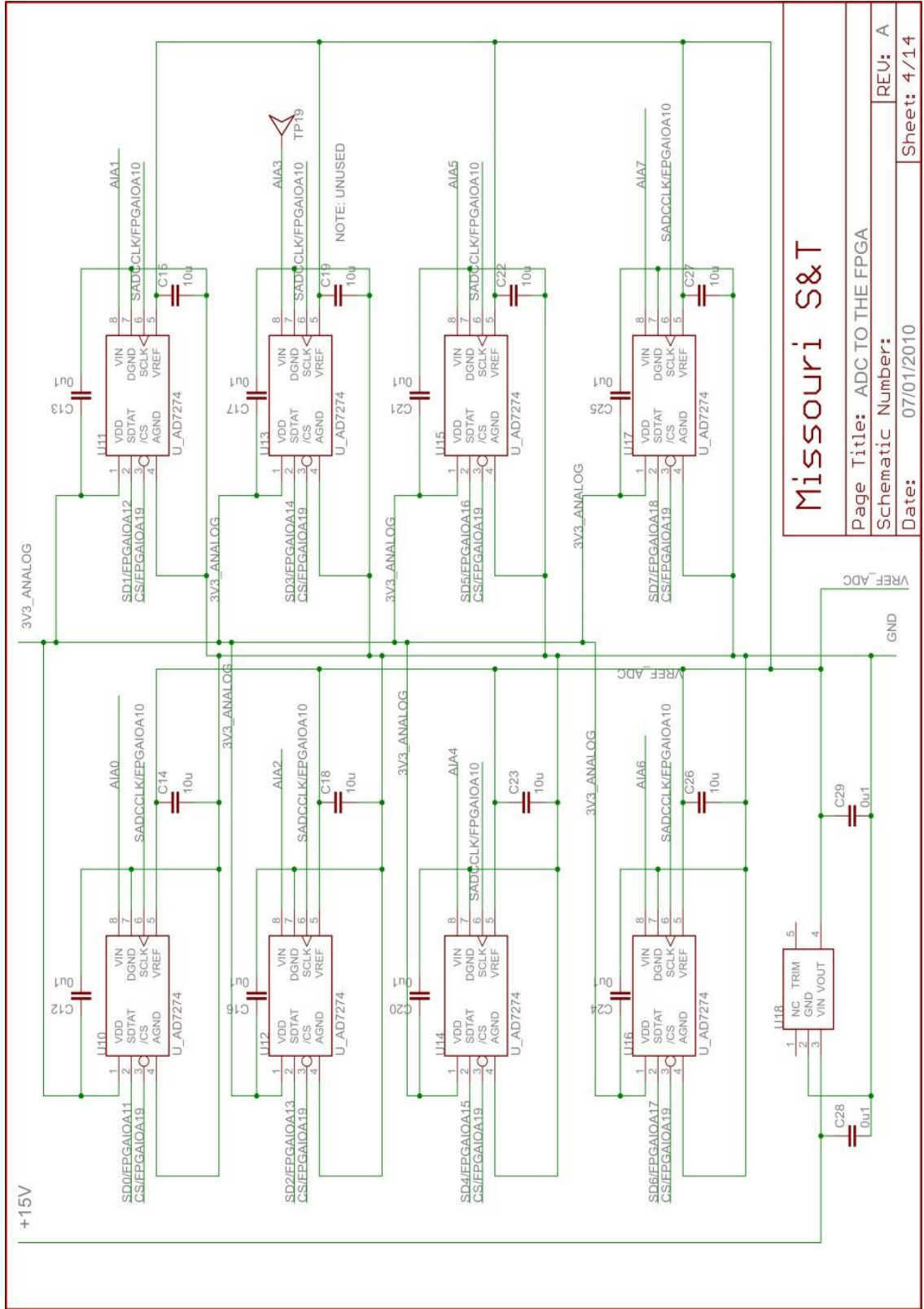
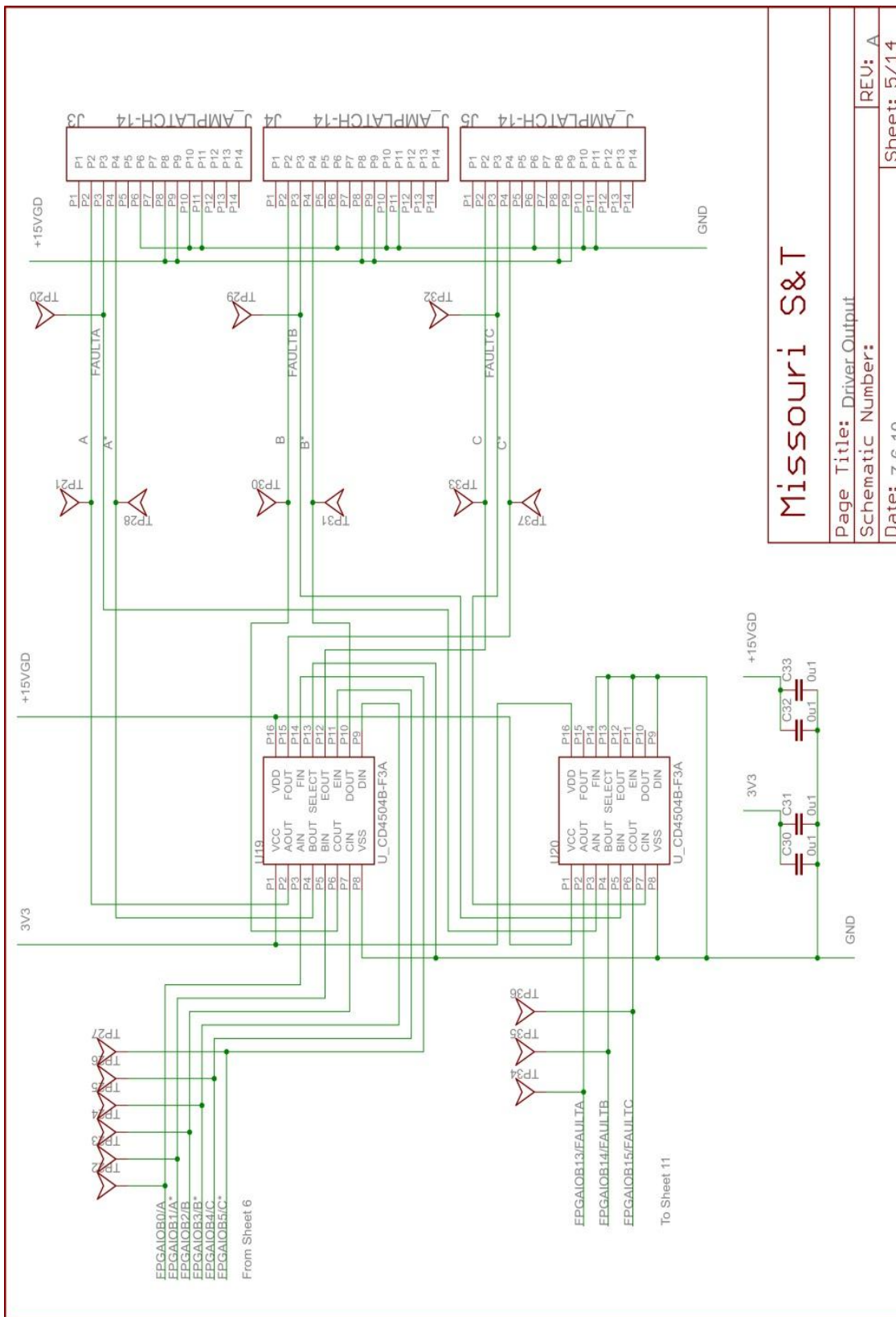


Figure A.4. The ADC AD7276 Circuit.



Missouri S&T

Page Title: Driver Output
 Schematic Number:
 Date: 7-6-10

REV: A
 Sheet: 5/14

Figure A.5. Level Shifters Circuit.

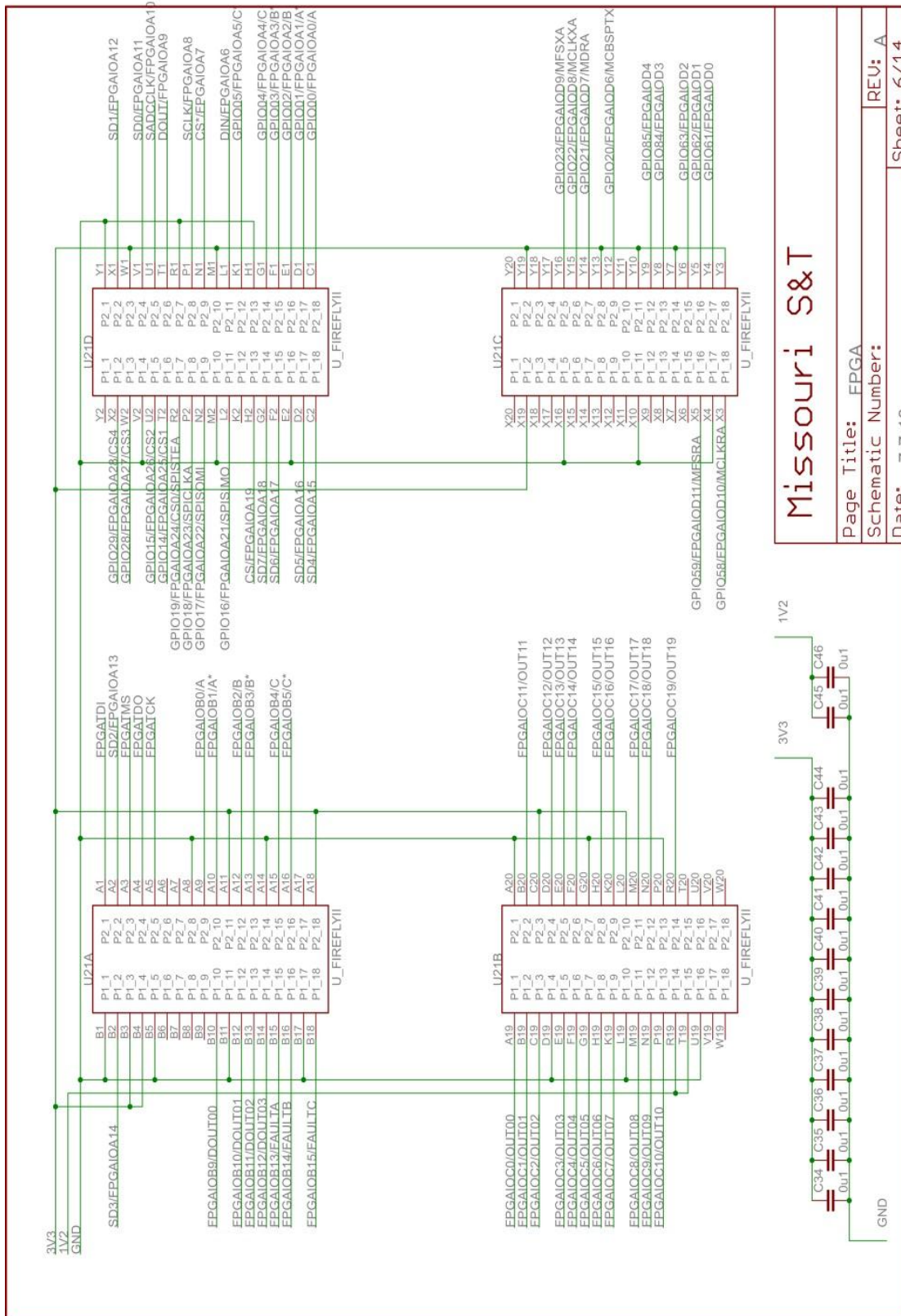


Figure A.6. The FPGA Pin Out.

<h1>Missouri S&T</h1>	
Page Title: FPGA	REU: A
Schematic Number:	Sheet: 6/14
Date: 7-7-10	

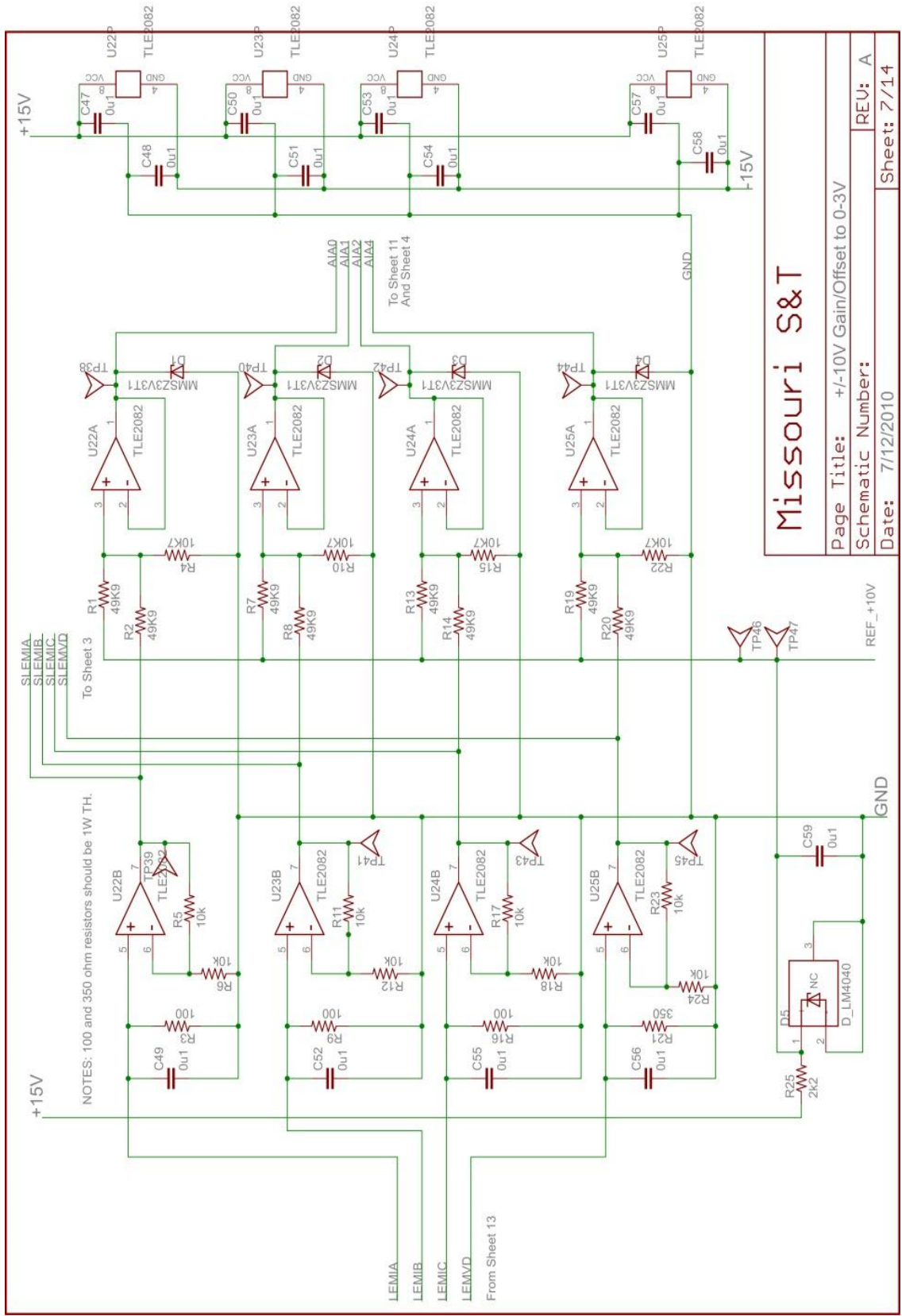


Figure A.7. 0-3V Gain-Offset Circuit.

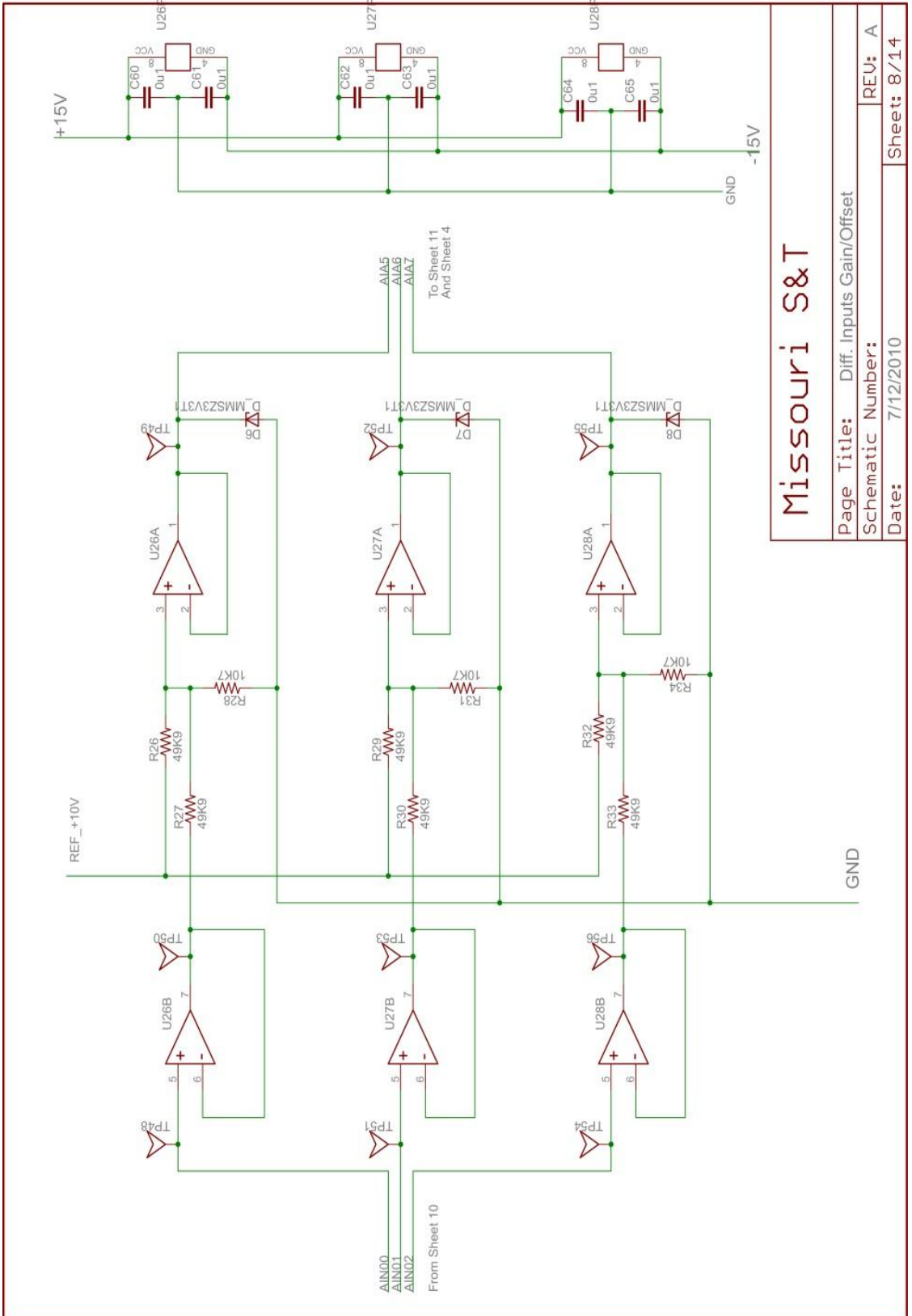


Figure A.8. Differential Input Gain-Offset Circuit.

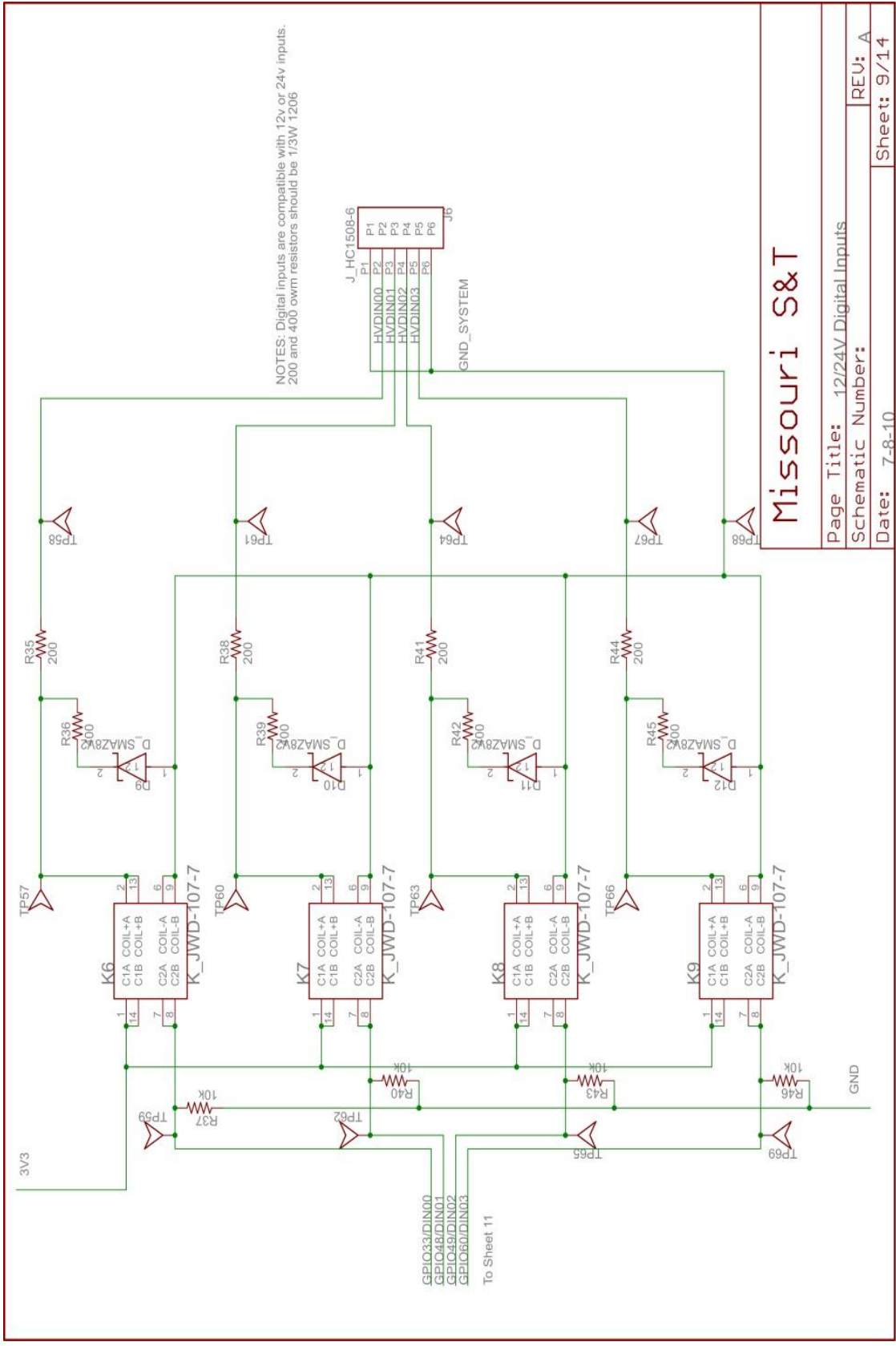


Figure A.9. Digital Inputs Circuit.

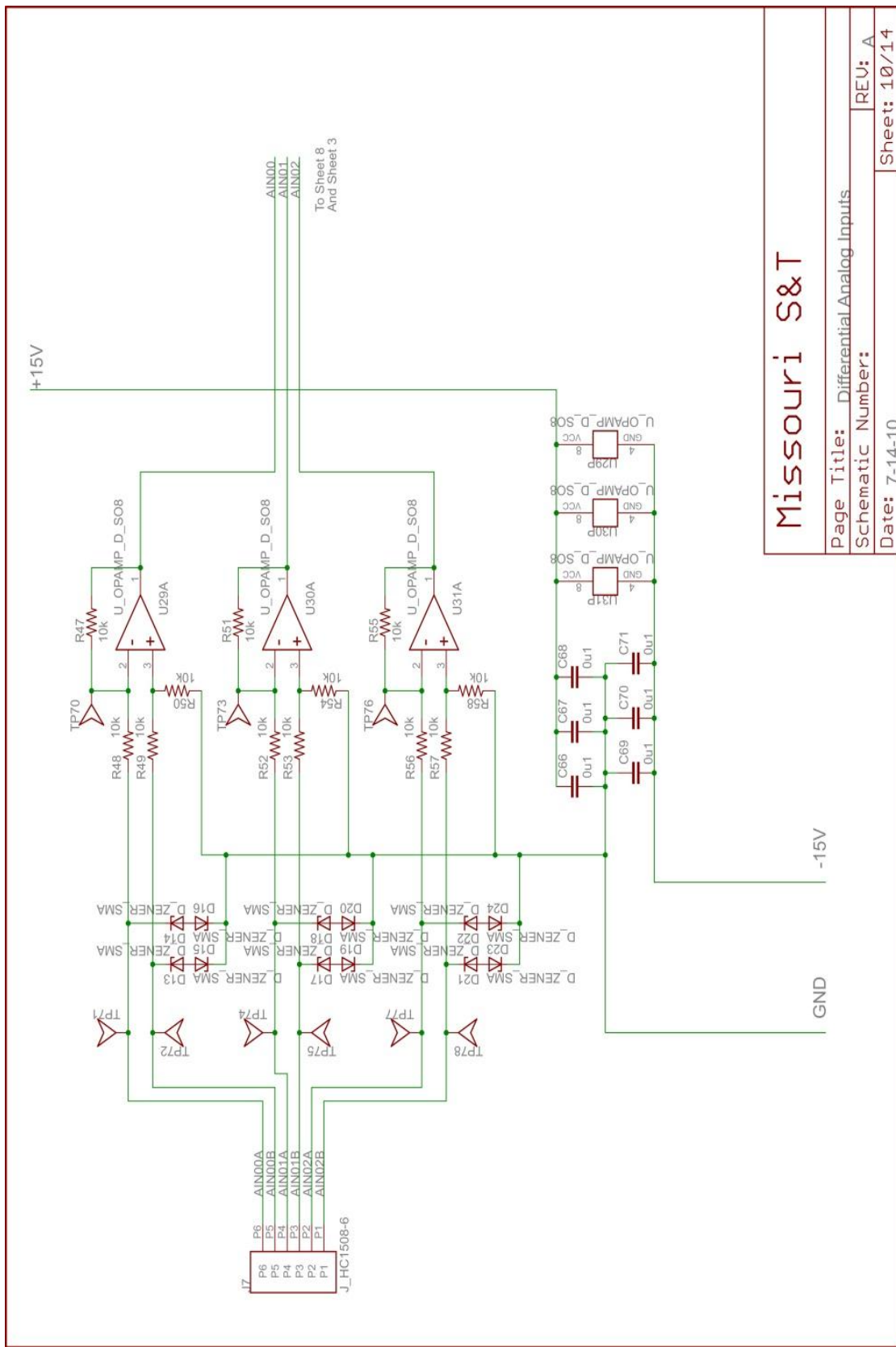


Figure A.10. Differential Amplifiers Circuit.



Figure A.11. The DSP Pin Out.

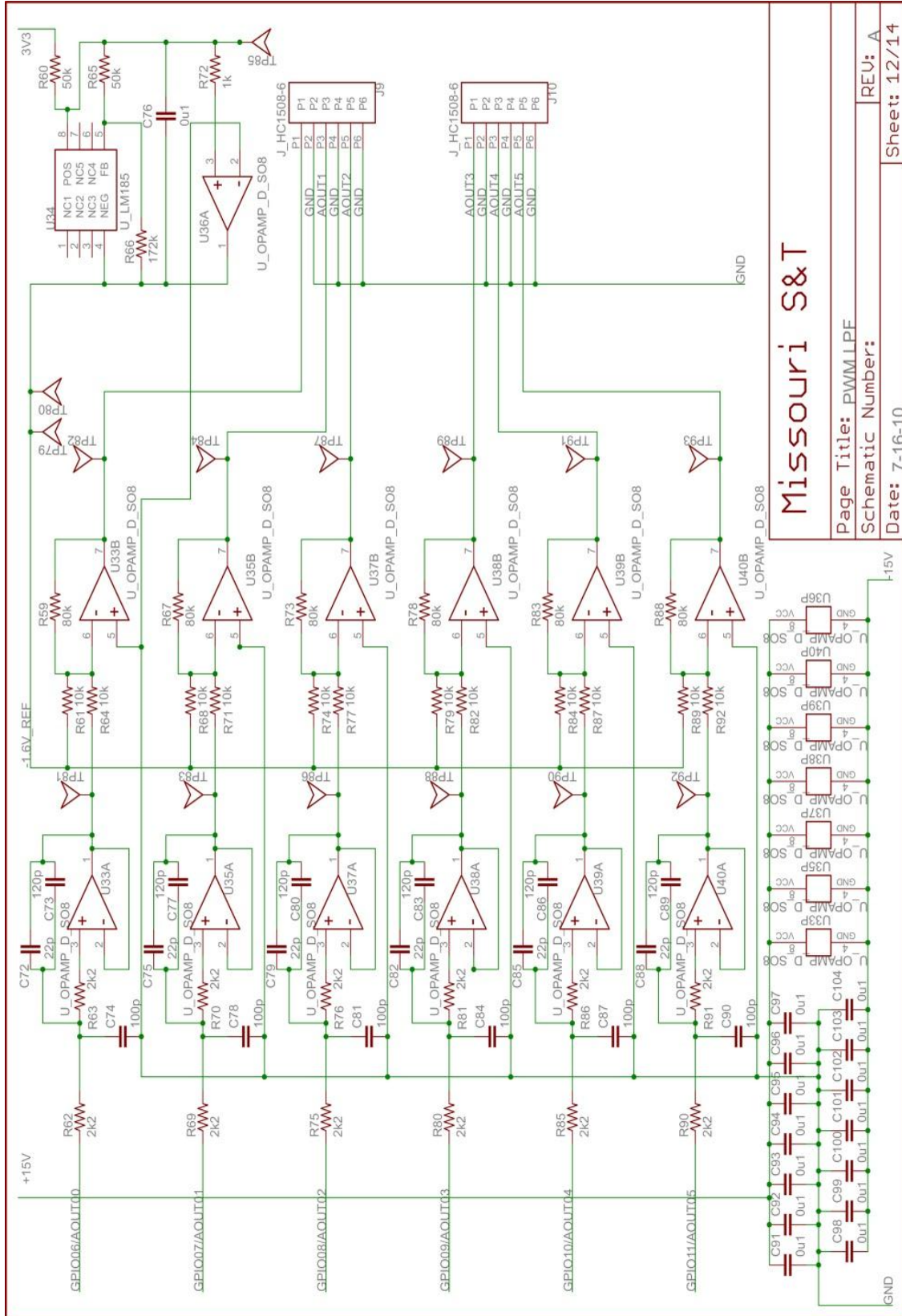


Figure A.12. The Sallen Key LPF.

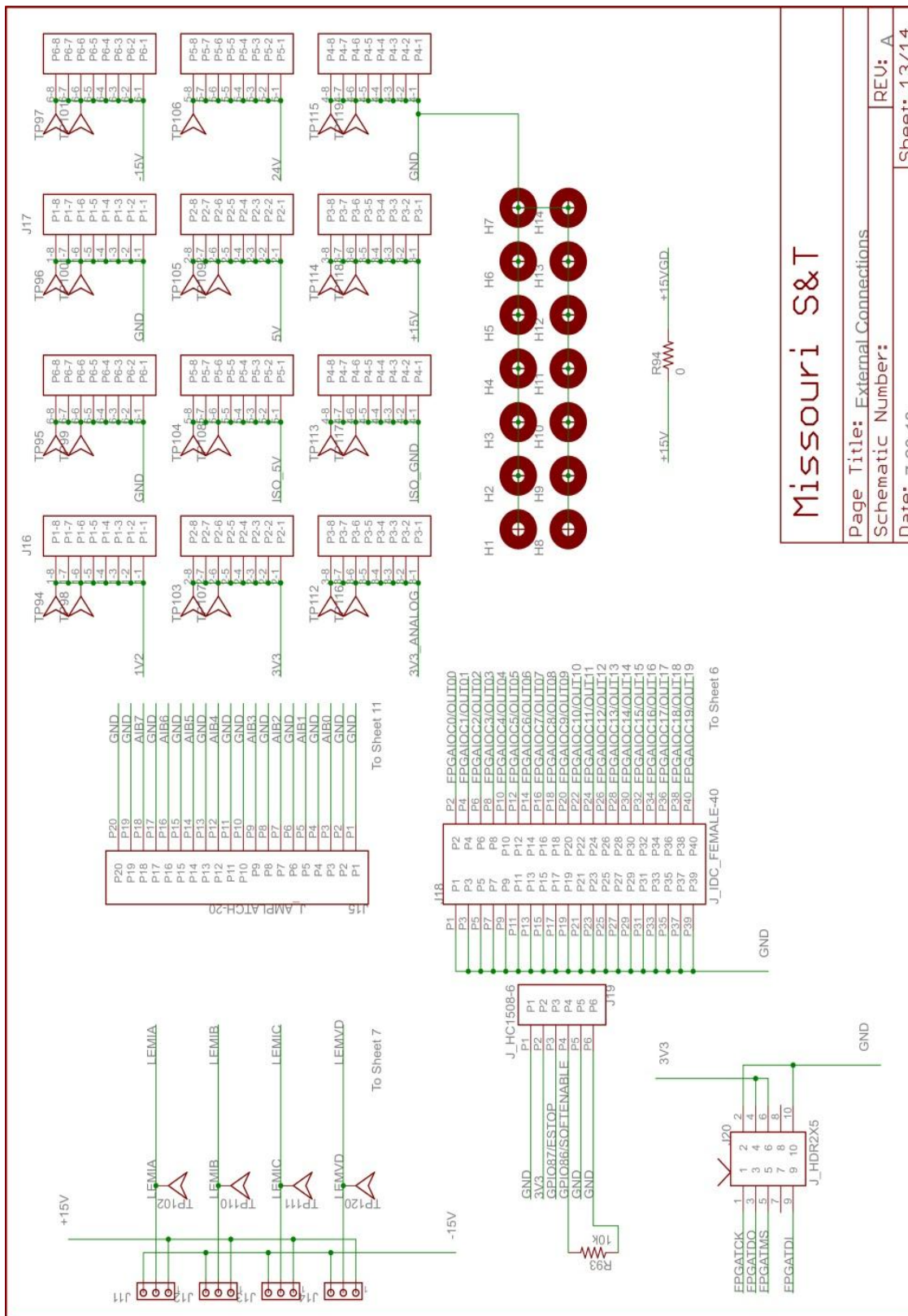
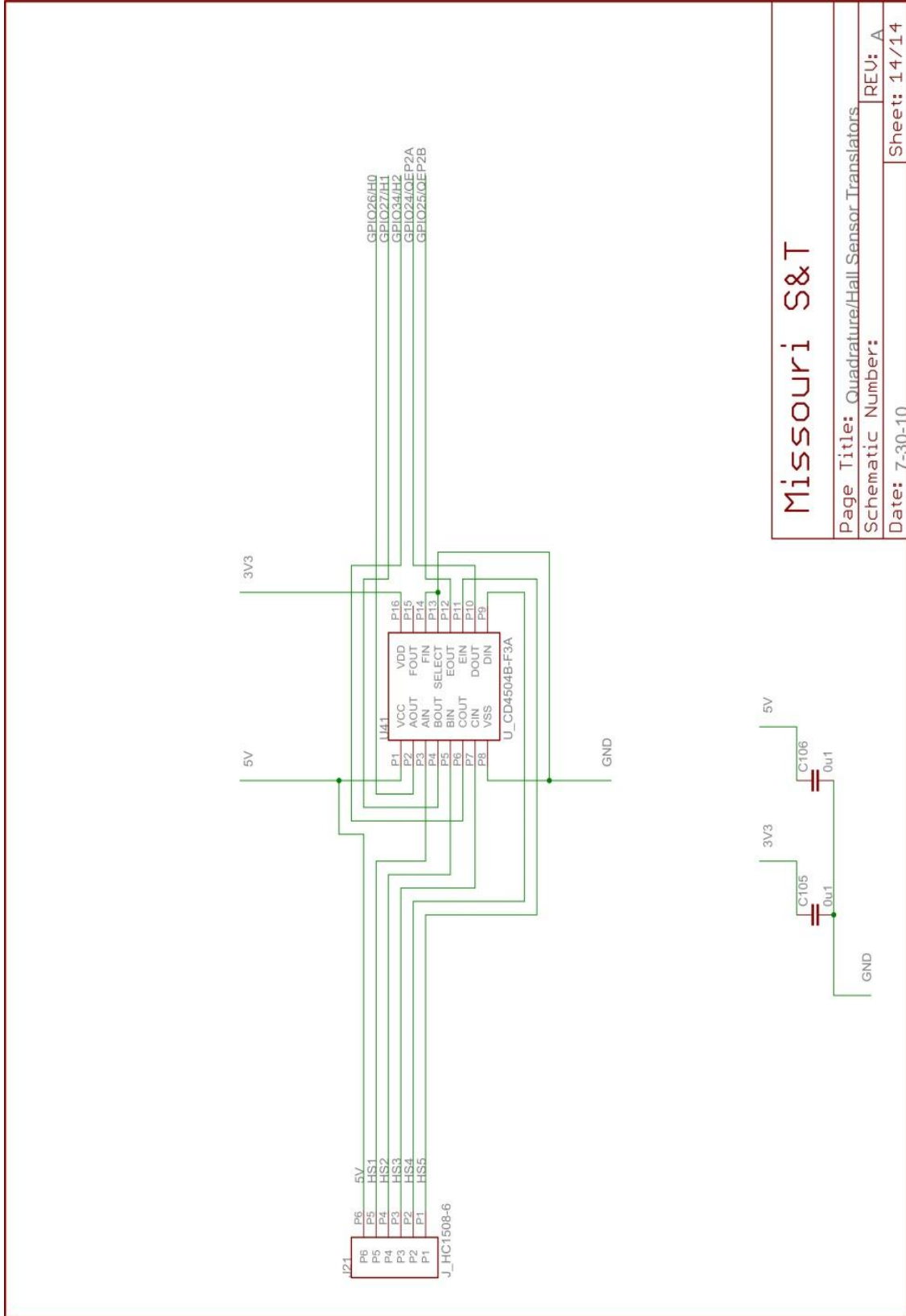


Figure A.13. The Connectors Pin Out.



Missouri S&T	
Page Title: Quadrature/Hall-Sensor Translators	REV: A
Schematic Number:	Sheet: 14/14
Date: 7-30-10	

Figure A.14. The Hall effect Signals Level Shitter Circuit.

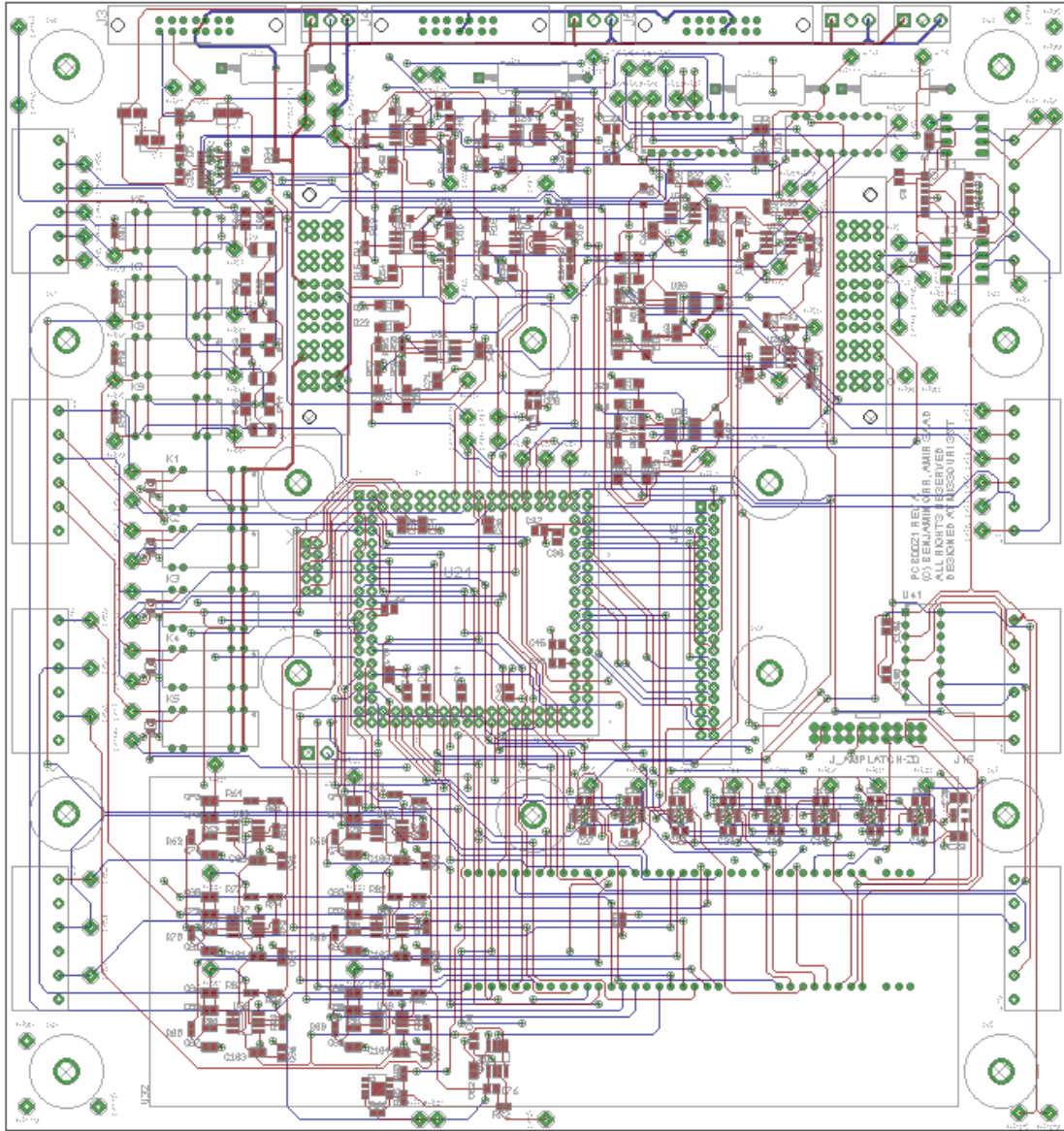
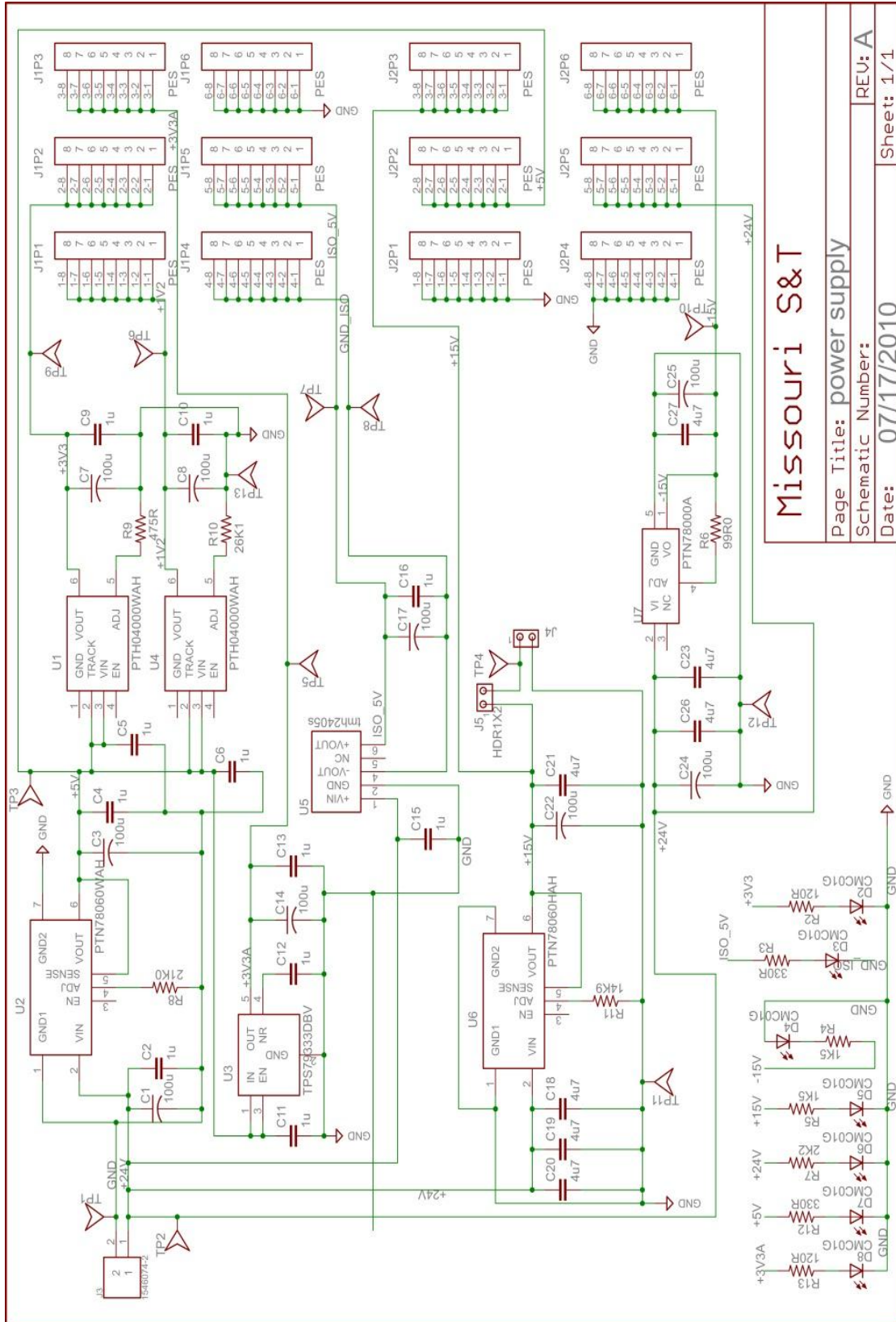


Figure A.15. The Signal Processing Board Top Layer.



Missouri S&T

Page Title: power supply

Schematic Number:

Date: 07/17/2010

REV: A

Sheet: 1/1

Figure A.16. The Power Supply Schematic.

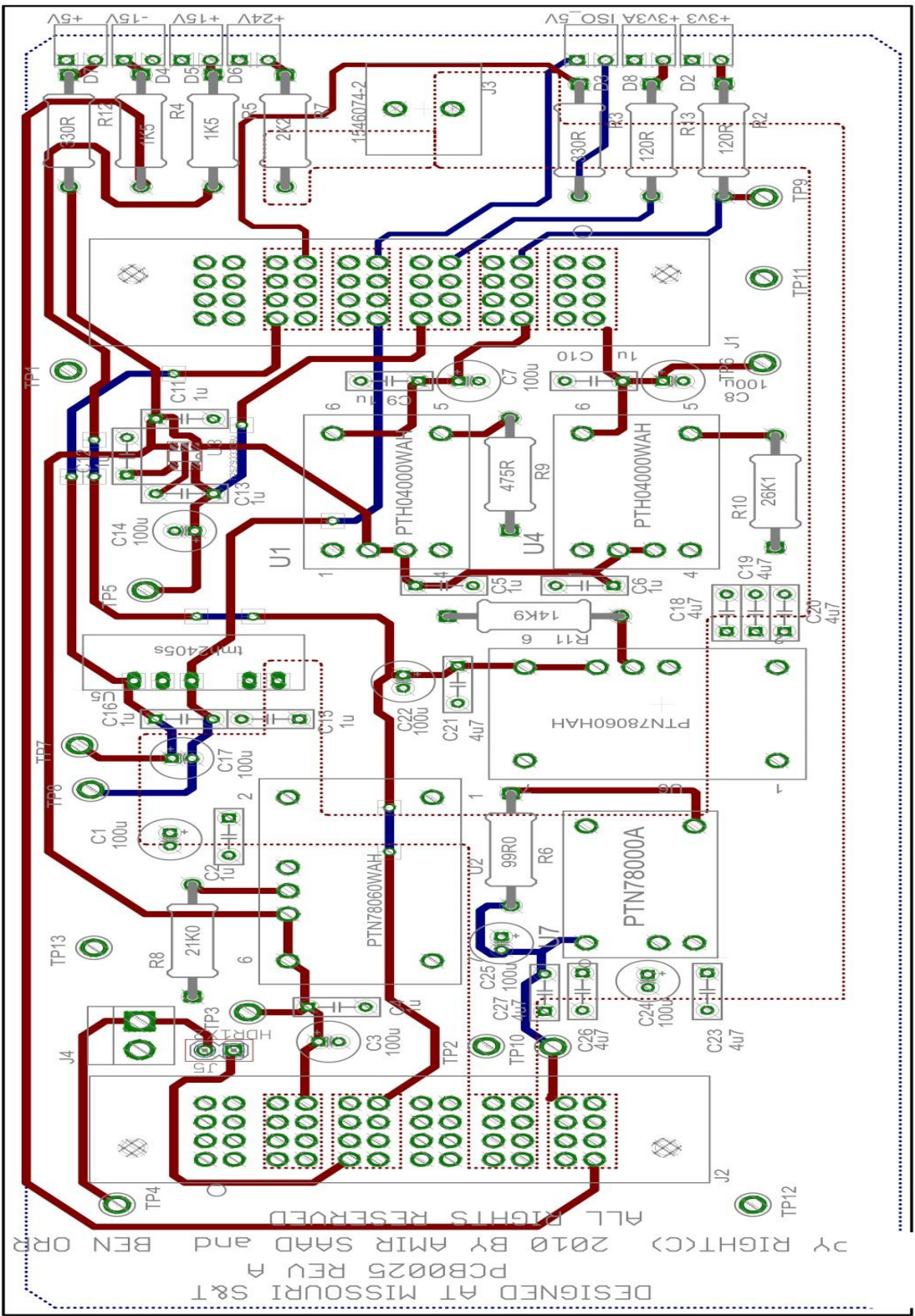


Figure A.17. The Power Supply Board Top Layer.

APPENDIX B.
VHDL CODES OF THE DESIGN

This appendix contains the VHDL programs of the up mode, down mode, and up-down mode PWMs, also it includes the speed observer program. The comments are denoted by text that starts with double hyphen (--) and green font.

This is a program for up mode counter PWM.

--This program has been written in VHDL for PWM using up mode counter. The program has been developed by Amir Saad at
- Missouri University of Science and Technology in Aug. 2011 . Copy right (c) For Amir Saad. All rights reserved 2011.

```

Library ieee;
use ieee.std_logic_1164.all;
use ieee.std_logic_unsigned.all;
use ieee.std_logic_arith.all;

ENTITY aes_pwm_up is
  generic ( n: natural := 12);-- n can be changed as needed
  port(
    --input signales
    iStart : in std_logic;    -- pulse at start
    iD      : in std_logic_vector(n-1 downto 0); --used for 12 bit input data value
    iClk    : in std_logic;
    iReset  : in std_logic;
    iRed    : in std_logic_vector (3 downto 0); -- rising edge counter input data
    iFed    : in std_logic_vector (3 downto 0); -- falling edge counter output data
    --Output signals
    oQ      : out std_logic;
    oQ1     : out std_logic;
    oQ2     : out std_logic;
    oQ3     : out std_logic;
    oQ4     : out std_logic;
    oQ_inv  : out std_logic;
    oQ1_inv : out std_logic;
    oQ2_inv : out std_logic;
    oQ3_inv : out std_logic;
    oQ4_inv : out std_logic;
    oDone   : out std_logic;
    oDone_fed : out std_logic;
    oDone_red : out std_logic;
    Constant C_min : std_logic_vector(n-1 downto 0):=(others=>'0');
    Constant C_max : std_logic_vector(n-1 downto 0):=(others=>'1');
  );
end aes_pwm_up ;

Architecture Behavioral of aes_pwm_up is
  signal lDreg : std_logic_vector(n-1 downto 0); -- register output
  signal lCount : std_logic_vector(n-1 downto 0); -- counter output
  signal lFed : std_logic_vector(3 downto 0); -- falling edge register output
  signal lRed : std_logic_vector(3 downto 0); -- rising edge register output
  signal lCount_red : std_logic_vector(3 downto 0); -- rising edge counter output
  signal lCount_fed : std_logic_vector(3 downto 0); -- falling edge counter output
  signal lQint : std_logic;
  signal lPreQint : std_logic;
  signal lQ1 : std_logic;
  signal lQ2 : std_logic;
  signal lQ3 : std_logic;
  signal lQ4 : std_logic;
  signal lRedEn : std_logic;
  signal lFedEn : std_logic;

Begin
  process (iClk,iReset,iStart,lQint,lDreg,lCount,lCount_fed,lCount_red,lQ1,lQ2,lQ3,lQ4,lFed,lRed,lRedEn,lFedEn,lPreQint)
  Begin
    -- Initializations
    if (iReset = '0') then
      lCount <= C_min;
      lDreg <= C_min;
      lFed <= "0000";
      lRed <= "0000";
      lQint <='0';
      lQ1 <='0';
      lQ2 <='0';
      lQ3 <='0';
      lQ4 <='0';
      lRedEn <='0';
      lFedEn <='0';
    end if;
  end process;
end Behavioral;

```

```

lCount_red<="0000";
lCount_fed<="0000";

elsif ( rising_edge(iClk) ) then

    if (lCount=C_max) then
        oDone <= '1';
        lCount<= C_min;
    Else
        lCount<=lCount+1;
        oDone <= '0';
    End if ;

-----
--rising edge counter
    if (lRedEn='1') then
        lCount_red<=lCount_red +1;
        oDone_red<='0';

    Else

        lRedEn<='0';
        oDone_red<='1';

    End if;

-----
--falling edge counter
    if (lFedEn='1') then
        lCount_fed<=lCount_fed +1;
        oDone_fed<='0';

    Else

        lFedEn<='0';
        oDone_fed<='1';

    End if;

-----

if (lQint='1' and lPreQint='0') then
    lRedEn          <='1';
    lFedEn          <='0';
    lCount_red<="0000";
    lCount_fed<="0000";

Else

    if (lCount_red>=lRed) then
        lRedEn          <='0';
        lCount_red<=lCount_red;

    End if;

End if;

-----

if (lQint='0' and lPreQint='1') then
    lFedEn          <='1';
    lRedEn          <='0';
    lCount_fed<="0000";
    lCount_red<="0000";

Else

    if (lCount_fed>=lFed) then
        lFedEn          <='0';

    End if;

End if;

-----

    if (lCount >= lDreg) then
        lQint<='1';

    Else

        lQint <='0';

    End if;

-----

if ( lCount >=lDreg or lCount_fed<= lFed ) then
    lQ1          <= '1';

Else

    lQ1          <='0';

End if;

```

```

End if;
-----
if ( ICount_red >= IRed ) then
    IQ2    <= '1';
    Else
    IQ2    <='0';
End if;
-----

IQ3    <= IQ1 and IQ2;
-----
if ( ICount_fed >= IFed) then
    IQ4    <= '1';
Else
    IQ4    <='0';
End if;
-----

if ( iStart ='1') then
    IDreg <= iD;
    IFed <= iFed;
    IRed <= iRed;
End if;
End if;
-----

```

```

End process ;
oQ    <= IQint;
oQ1   <=   IQ1;
oQ2   <=   IQ2;
oQ3   <=   IQ3;
oQ4   <=   IQ4;
oQ_inv <= not (IQint);
oQ1_inv <=   not (IQ1);
oQ2_inv <=   not (IQ2);
oQ3_inv <=   not (IQ3);
oQ4_inv <=   not (IQ4);

```

```

End Behavioral ;
-----
-----

```

This is a program for down mode counter PWM.

```
-----
-----
This program has been written in VHDL for PWM using down mode counter. The program has
been developed by Amir
Saad at Missouri University of Science and Technology in Aug. 2011. Copy right (c) For
Amir Saad. All rights reserved 2011.
-----
-----
```

```
Library ieee;
use ieee.std_logic_1164.all;
use ieee.std_logic_unsigned.all;
use ieee.std_logic_arith.all;

ENTITY aes_pwm_dn is
    generic ( n: natural := 12);-- n can be changed as needed
    port(
        --input signales
        iStart : in std_logic;    -- pulse at start
        iD      : in std_logic_vector(n-1 downto 0 ); --used for 12 bit input
data value
        iClk    : in std_logic;
        iReset  : in std_logic;
        iRed    : in std_logic_vector (3 downto 0); -- rising edge counter
input data
        iFed    : in std_logic_vector (3 downto 0); -- falling edge
counter output data
        --Output signals
        oQ      : out std_logic;
        oQ1     : out std_logic;
        oQ2     : out std_logic;
        oQ3     : out std_logic;
        oQ4     : out std_logic;
        oQ_inv  : out std_logic;
        oQ1_inv : out std_logic;
        oQ2_inv : out std_logic;
        oQ3_inv : out std_logic;
        oQ4_inv : out std_logic;
        oDone   : out std_logic;
        oDone_fed : out std_logic;
        oDone_red : out std_logic;
        Constant C_min : std_logic_vector(n-1 downto
0):=(others=>'0');
        Constant C_max : std_logic_vector(n-1 downto
0):=(others=>'1');
    end aes_pwm_dn ;

Architecture Behavioral of aes_pwm_dn is
    signal lDreg : std_logic_vector(n-1 downto 0); -- register output
    signal lCount : std_logic_vector(n-1 downto 0); -- counter output
    signal lFed : std_logic_vector(3 downto 0); -- falling edge register
output
    signal lRed : std_logic_vector(3 downto 0); -- rising edge register output
    signal lCount_red : std_logic_vector(3 downto 0); -- rising edge counter
output
    signal lCount_fed : std_logic_vector(3 downto 0); -- falling edge counter
output
    signal lQint : std_logic;
    signal lPreQint : std_logic;
    signal lQ1 : std_logic;
    signal lQ2 : std_logic;
    signal lQ3 : std_logic;
    signal lQ4 : std_logic;
    signal lRedEn : std_logic;
    signal lFedEn : std_logic;

Begin
```



```

process
(iClk,iReset,iStart,lQint,lDreg,lCount,lCount_fed,lCount_red,lQ1,lQ2,lQ3,lQ4,lFed,lRed,lRedEn,lFedEn,lPreQint)
Begin
-- Initializations
  if (iReset = '0' ) then
    lCount <= C_max;
    lDreg <= C_min;
    lQint <='0';
  elsif (rising_edge(iClk)) then

    if (lCount=C_min) then
      oDone <= '1';
      lCount<= C_max;
    Else
      lCount<=lCount-1;
      oDone <= '0';
    End if ;

-----
    --rising edge counter
    if (lRedEn='1') then
      lCount_red<=lCount_red +1;
      oDone_red<='0';
    Else
      lRedEn<='0';
      oDone_red<='1';
    End if;

-----
    --falling edge counter
    if (lFedEn='1') then
      lCount_fed<=lCount_fed +1;
      oDone_fed<='0';
    Else
      lFedEn<='0';
      oDone_fed<='1';
    End if;

-----

    if (lQint='1' and lPreQint='0') then
      lRedEn <='1';
      lFedEn <='0';
      lCount_red <="0000";
      lCount_fed <="0000";
    Else
      if (lCount_red>=lRed) then
        lRedEn <='0';
        lCount_red <=lCount_red;
      End if;
    End if;

-----

    if (lQint='0' and lPreQint='1') then
      lFedEn <='1';
      lRedEn <='0';
      lCount_fed <="0000";
      lCount_red <="0000";
    Else
      if (lCount_fed>=lFed) then
        lFedEn <='0';
      End if;
    End if;

-----

    if (lCount >= lDreg) then
      lQint<='1';

    Else
      lQint <='0';
    End if;

-----

    if ( lCount >=lDreg or lCount_fed<= lFed ) then
      lQ1 <= '1';
    Else

```

```

                                lQ1      <='0';
End if;
-----
if ( lCount_red >= lRed ) then
                                lQ2      <= '1';
                                Else
                                lQ2      <='0';
End if;
-----

lQ3      <= lQ1 and lQ2;
-----
if ( lCount_fed >= lFed) then
                                lQ4      <= '1';
                                Else
                                lQ4      <='0';
End if;
-----

if ( iStart ='1') then
                                lDreg <= iD;
                                lFed  <= iFed;
                                lRed  <= iRed;
End if;
End if;
-----
End process ;

oQ      <= lQint;
oQ1     <= lQ1;
oQ2     <= lQ2;
oQ3     <= lQ3;
oQ4     <= lQ4;
oQ_inv  <= not (lQint);
oQ1_inv <= not (lQ1);
oQ2_inv <= not (lQ2);
oQ3_inv <= not (lQ3);
oQ4_inv <= not (lQ4);

End Behavioral ;
-----

```

This is a program for up/down mode counter PWM.

```

-----
-- This program has been written in VHDL for PWM using up/dn mode counter. The program
has been developed by Amir
-- Saad at Missouri University of Science and Technology in Aug. 2011. Copy right (c) For
Amir Saad. All rights reserved 2011.
-----

Library ieee;
use ieee.std_logic_1164.all;
use ieee.std_logic_unsigned.all;
use ieee.std_logic_arith.all;

ENTITY aes_pwm_updn is
    generic ( n: natural :=12);-- n can be changed as needed
    port(
        --input signales
        iStart : in std_logic;    -- pulse at start
        iD      : in std_logic_vector(n-1 downto 0 ); --used for 12 bit
input data value
        iClk   : in std_logic;
        iReset : in std_logic;
        iRed   : in std_logic_vector (3 downto 0); -- rising edge counter
input data
        iFed   : in std_logic_vector (3 downto 0); -- falling edge
counter output data
        iClkDiv : in std_logic_vector(7 downto 0); -- clock divider for PWM
        --Output signals
        oQ      : out std_logic;
        oQ1     : out std_logic;
        oQ2     : out std_logic;
        oQ3     : out std_logic;
        oQ4     : out std_logic;
        oQ_inv  : out std_logic;
        oQ1_inv : out std_logic;
        oQ2_inv : out std_logic;
        oQ3_inv : out std_logic;
        oQ4_inv : out std_logic;
        oDone   : out std_logic;
        oDone_fed : out std_logic;
        oDone_red : out std_logic);
        Constant C_min : std_logic_vector(n-1)          downto
0):=(others=>'0');
        Constant C_max : std_logic_vector(n-1)          downto
0):=(others=>'1');
    end aes_pwm_updn;

Architecture Behavioral of aes_pwm_updn is
    signal lDIR      : std_logic; --Direction of the of the PWM
    signal lDreg     : std_logic_vector(n-1 downto 0); -- register output
    signal lCount    : std_logic_vector(n-1 downto 0); -- counter output
    signal lFed      : std_logic_vector(3 downto 0); -- falling edge register
output
    signal lRed      : std_logic_vector(3 downto 0); -- rising edge register output
    signal lCount_red : std_logic_vector(3 downto 0); -- rising edge counter
output
    signal lCount_fed : std_logic_vector(3 downto 0); -- falling edge counter
output
    signal lCount_div : std_logic_vector(7 downto 0); -- counter for clock
divider
    signal lQint     : std_logic;
    signal lPreQint  : std_logic;
    signal lQ1       : std_logic;
    signal lQ2       : std_logic;
    signal lQ3       : std_logic;
    signal lQ4       : std_logic;
    signal lRedEn    : std_logic;
    signal lFedEn    : std_logic;

```

```

Begin
process
(iClk,iReset,iStart,lDIR,lQint,lDreg,lCount,lCount_fed,lCount_red,lQ1,lQ2,lQ3,lQ4,lFed,lRed,
lRedEn,lFedEn,lPreQint)
Begin
-- Initializations
  if (iReset = '0') then
    lCount <= C_min;
    lDIR <= '0';
    lDreg <= C_min;
    lFed <= "0000";
    lRed <= "0000";
    lQint <='0';
    lQ1 <='0';
    lQ2 <='0';
    lQ3 <='0';
    lQ4 <='0';
    lRedEn <='0';
    lFedEn <='0';
    lCount_red <="0000";
    lCount_fed <="0000";
    lCount_div <= "00000000";
  elsif ( rising_edge(iClk) ) then
    if (lCount_div = iClkDiv) then
      lCount_div <= "00000000";
      if (lDIR = '1') then
        if (lCount= C_max) then
          lDIR <= '0';
          oDone<= '0';
          lCount<=lCount-1;
        Else
          lCount<=lCount+1;
          oDone<= '0';
        End if;
      Else
        if (lCount= C_min) then
          lDIR<='1';
          oDone<= '1';
          lCount<=lCount + 1;
        Else
          oDone<= '0';
          lCount<=lCount - 1;
        End if ;
      End if ;
    End if ;
    lCount_div <= lCount_div + 1;
  end if;
  lPreQint<=lQint;
-----
  --rising edge counter
  if (lRedEn='1') then
    lCount_red<=lCount_red +1;
    oDone_red<='0';
  Else
    lRedEn<='0';
    oDone_red<='1';
  End if;
-----
  --falling edge counter
  if (lFedEn='1') then
    lCount_fed<=lCount_fed +1;
    oDone_fed<='0';
  Else
    lFedEn<='0';
    oDone_fed<='1';
  End if;
-----

```

```

if (lQint='1' and lPreQint='0') then
    lRedEn      <='1';
    lFedEn      <='0';
    lCount_red  <="0000";
    lCount_fed  <="0000";
Else
    if (lCount_red>=lRed) then
        lRedEn      <='0';
        lCount_red  <=lCount_red;
    End if;
End if;
-----

if (lQint='0' and lPreQint='1') then
    lFedEn      <='1';
    lRedEn      <='0';
    lCount_fed  <="0000";
    lCount_red  <="0000";
Else
    if (lCount_fed>=lFed) then
        lFedEn      <='0';

    End if;
End if;
-----

    if (lCount >= lDreg) then
        lQint<='1';

    Else
        lQint <='0';
    End if;
-----

if ( lCount >=lDreg or lCount_fed<= lFed ) then
    lQ1      <= '1';
    Else
        lQ1      <='0';
End if;
-----

if ( lCount_red >= lRed ) then
    lQ2      <= '1';
    Else
        lQ2      <='0';
End if;
-----

lQ3      <= lQ1 and lQ2;
-----

if ( lCount_fed >= lFed) then
    lQ4      <= '1';
Else
    lQ4      <='0';
End if;
-----

if ( iStart ='1') then
    lDreg <= iD;
    lFed <= iFed;
    lRed <= iRed;
End if;
End if;
-----

End process ;
oQ      <= lQint;
oQ1     <= lQ1;
oQ2     <= lQ2;
oQ3     <= lQ3;
oQ4     <= lQ4;
oQ_inv  <= not (lQint);
oQ1_inv <= not (lQ1);
oQ2_inv <= not (lQ2);

```

```
oQ3_inv <= not (lQ3);  
oQ4_inv <= not (lQ4);  
  
End Behavioral ;
```

This is a program for speed observer.

```
-----
-- This program has been written in VHDL for hybrid speed observer to estimate the rotor
positions on continuous basis using the          -- information available through the Hall-
effect sensors. The program has been developed by Amir Saad at Missouri University of
-- Science and Technology in Aug. 2011. Copy right (c) For Amir Saad. All rights reserved
2011.
-----
```

```
Library ieee;
use ieee.std_logic_1164.all;
use ieee.std_logic_unsigned.all;
use ieee.std_logic_arith.all;
library floatfixlib;
use floatfixlib.fixed_pkg.all;
use floatfixlib.float_pkg.all;

ENTITY aes_speed_observer is
  generic (  n: natural := 24;-- n&m can be change depending on the precision of
the angles
            m: natural := 24;-- the fraction part of Wr
            r: natural := 52;-- the precision of Cos phi
            s: natural := 5;-- the integer part of the time
            x: natural := 32;-- the integer part of Wr
            F: natural := 12;
            y: natural := 24;-- the number of the bits in the counter
            a: real := 0.898794;
            b: real := 0.438371;
            c: real := 0.0000000417;
            d: real := 1.0472;
            e: real := 0.1591549431;
            z: natural :=8;
            q : natural := 12 );

  port(
    --input signals
    iStart : in std_logic;          -- pulse at start
    iHa    : in std_logic;          -- Hall effect sensor signal
    iHb    : in std_logic;          -- Hall effect sensor signal
    iHc    : in std_logic;          -- Hall effect sensor signal
    iClk   : in std_logic;          -- the clock signal
    iReset : in std_logic;          -- reset signal

    --Output signals
    oDone  : out std_logic;
    oT1    : out std_logic;
    oT2    : out std_logic;
    oT3    : out std_logic;
    oWr    : out sfixed(F-1 downto 0); -- pulse done when end

the operation
    oSin_th_r : out sfixed(F-1 downto 0); --
    oCos_th_r : out sfixed(F-1 downto 0);
    oFreq     : out sfixed(F-1 downto 0)
  );

  Constant C_min : std_logic_vector(y-1 downto
0):=(others=>'0');
  Constant C_max : std_logic_vector(y-1 downto
0):=(others=>'1');

  end aes_speed_observer;

Architecture Behavioral of aes_speed_observer is
  signal lCount : std_logic_vector(y-1 downto 0); -- counter output
  signal lCount_div : std_logic_vector(7 downto 0); -- counter for
clock divider
  signal lSin_th_r_temp : sfixed (0 downto-11);
```

```

signal lCos_th_r_temp : sfixed (0 downto -11);
signal lWr_temp       : sfixed (9  downto -2);
signal lFreq_temp     : sfixed (9  downto -2);
signal Cos_phi        : sfixed (0  downto -n);
signal Sin_phi        : sfixed (0  downto -n);
signal lDone          : std_logic;
signal T              : sfixed (s  downto -x);--Time between the two
transitions
signal Ts             : sfixed (0  downto -x);--sampling time
signal fs             : sfixed (26 downto 0);--sampling frequency
signal lT1_temp      : std_logic;-- transition in Ha
signal lT2_temp      : std_logic;-- transition in Hb
signal lT3_temp      : std_logic;-- transition in Hc
signal tCount        : sfixed (y-1 downto 0);

Begin
  process
    (iClk,iReset,iStart,lCount,lDone,lSin_th_r_temp,lCos_th_r_temp,lFreq_temp,lT1_temp,lT2_t
mp,lT3_temp)

    variable lFreq      : sfixed (q-1 downto -m);
    variable lSin_th_r_int : sfixed (0  downto -n);
    variable lCos_th_r_int : sfixed (0  downto -n);
    variable lSin_th_r_new : sfixed (0  downto -n);
    variable lCos_th_r_new : sfixed (0  downto -n);
    variable lSin_th_r    : sfixed (0  downto -n);
    variable lCos_th_r    : sfixed (0  downto -n);
    variable lMaxSin      : sfixed (0  downto -n);
    variable lMinSin      : sfixed (0  downto -n);
    variable lMaxCos      : sfixed (0  downto -n);
    variable lMinCos      : sfixed (0  downto -n);
    variable lT1          : std_logic;          -- variable transition in Ha
    variable lT2          : std_logic;          -- variable transition in Hb
    variable lT3          : std_logic;          -- variable transition in Hc
    variable lWr          : sfixed (10 downto -m);
    output variable lHa_reg : std_logic;          -- variable register A
    output variable lHb_reg : std_logic;          -- variable register
    B output variable lHc_reg : std_logic;          -- variable register C
    output variable lPre_Ha_reg : std_logic;      -- variable register A pre-
    output variable lPre_Hb_reg : std_logic;      -- variable register B pre-
    output variable lPre_Hc_reg : std_logic;      -- variable register C pre-
    output
  Begin
    -- Initializations ,

    if (iReset = '0') then

      lWr      := to_sfixed(0,lWr'high,lWr'low);
      lFreq    := to_sfixed(0,lFreq'high,lFreq'low);
      lCount  <= C_min;
      lHa_reg  := '0';
      lHb_reg  := '0';
      lHc_reg  := '0';
      lDone   <= '0';

      -- intitial conditions

      If (lHa_reg='0' and lHb_reg='0' and lHc_reg='1' ) then
        lSin_th_r_int := to_sfixed(-
0.8660254,lSin_th_r_int'high,lSin_th_r_int'low);
        lCos_th_r_int := to_sfixed(-0.5,lCos_th_r_int'high,lCos_th_r_int'low);
      Eelsif (lHa_reg='0' and lHb_reg='1' and lHc_reg='0') then
        lSin_th_r_int :=
to_sfixed(0.8660254,lSin_th_r_int'high,lSin_th_r_int'low);
        lCos_th_r_int := to_sfixed(-0.5,lCos_th_r_int'high,lCos_th_r_int'low);
      Eelsif (lHa_reg='0' and lHb_reg='1' and lHc_reg='1' ) then
        lSin_th_r_int := to_sfixed(0,lSin_th_r_int'high,lSin_th_r_int'low);
        lCos_th_r_int := to_sfixed(-1,lCos_th_r_int'high,lCos_th_r_int'low);

```



```

Elsif (lHa_reg='1' and lHb_reg='0' and lHc_reg='0' ) then
    lSin_th_r_int := to_sfixed(0,lSin_th_r_int'high,lSin_th_r_int'low);
    lCos_th_r_int := to_sfixed(1,lCos_th_r_int'high,lCos_th_r_int'low);
Elsif (lHa_reg='1' and lHb_reg='0' and lHc_reg='1' ) then
    lSin_th_r_int := to_sfixed(-
0.8660254,lSin_th_r_int'high,lSin_th_r_int'low);
    lCos_th_r_int := to_sfixed(0.5,lCos_th_r_int'high,lCos_th_r_int'low);
Elsif (lHa_reg='1' and lHb_reg='1' and lHc_reg='0' ) then
    lSin_th_r_int :=
to_sfixed(0.8660254,lSin_th_r_int'high,lSin_th_r_int'low);
    lCos_th_r_int := to_sfixed(0.5,lCos_th_r_int'high,lCos_th_r_int'low);
Elsif (lHa_reg='1' and lHb_reg='1' and lHc_reg='1' ) then
    lSin_th_r_int := to_sfixed(0,lSin_th_r_int'high,lSin_th_r_int'low);
    lCos_th_r_int := to_sfixed(0,lCos_th_r_int'high,lCos_th_r_int'low);
End if;

if (lHa_reg='0' and lHb_reg='0' and lHc_reg='1' ) then
    lMaxSin := to_sfixed(-0.5,lMaxSin'high,lMaxSin'low);
    lMinSin := to_sfixed(-1,lMaxSin'high,lMaxSin'low);
    lMaxCos := to_sfixed(0,lMaxCos'high,lMaxCos'low);
    lMinCos := to_sfixed(-0.8660254,lMaxCos'high,lMaxCos'low);
Elsif (lHa_reg='0' and lHb_reg='1' and lHc_reg='0' ) then
    lMaxSin := to_sfixed(1,lMaxSin'high,lMaxSin'low);
    lMinSin := to_sfixed(0.5,lMaxSin'high,lMaxSin'low);
    lMaxCos := to_sfixed(0,lMaxCos'high,lMaxCos'low);
    lMinCos := to_sfixed(-0.8660254,lMaxCos'high,lMaxCos'low);
Elsif (lHa_reg='0' and lHb_reg='1' and lHc_reg='1' ) then
    lMaxSin := to_sfixed(-0.5,lMaxSin'high,lMaxSin'low);
    lMaxCos := to_sfixed(-0.8660254,lMaxCos'high,lMaxCos'low);
    lMinCos := to_sfixed(-1,lMaxCos'high,lMaxCos'low);
Elsif (lHa_reg='1' and lHb_reg='0' and lHc_reg='0' ) then
    lMaxSin := to_sfixed(0.5,lMaxSin'high,lMaxSin'low);
    lMinSin := to_sfixed(-0.5,lMaxSin'high,lMaxSin'low);
    lMaxCos := to_sfixed(1,lMaxCos'high,lMaxCos'low);
    lMinCos := to_sfixed(0.8660254,lMaxCos'high,lMaxCos'low);
Elsif (lHa_reg='1' and lHb_reg='0' and lHc_reg='1' ) then
    lMaxSin := to_sfixed(-0.5,lMaxSin'high,lMaxSin'low);
    lMinSin := to_sfixed(-1,lMaxSin'high,lMaxSin'low);
    lMaxCos := to_sfixed(0.8660254,lMaxCos'high,lMaxCos'low);
    lMinCos := to_sfixed(0,lMaxCos'high,lMaxCos'low);
Elsif (lHa_reg='1' and lHb_reg='1' and lHc_reg='0' ) then
    lMaxSin := to_sfixed(1,lMaxSin'high,lMaxSin'low);
    lMinSin := to_sfixed(0.5,lMaxSin'high,lMaxSin'low);
    lMaxCos := to_sfixed(0.8660254,lMaxCos'high,lMaxCos'low);
    lMinCos := to_sfixed(0,lMaxCos'high,lMaxCos'low);
End if;
-- Now we can calculate sine and cosine theata_r in the initial conditions mode

    Cos_phi <= to_sfixed(a,Cos_phi'High,Cos_phi'Low); -- in this case phi
tken as 26 degrees
    Sin_phi <= to_sfixed(b,Sin_phi'High,Sin_phi'Low); -- in this case phi
tken as 26 degrees
    Ts <= to_sfixed(c,Ts'High,Ts'Low); -- Sampling time
    fs <= to_sfixed(24000000,fs'High,fs'Low); -- Sampling frequency
    lSin_th_r :=
resize((lSin_th_r_int*Cos_phi)+(lCos_th_r_int*Sin_phi),lSin_th_r'High,lSin_th_r'Low);
    lCos_th_r := resize((lCos_th_r_int*Cos_phi)-
(lSin_th_r_int*Sin_phi),lCos_th_r'High,lCos_th_r'Low);

-- Bounding conditions
elsif ( rising_edge(iClk)) then
    Cos_phi <= to_sfixed(a,Cos_phi'High,Cos_phi'Low); -- in this case phi
tken as 26 degrees
    Sin_phi <= to_sfixed(b,Sin_phi'High,Sin_phi'Low); -- in this
case phi tken as 26 degrees
    Ts <= to_sfixed(c,Ts'High,Ts'Low); -- Sampling time
    fs <= to_sfixed(24000000,fs'High,fs'Low); -- Sampling frequency
    lHa_reg := iHa;
    lHb_reg := iHb;

```

```

lHc_reg      :=      iHc;

lT1          :=      (lPre_Ha_reg xor lHa_reg);
lT2          :=      (lPre_Hb_reg xor lHb_reg);
lT3          :=      (lPre_Hc_reg xor lHc_reg);

-- Counter to count the time between the transitions

if (lCount= C_max) then
    lCount<= C_min;
    oDone  <= '0';
Else
    lCount<=lCount+1;
End if ;

-----
-----

If      (lT1 ='1' or lT2 ='1' or lT3 ='1') then
lCount <= C_min;
lDone  <='1';
tCount <= to_sfixed(lCount,tCount'High,tCount'low);
lWr    :=  resize((to_sfixed(1.0472,1,-6)*fs/tCount),lWr'High,lWr'Low);--T is the
time between tow transition = lCount*sampling time(Ts)
lCount <= C_min;
lFreq  :=  resize(to_sfixed(e,0,-24)*lWr,lFreq'High,lFreq'Low);-- this is
temporary value for lFreq

Else
    lDone  <= '0';
End if;

if      (lT1 ='1' and lHb_reg='1') then
lSin_th_r_int := to_sfixed(1,lSin_th_r_int'high,lSin_th_r_int'low);
lCos_th_r_int := to_sfixed(0,lCos_th_r_int'high,lCos_th_r_int'low);
Elsif    (lT1 ='1' and lHc_reg='1') then
lSin_th_r_int := to_sfixed(-1,lSin_th_r_int'high,lSin_th_r_int'low);
lCos_th_r_int := to_sfixed(0,lCos_th_r_int'high,lCos_th_r_int'low);
Elsif    (lT2 ='1' and lHa_reg='1') then
lSin_th_r_int := to_sfixed(0.5,lSin_th_r_int'high,lSin_th_r_int'low);
lCos_th_r_int := to_sfixed(0.8660254,lCos_th_r_int'high,lCos_th_r_int'low);
Elsif    (lT2 ='1' and lHc_reg='1') then
lSin_th_r_int := to_sfixed(-0.5,lSin_th_r_int'high,lSin_th_r_int'low);
lCos_th_r_int := to_sfixed(-0.8660254,lCos_th_r_int'high,lCos_th_r_int'low);
Elsif    (lT3 ='1' and lHa_reg='1') then
lSin_th_r_int := to_sfixed(-0.5,lSin_th_r_int'high,lSin_th_r_int'low);
lCos_th_r_int := to_sfixed(0.8660254,lCos_th_r_int'high,lCos_th_r_int'low);
Elsif    (lT3 ='1' and lHb_reg='1') then
lSin_th_r_int := to_sfixed(0.5,lSin_th_r_int'high,lSin_th_r_int'low);
lCos_th_r_int := to_sfixed(-0.8660254,lCos_th_r_int'high,lCos_th_r_int'low);
End if;

if      (lHa_reg='0' and lHb_reg='0' and lHc_reg='1' ) then
lMaxSin := to_sfixed(-0.5,lMaxSin'high,lMaxSin'low);
lMinSin := to_sfixed(-1,lMaxSin'high,lMaxSin'low);
lMaxCos := to_sfixed(0,lMaxCos'high,lMaxCos'low);
lMinCos := to_sfixed(-0.8660254,lMaxCos'high,lMaxCos'low);
Elsif    (lHa_reg='0' and lHb_reg='1' and lHc_reg='0' ) then
lMaxSin := to_sfixed(1,lMaxSin'high,lMaxSin'low);
lMinSin := to_sfixed(0.5,lMaxSin'high,lMaxSin'low);
lMaxCos := to_sfixed(0,lMaxCos'high,lMaxCos'low);
lMinCos := to_sfixed(-0.8660254,lMaxCos'high,lMaxCos'low);
Elsif    (lHa_reg='0' and lHb_reg='1' and lHc_reg='1' ) then
lMaxSin := to_sfixed(-0.5,lMaxSin'high,lMaxSin'low);
lMaxCos := to_sfixed(-0.8660254,lMaxCos'high,lMaxCos'low);
lMinCos := to_sfixed(-1,lMaxCos'high,lMaxCos'low);
Elsif    (lHa_reg='1' and lHb_reg='0' and lHc_reg='0' ) then
lMaxSin := to_sfixed(0.5,lMaxSin'high,lMaxSin'low);
lMinSin := to_sfixed(-0.5,lMaxSin'high,lMaxSin'low);
lMaxCos := to_sfixed(1,lMaxCos'high,lMaxCos'low);

```

```

lMinCos := to_sfixed(0.8660254,lMaxCos'high,lMaxCos'low);
Elsif (lHa_reg='1' and lHb_reg='0' and lHc_reg='1' ) then
lMaxSin := to_sfixed(-0.5,lMaxSin'high,lMaxSin'low);
lMinSin := to_sfixed(-1,lMaxSin'high,lMaxSin'low);
lMaxCos := to_sfixed(0.8660254,lMaxCos'high,lMaxCos'low);
lMinCos := to_sfixed(0,lMaxCos'high,lMaxCos'low);
Elsif (lHa_reg='1' and lHb_reg='1' and lHc_reg='0' ) then
lMaxSin := to_sfixed(1,lMaxSin'high,lMaxSin'low);
lMinSin := to_sfixed(0.5,lMaxSin'high,lMaxSin'low);
lMaxCos := to_sfixed(0.8660254,lMaxCos'high,lMaxCos'low);
lMinCos := to_sfixed(0,lMaxCos'high,lMaxCos'low);
End if;

lCos_th_r_new := resize(lCos_th_r_int
(lWr*lSin_th_r_int)*Ts,lCos_th_r'High,lCos_th_r'Low); --intigration -
lSin_th_r_new := resize(lSin_th_r_int
(lWr*lCos_th_r_int)*Ts,lSin_th_r'High,lSin_th_r'Low); --intigration +

lT1_temp <= lT1;
lT2_temp <= lT2;
lT3_temp <= lT3;

-- integral limitations
if (lSin_th_r_new >= lMaxSin) then
lSin_th_r_new := lMaxSin;
Elsif (lSin_th_r_new <= lMinSin) then
lSin_th_r_new := lMinSin;
End if;

If (lCos_th_r_new >= lMaxCos) then
lCos_th_r_new := lMaxCos;
Elsif (lCos_th_r_new <= lMinCos) then
lCos_th_r_new := lMinCos;
End if;

-- calculating the sine theata_r and cosine theata_r for the starting mode
lSin_th_r :=
resize((lSin_th_r_new*cos_phi)+(lCos_th_r_new*sin_phi),lSin_th_r'High,lSin_th_r'Low);
lCos_th_r := resize((lCos_th_r_new*cos_phi)-
(lSin_th_r_new*sin_phi),lCos_th_r'High,lCos_th_r'Low);
lSin_th_r_int := lSin_th_r_new;
lCos_th_r_int := lCos_th_r_new;
lPre_Ha_reg := lHa_reg;
lPre_Hb_reg := lHb_reg;
lPre_Hc_reg := lHc_reg;

-- Because Quartus II don't recognize the fraction part we need to change them to real
part
lFreq_temp <= resize(lFreq ,lFreq_temp'high,lFreq_temp'low);
lWr_temp <= resize(lWr ,lWr_temp'high ,lWr_temp'low );
lFreq_temp <= resize(lFreq ,lFreq_temp'high,lFreq_temp'low);
lSin_th_r_temp <=
resize(lSin_th_r,lSin_th_r_temp'high,lSin_th_r_temp'low);
lCos_th_r_temp <=
resize(lCos_th_r,lCos_th_r_temp'high,lCos_th_r_temp'low);

End if;
oDone <= lDone;
End process ;

oSin_th_r <= lSin_th_r_temp;
oCos_th_r <= lCos_th_r_temp;
oWr <= lWr_temp;
oFreq <= lFreq_temp;
oT1 <= lT1_temp;
oT2 <= lT2_temp;
oT3 <= lT3_temp;

End Behavioral;

```

BIBLIOGRAPHY

- [1] A. Raskin and S. Shah, "The Emergence of Hybrid Vehicles," AllianceBernstein.
- [2] M. Umeda, H. Itoh, S. Hashimoto, M. Hirata, J. Tsujimura, and S. Kato, "Permanent magnet motor for EV," in *Proc. Power Electronics and Drive Systems, 1995., Proceedings of 1995 International Conference on*, 1995, pp. 792-796 vol.2.
- [3] M. Mekhiche, S. Nichols, J. L. Kirtley, J. Young, D. Boudreau, and R. Jodoin, "High-speed, high-power density PMSM drive for fuel cell powered HEV application," in *Proc. Electric Machines and Drives Conference, 2001. IEMDC 2001. IEEE International*, 2001, pp. 658-663.
- [4] M. J. Corley and R. D. Lorenz, "Rotor position and velocity estimation for a salient-pole permanent magnet synchronous machine at standstill and high speeds," *Industry Applications, IEEE Transactions on*, vol. 34, pp. 784-789.
- [5] W. Limei and R. D. Lorenz, "Rotor position estimation for permanent magnet synchronous motor using saliency-tracking self-sensing method," in *Proc. Industry Applications Conference, 2000. Conference Record of the 2000 IEEE*, 2000, vol. 1, pp. 445-450 vol.1.
- [6] Z.-y. Zhou, Z. Xu, and T.-c. Li, "FPGA implementation of a new hybrid rotor position estimation scheme based on three symmetrical locked Hall effect position sensors," in *Proc. Power Electronics and Motion Control Conference, 2004. IPEMC 2004. The 4th International*, 2004, vol. 3, pp. 1592-1596 Vol.3.
- [7] S. Jiang, J. Liang, Y. Liu, K. Yamazaki, and M. Fujishima, "Modeling and cosimulation of FPGA-based SVPWM control for PMSM," in *Proc. Industrial Electronics Society, 2005. IECON 2005. 31st Annual Conference of IEEE*, 2005, pp. 6 pp.
- [8] X. Z. Qi, Xiaomin; Wang, Changsong; Wang, Xu; and Zhou, Ke, "Rotor position estimation for a sensorless PMSM using high-frequency signal injection method," in *Proc. Information, Computing and Telecommunication, 2009. YC-ICT '09. IEEE Youth Conference on*, 2009, pp. 54-57.
- [9] B. Zheng, L. Wu, A. Lin, F. Li, C. Yuan, and J. Dang, "Study of a new detection technology for sensorless PMSM drive with flux linkage observer," in *Proc. Consumer Electronics, Communications and Networks (CECNet), 2011 International Conference on*, 2011, pp. 1691-1694.

- [10] S. Zaim, J. P. Martin, B. Nahid-Mobarakeh, and F. Meibody-Tabar, "High performance low cost control of a permanent magnet wheel motor using a hall effect position sensor," in *Proc. Vehicle Power and Propulsion Conference (VPPC), 2011 IEEE*, 2011, pp. 1-6.
- [11] P. Thiemann, C. Mantala, J. Hordler, *et al.*, "PMSM sensorless rotor position detection for all speeds by Direct Flux Control," in *Proc. Industrial Electronics (ISIE), 2011 IEEE International Symposium on*, 2011, pp. 673-678.
- [12] M. a. P. Seilmeier, B., "Modeling of PMSM with multiple saliencies using a stator-oriented magnetic circuit approach," in *Proc. Electric Machines & Drives Conference (IEMDC), 2011 IEEE International*, 2011, pp. 131-136.
- [13] K. C. Sam-Young, Choi; Kyeongjin, Lee; and Wootaik, Lee, "An Improved Rotor Position Estimation With Vector-Tracking Observer in PMSM Drives With Low-Resolution Hall-Effect Sensors," *Industrial Electronics, IEEE Transactions on*, vol. 58, pp. 4078-4086.
- [14] Texas Instruments, "Non-Inverting Attenuation with Positive Offset " accessed on, <http://www-k.ext.ti.com/srvs/cgi-bin/webcgi.exe?Company={5761bcd8-11f5-4e08-84e0-8167176a4ed9},kb=analog.case=obj%2835457%29.new>.
- [15] D. L. Terrell, *OP AMPS Design, Application, and Troubleshooting*, Second ed, 1996.
- [16] Texas Instruments, "FilterPro™ User's Guide," accessed on, www.ti.com/lit/an/sbfa001c/sbfa001c.pdf.
- [17] Texas Instruments "CMOS Hex Voltage-Level shifter for TTL-to-CMOS or CMOS-to-TTL Operation," accessed on, <http://www.ti.com/lit/ds/symlink/cd4504b-mil.pdf>.
- [18] Analog Devices, "AD 7276 8-Bit ADCs in 6-Lead TSOT," accessed on, http://www.analog.com/static/imported-files/data_sheets/AD7276_7277_7278.pdf.
- [19] Analog Devices, Inc, "Quad-Channel Digital Isolators," accessed on, http://www.analog.com/static/imported-files/data_sheets/ADUM1410_1411_1412.pdf.
- [20] National Instruments, "Optical Encoder Fundamentals," accessed on, <http://zone.ni.com/devzone/cda/tut/p/id/4672>.
- [21] TI, "INDUSTRIAL CAN TRANSCEIVER," accessed on, <http://www.ti.com/lit/ds/symlink/sn65hvd251.pdf>.

- [22] Basic Electronics Tutorials "Differential Amplifier," accessed on, http://www.electronics-tutorials.ws/opamp/opamp_5.html.
- [23] TI, "Digital Signal Controllers (DSCs)," accessed on, <http://www.ti.com/lit/ds/symlink/tms320f28335.pdf>.
- [24] Altera corporation, "FPGA and CPLD Design Flow," accessed on, <http://www.altera.com/products/software/flows/fpga/flo-fpga.html>.
- [25] Samtec Inc., accessed on, <http://www.samtec.com/ProductInformation/TechnicalSpecifications/Overview.aspx?series=PES>.
- [26] K. Corzine, "Rotor Position Measurement, EE305," Missouri S&T.
- [27] Control Science Inc., "Resolvers as Velocity and Position Encoding Devices," accessed on, http://www.controlsciences.com/resolver_application_data.shtml.
- [28] Advanced Micro Controls, Inc., "What is the Resolver," accessed on, <http://www.amci.com/tutorials/tutorials-what-is-resolver.asp>.
- [29] Z. Chen, M. Tomita, S. Doki, and S. Okuma, "New adaptive sliding observers for position- and velocity-sensorless controls of brushless DC motors," *Industrial Electronics, IEEE Transactions on*, vol. 47, pp. 582-591.
- [30] T. Furuhashi, S. Sangwongwanich, and S. Okuma, "A position and velocity sensorless control of brushless DC motors using an adaptive sliding observer," in *Proc. Industrial Electronics Society, 1990. IECON '90., 16th Annual Conference of IEEE*, 1990, pp. 1188-1192 vol.2.
- [31] E. Ramsden, *Hall-Effect Sensors Theory and Applications*: Elsevier Inc., Copyright © 2006.
- [32] K. A. Corzine and S. D. Sudhoff, "A hybrid observer for high performance brushless DC motor drives," *Energy Conversion, IEEE Transactions on*, vol. 11, pp. 318-323.
- [33] vhdl.org, "Fixed point package user's guide," accessed on, http://www.eda.org/fphdl/Fixed_ug.pdf.

VITA

Amir Saad was born in Omdurman, Sudan. He completed his Bachelor of Science (B.S.) in Electronic Engineering Technology specialized in Medical Electronics Engineering from University of Gezira, Wad Medani, Sudan in DEC 1998. He joined his Master of Science program in Electrical Engineering at Missouri University of Science and Technology in January 2010 and will receive his Master's degree in Electrical Engineering from Missouri University of Science and Technology in May 2012. He has worked at different companies before making his way back for a higher degree and after graduation will join Caterpillar Inc. at Advance Components Group.